

**Comparison and optimization of tissue clearing and vascular labeling
techniques for high-resolution imaging of the cortical vasculature in rodents**

Maria Matossian

Department of Biological and Biomedical Engineering

McGill University, Montreal

12/2021 of initial thesis submission

A thesis submitted to McGill University in partial fulfillment of the requirements of the degree
of Master of Biological and Biomedical Engineering

© Maria Matossian 2021

List of Tables

Table 1. Incubation steps and durations for 3DISCO clearing	39
Table 2. Incubation steps and durations for iDISCO+ clearing	40
Table 3. Summary of experiments	42
Table 4. Indication of dye type and concentration used for each coronal slab	45
Table 5. Experimental design for labeling by immersion applied 5 mouse brains	45
Table 6. Mean and standard deviation values of the signal-to-background ratio for each mouse from each region of interest.	72

List of Figures

Figure 1. Evaluation of EGFP fluorescence preservation and tissue clearing results based on different incubation parameters	19
Figure 2. Comparison of EGFP fluorescence preservation between sDISCO and 3DISCO.	21
Figure 3. Fluorescence imaging of different dyes with 3DISCO and FDISCO clearing.	22
Figure 4. Brain clearing and vessel imaging with MACS.	25
Figure 5. CUBIC clearing progress and imaging of vessels.	26
Figure 6. Demonstration of rat liver vasculature intensity obtained with a confocal microscope at different imaging depths	27
Figure 7. List of CUBIC cocktails and protocols.	29
Figure 8. Lectin labeling of brain and liver vasculature	34
Figure 9. Cutting plan for experiments.	44
Figure 10. Example of capillary and background signal sampling across the cortical depths.	50
Figure 11. Comparison of clearing results based on different incubation conditions.	51
Figure 12: Demonstration of whole-brain clearing performance using different organic solvent protocols.	52
Figure 13: Example of CUBIC clearing progress of a whole brain.	53
Figure 14. Clearing results from 3 mm thick coronal brain slabs using iDISCO+ and 3DISCO.	55
Figure 15. Comparison of iDISCO+ and 3DISCO clearing after 1 and 2 days of refractive index matching.	56
Figure 16. Depiction of clearing artifacts.	56
Figure 17. Demonstration of final clearing results from rat coronal brain slabs using 3 different clearing methods.	57
Figure 18. Depiction of vascular staining results using DISCO clearing methods in a mouse.	59-60
Figure 19. Depiction of blood vessel images from a CUBIC cleared mouse coronal slab. An overview of a coronal slab cleared with CUBIC is shown on the left with a magnified view of the orange square on the right.	60
Figure 20. Depiction of vascular labeling results using DISCO clearing methods in a rat.	64-65

Figure 21. Comparison of signal-to-background ratio and signal and background intensities between clearing protocols.	66
Figure 22. Comparison of signal-to-background ratio and signal and background intensities between different dye volumes.	67
Figure 23. Depiction of vascular labeling results using the iDISCO+ clearing method in a rat.	68
Figure 24. Average intensity z-projection of 10 planes using a single point confocal microscope (LSM880) from a 2 mm thick rat coronal brain slab.	70
Figure 25. Vascular imaging results from 4 mice injected with different volumes of Alexa Fluor 594.	73
Figure 26. Signal to background ratio from 5 different regions of interest (ROI) in mouse brains.	74
Figure 27. Imaging results obtained from iDISCO+ and 3DISCO clearing and labeling with 4 different volumes of WGA Alexa Fluor 594.	75
Figure 28. Comparison of clearing between different coronal slab thicknesses from mice of different ages.	77
Figure 29. Imaging the vasculature in slabs with different thicknesses obtained from 2 mice of different ages.	78
Figure 30. Observation of inhomogeneous labeling.	78
Figure 31. Depiction of the progress of CUBIC clearing applied to coronal slabs of different thicknesses from mice of varying age.	79
Figure 32. Demonstration of blood vessels labeling with dextran-FITC and CUBIC clearing.	81
Figure 33. CUBIC delipidation progress of 3 different mice brains used for labeling by immersion.	83
Figure 34. Labeling by immersion with DyLight 649 performed after delipidation.	85
Figure 35. Labeling by immersion with 4 different protocols.	87

ACKNOWLEDGMENTS

This work would not have been possible without the help of Aleksandra, Victor, and Tiago who performed dye injections and rodent perfusions throughout my research. I would also like to thank Deepthi who works on aqueous tissue clearing. Our discussions and sharing of knowledge on tissue clearing and imaging were insightful.

Additionally, I would like to thank all the staff members from McGill's Advanced Bioimaging Facility, Montreal Neurological Institute's microscopy facility, and the microscopy platform manager at St-Justine's. They provided me with training, knowledge, and support for using microscopes, data processing, and analysis software.

I would also like to show gratitude to my Professor, Amir Shmuel, for his constant support, guidance, and patience. He showed me how to conduct research and how to think scientifically in terms of planning, executing, and analyzing.

Finally, I am very thankful to my family for their support, their belief in me, and their never-ending encouragement.

FUNDING

The funding obtained for this work includes:

1. Canadian Institute of Health Research (MOP-102599; AS)
2. The Natural Sciences and Engineering Research Council of Canada (R GPIN- 2015-05103; AS)
3. FRQS' Quebec Bio-Imaging Network
4. Canada First Research Excellence Fund awarded to McGill University for the Healthy Brains for Healthy Lives Initiative

CONTRIBUTION OF AUTHORS

The candidate served as the main researcher for this project. She carried out the review of the literature on methods of tissue staining and clearing. She took part in the vascular labeling and tissue collection processes. She performed tissue clearing, tissue imaging, and data processing. The candidate compared different protocols and wrote the thesis.

Dr. Aleksandra Beata Bortel, Mihai Victor Mocanu, and Tiago David performed the animal procedures for obtaining the brain samples.

Deepthi David participated in obtaining part of the data and shared her knowledge on aqueous tissue clearing methods.

Dr. Amir Shmuel initiated the research project, advised on how to plan and perform the data acquisition and data analysis, evaluated and gave feedback on the results, and edited the thesis manuscript.

CONTRIBUTION TO THE WRITING OF SPECIFIC CHAPTERS

The abstract was written and translated to French by the candidate and edited by Dr. Shmuel.

Chapter I – The introduction was written by the candidate and edited by Dr. Shmuel.

Chapter II – The review and the background of the thesis were written by the candidate and edited by Dr. Shmuel.

Chapter III – The methods section was written by the candidate and edited by Dr. Shmuel.

Chapter IV – The figures and results were prepared and analyzed by the candidate. The chapter was written by the candidate and edited by Dr. Shmuel.

Chapter V – The discussion was written by the candidate and edited by Dr. Shmuel.

Conferences and presentations related to this work

Student Symposium

Maria Matossian, Dr. Aleksandra Beata Bortel, and Dr. Amir Shmuel. Optimization of tissue clearing and vasculature labeling methods to study the neocortical vasculature. Department of Biological and Biomedical Engineering, McGill University, Montreal, QC, Canada. February 26, 2021.

Poster Presentation

Maria Matossian, Dr. Aleksandra Beata Bortel, Deepthi Thommana, Mihai Victor Mocanu, and Dr. Amir Shmuel. A comparison of tissue clearing techniques for high-resolution imaging of the cortical vasculature. Society for Neuroscience Annual Conference, Online, November 11, 2021.

ENGLISH ABSTRACT

Introduction and Background

To gain a clear understanding of the mechanisms underlying Blood Oxygenation Level-Dependent functional magnetic resonance imaging in the brain, we need to quantify the structural organization and the density of blood vessels in the brain. However, obtaining a whole cerebral vascular map at the capillary level is challenging. We need to obtain homogeneous labeling of the vessels, image deep into the brain while maintaining the labeling dye's fluorescence and manage large data sets.

Objective

The goal of our current project is to compare and optimize methods for labeling blood vessels and tissue clearing to obtain high-resolution images of neocortical vessels in mice and rats.

Methods

To this end, we compared vasculature labeling methods, including (1) injecting the dye in vivo to the vascular system intracardially or through the tail vein and (2) in vitro staining by immersion. We evaluated the labeling by 3 different dyes, including Fluorescein Isothiocyanate-Dextran, wheat germ agglutinin Alexa fluor, and Lycopersicon esculentum (Tomato) lectin DyLight. We also compared three different clearing methods: CUBIC (clear, unobstructed brain/body imaging cocktails and computational analysis), 3DISCO (three-dimensional imaging of solvent-cleared organs), and iDISCO+ (Immunolabeling-enabled 3DISCO plus). We varied additional parameters such as the tissue slab thickness, the dye volume injected in mice of the same age, and the mouse age while keeping a constant fluorophore volume. We evaluated the labeling quality with an Opera Phenix High-Content Screening microscope, a single-point confocal microscope, and a quantitative estimation of signal to background fluorescence ratio.

Results

We found that organic solvents cleared coronal brain slabs within days, significantly faster than the CUBIC protocol that required weeks for clearing similar slabs. With CUBIC, the clearing time increased with coronal slab thickness. Based on our Opera Phenix images, we found homogenous vasculature labeling throughout the cortex was possible with intravascular labeling

protocols, especially with tail vein injection of Alexa Fluor. We found that the quality of the perfusion impacts the quality of labeling. We performed a quantitative analysis of the signal-to-background ratio of mice stained with different volumes of 1.67 mg/ml Alexa Fluor. We found that using 250 μ l and 200 μ l volumes gave a higher signal-to-background ratio relative to 100 μ l. We observed similar results in rats. Intravenous labeling with 1.2 ml of Alexa Fluor (1.67 mg/ml) gave a greater signal-to-background ratio compared to 0.6 ml. Additionally, imaging with CUBIC cleared samples gave a higher background signal relative to the DISCO methods. Finally, based on quantitative analysis, we found that iDISCO+ provided a greater signal-to-background ratio compared to 3DISCO.

Conclusion

Hence, tail vein injections of Alexa Fluor in rats and tissue clearing with iDISCO+ enable good vessel labeling, tissue clearing, and imaging results.

RÉSUMÉ FRANÇAIS

Introduction et contexte

Pour mieux comprendre les mécanismes sous-jacents à l'imagerie par résonance magnétique fonctionnelle dépendant du niveau d'oxygénation du sang dans le cerveau, nous voulons quantifier l'organisation structurale et la densité des vaisseaux sanguins du cerveau. Cependant, il est difficile d'obtenir l'architecture complète des vaisseaux sanguins au niveau capillaire. Nous devons marquer les vaisseaux d'une manière homogène, obtenir des imageries microscopiques du cerveau en profondeur tout en maintenant la fluorescence du marqueur et en gérant de grands ensembles de données.

Objectif

L'objectif de notre projet actuel est de comparer et d'optimiser les méthodes de marquage des vaisseaux sanguins et les méthodes de rendre les indices de réfraction du cerveau homogène. Ainsi, nous pourrions obtenir des images en haute résolution des vaisseaux néocorticaux avec les souris et les rats.

Méthodes

À cette fin, nous avons comparé les méthodes de marquage vasculaire, y compris (1) l'injection du colorant dans le système vasculaire par voie intracardiaque ou par la veine caudale et (2) la coloration par immersion du cerveau. Nous avons évalué 3 marqueurs différents, dont l'isothiocyanate de fluorescéine-dextran, l'agglutinine de germe de blé Alexa fluor et la lectine DyLight de *Lycopersicon esculentum* (tomate). Nous avons également comparé trois méthodes d'homogénéisation d'indice de réfraction: CUBIC (cocktails d'imagerie cérébrale/corps clairs et non obstrués et analyse informatique), 3DISCO (imagerie tridimensionnelle d'organes nettoyés au solvant) et iDISCO+ (3DISCO plus compatible avec l'immunoétiquetage). Nous avons examiné des paramètres supplémentaires tels que la variation du volume de fluorophore injecté chez des souris du même âge et la variation de l'âge des souris tout en gardant un volume de fluorophore constant. Nous avons évalué la qualité de marquage avec un microscope "Opera Phenix High-Content Screening" et avec un microscope confocale monopoint. Ensuite, nous avons effectué une estimation quantitative du rapport signal/bruit.

Résultats

Nous avons constaté que les solvants organiques nettoyaient les sections du cerveau en quelques jours. En comparaison, le protocole CUBIC prend des semaines. De plus, avec CUBIC, le temps d'homogénéisation de l'indice de réfraction augmente avec l'épaisseur de notre section de tissu cérébrale. Basé sur nos images d'Opera Phenix, nous avons constaté qu'un marquage homogène du système vasculaire du cortex cérébral était possible en utilisant des protocoles de marquage intravasculaire. Ceci était possible, en particulier, avec l'injection d'Alexa Fluor dans la veine caudale. Nous avons constaté que la qualité de la perfusion impacte la qualité de marquage. Nous avons effectué une analyse quantitative du rapport signal/bruit pour les souris dont leur vaisseaux sanguins ont été étiquette avec différents volumes d'Alexa Fluor (1,667 mg/ml). Nous avons constaté que l'utilisation de volumes de 200 μ l et 250 μ l donnait un rapport signal/bruit plus élevé par rapport à 100 μ l. Nous avons observé des résultats similaires chez les rats. Le marquage des vaisseaux par la veine caudale avec 1,2 ml d'Alexa Fluor (1,67 mg/ml) a donné un rapport signal/bruit supérieur à celui de 0,6 ml. De plus, l'imagerie microscopique des section du cerveau nettoyés avec CUBIC a donné un signal de bruit de fond plus élevé par rapport aux méthodes DISCO. Finalement, sur la base d'une analyse quantitative, nous avons constaté qu'iDISCO+ offrait un rapport signal/bruit plus élevé comparé à 3DISCO.

Conclusion

Par conséquent, les injections d'Alexa Fluor dans la veine caudale chez les rats et le nettoyage des sections de cerveau avec iDISCO+ permettent de bonnes capacités de nettoyage et d'imagerie.

THESIS OUTLINE

I.	Introduction	14
	a. Rational	14
	b. Objectives	15
	c. Proposed solutions and approaches	16
II.	Review and background	17
	a. Clearing with organic solvents	17
	b. Clearing with aqueous solvents	24
	c. Vasculature labelling	30
	i. Dye selection	30
	ii. Labelling methods	33
III.	Development of methodology	35
	a. Overview	35
	b. Perfusion and staining the cerebral vasculature	36
	c. Clearing methods	38
	d. Experimental setup for comparing different methods together	41
	e. Imaging the brain slabs	45
	i. Opera Phenix High-Content Screening Microscope	46
	ii. Zeiss LSM-880 with AiryScan detector microscope	47
	f. Visualization of data	47
	g. Quantitative analysis	48
IV.	Research findings	50
	a. Preliminary clearing results of whole brains & hemispheres	50
	b. Comparison of clearing protocols 3DISCO, iDISCO+, and CUBIC: Experiment 1-3	53
	i. Clearing results in mice: Experiment 1	53
	ii. Clearing results in rat: Experiment 3	57
	iii. Imaging results in mice: Experiment 2	58
	iv. Imaging results in rat: Experiment 3	61
	c. Dye volume selection: Experiment 4	71
	d. Effects of clearing on age and tissue thickness: Experiment 5 and 6	76
	i. Clearing results using the iDISCO+ protocol: Experiment 5	76
	ii. Imaging results from iDISCO+ protocol: Experiment 5	77
	iii. Clearing results from CUBIC protocol: Experiment 6	79
	iv. Imaging results from CUBIC protocol: Experiment 6	80
	e. Staining by immersion: Experiment 7	82
V.	Discussion	88
VI.	References	98

CHAPTER I – INTRODUCTION

a. Rational

Ex-vivo three-dimensional study of organs, more specifically vascular structures, permits researchers to answer questions related to tumors such as the tumor stage (Tanaka et al., 2018) or the presence of angiogenesis (Li et al., 2014). It can also help understand how the structural organization of blood vessels (or the nervous system) can be altered following a disease or an injury (Todorov et al., 2020). Furthermore, it can give a more accurate understanding of brain imaging data such as functional magnetic resonance imaging (fMRI) which relies on the hemodynamic changes in the blood vessels. As for our main interest, these ex-vivo studies could help us understand the structural organization of the vessels in the cortical layers of the brain. In turn, this could potentially help clarify cortical depth-dependent fMRI signals. They are often influenced by large draining veins spanning across the cortical layers, which makes it difficult to determine from which laminae the blood vessels drain the blood (Huber et al. 2021, Uludağ and Blinder, 2018).

A commonly used ex-vivo method is histology. Here, tissue samples are dissected, cut into numerous 2D thin slices, and stained one by one. This precedes imaging of the sections through high-resolution microscopes (Pichat et al., 2018). However, forming the 3D reconstruction brings forward a set of challenges. For instance, the occurrence of deformations can cause state-of-the-art image registration techniques to have inaccuracies of up to 30% (Wang et al., 2015). Fortunately, additional resources, such as medical images (i.e.: MRI) of the organ of interest, can help avoid alignment artifacts during reconstruction as they provide a reference or ‘structural ground truth’ (Pichat et al., 2018). Histology involves performing steps with great care and caution in order to minimize artifacts such as tissue distortion, uneven staining, loss of details, creation of folds or holes, etc. (Pichat et al., 2018).

Currently, an increasing number of alternative procedures are being proposed to study three-dimensional (3D) organ anatomy at high resolution. One method involves imaging whole organs of small animals or even small rodent bodies through means of tissue clearing and high-resolution microscopy imaging. Another option is to image tissues with micro-computed tomography or magnetic resonance imaging. However, cellular resolution imaging cannot be performed with these last two methods (Dodt et al., 2007, Rocha et al., 2019., d’Esposito et al.,

2015). Overall, these methods can allow for tissues to remain intact while reducing the experiment duration, required labor, and tissue processing artifacts related to histology.

Tissue clearing aims to make large/thick biological samples transparent by incubating them in a series of chemical solutions (Ariel, 2017). According to (Ertürk et al., 2012a), tissue clearing was first introduced around a century ago (Spalteholz, 1914), as was the idea of light sheet illumination explained by Dodt et al. (2007) (Siedentopf and Zsigmondy, 1903). However, this idea was not initially pursued due to the lack of scientific advancements enabling imaging deep in the tissue. Within the last decade, the concept of tissue clearing gained popularity. In fact, numerous methods are being developed to further advance the techniques. Therefore, many clearing approaches have been generated. A recently published review has divided them into 3 categories (Ueda et al., 2020). Namely, they are categorized as hydrophobic, hydrophilic, and hydrogel-based clearing methods where each method has its own set of advantages and limitations (Ueda et al., 2020).

The capability of rendering tissue transparent facilitates imaging of large tissue samples since it allows the light of microscopes to penetrate deep into the sample with minimal scattering and absorbance of light (Richardson and Lichtman, 2015). Beyond clearing methods, attention must be paid to the choice of imaging technology and to the selection of the dye or the antibody. The use of light-sheet fluorescent microscopes, also called ultra-microscopes, is one of the most commonly used methods to image large, cleared tissue samples as it allows for deep tissue imaging at high resolution while minimizing fluorescence bleaching (Dodt et al., 2007). Additionally, it is preferable if the dyes used are strong dyes: ideally, they should feature a long half-life, not be easily quenched by clearing solutions or microscope lasers, and have the capability to bind to the cells of interest.

b. Objectives

My thesis aims to first compare and optimize methods of vasculature labeling and tissue clearing. We want to identify the protocol with which we can obtain homogenous labeling of the brain's vessels. We also want our ideal protocol to give a minimal amount of physical distortion. My tissue samples should be transparent tissue such that we will have minimal light scattering and light absorption during microscopy imaging.

We hypothesize that

- Strong fluorophores will be able to withstand the clearing process without deterioration.
- For staining, allowing the dye to circulate through the vascular system (intracardiac and tail vein injection) will allow the fluorophore to stain the blood vessels homogeneously without staining the other cell bodies.
- Organic solvent-based clearing methods will have greater clearing capabilities compared to aqueous-based clearing. The organic solvent methods we focused on are 3DISCO (3-dimensional imaging of solvent-cleared organs) and iDISCO+ (immunolabeling-enabled DISCO). The aqueous-based clearing method is called CUBIC (clear, unobstructed brain imaging cocktails and computational analysis)

Following my thesis, we will conduct further studies from our lab to quantitatively analyze the organization and the density of blood vessels in the neocortex. This can make it possible to study the mechanisms underlying blood oxygenation-based and/or blood volume-based functional MRI.

c. Proposed solution and approach

As part of our optimization process,

- We evaluated the quality and homogeneity of the vessel labeling by comparing 3 different methods of staining: dye injection through the heart, dye injection through the tail vein, and incubation in the dye after brain extraction.
- We tested 3 different dyes: wheat germ agglutinin (WGA) Alexa fluor 594 and 647, Lycopersicon esculentum (Tomato) Lectin (LEL) DyLight 649, and Fluorescein isothiocyanate (FITC) dextran.
- We investigated the impact of age on the clearing by using mice of varying ages
- We investigated the impact of different tissue slab thicknesses on clearing.
- We varied the volume of dye used in mice and rats.
- We compared 3 clearing protocols: 3DISCO, iDISCO+, and CUBIC.

- We used a high-content screening Opera Phenix microscope to compare our different methods. We also used a single-point confocal microscope LSM880.

Our results show that: (1) The quality of the perfusion impacts the quality of the staining. For instance, we noticed patchy labeling in our microscopy images each time we had an indication that the brain's capillaries were likely severed during perfusion. (2) In vivo staining has the capacity to give brain-wide homogeneous labeling of the vasculature without staining other structures as well. (3) Although all clearing methods provided optically transparent tissues, organic solvents clear the brain significantly faster than CUBIC-related solutions. (4) CUBIC introduces variations in clearing duration as a function of tissue thickness and animal age. (5) Qualitatively and quantitatively, iDISCO+ provides a greater signal-to-noise ratio compared to the two other methods. (6) We found the best results from DISCO-cleared rat brain slabs that were stained through the tail vein with WGA Alexa Fluor 647.

CHAPTER II – REVIEW AND BACKGROUND

In this review, I present in-depth organic clearing protocols, the difficulties faced, and the solutions brought forward by various research groups. I also discuss aqueous-based clearing methods, especially the CUBIC-based protocols. Ultimately, all clearing methods have the same goal: to make the tissue of interest transparent. This involves a series of steps where the tissue is incubated into solutions that alter some of its compositions to let the light reach deeper tissue structures with minimal scattering (Ueda et al., 2020). In addition, this review goes over some of the fluorescent probes used for labeling vasculature and the different labeling methods.

a. Clearing with organic solutions

Hydrophobic methods make use of organic solutions. They have three major steps: dehydration, lipid extraction, and refractive index matching (Ariel, 2017). These techniques are capable of clearing thick tissue slices or whole rodent organs and bodies in just a matter of hours or days. A recurring challenge consists of their capability to preserve the fluorophore's signal. Depending on the research objectives, other difficulties may surface. For instance, organic solution clearing protocols will most of the time lead to tissue shrinkage limiting morphology preservation

(Renier et al., 2016). However, for larger size samples, shrinkage may serve as an advantage since it reduces the data size of microscopy images.

Initial methods used a combination of alcohols such as ethanol, and benzyl alcohol benzyl benzoate (BABB) (also known as Murray's clear) to clear tissues (Dodt et al., 2007). Dodt *et al.*, demonstrated the application through the reconstruction of 3D images of green fluorescent proteins (GFP) expressing neurons in mice. Subsequent studies have screened various chemicals in order to optimize the clearing process.

Instead of ethanol, Ertürk et al. proceeded with tetrahydrofuran (THF) as their dehydrating agent, since ethanol seemed to rapidly degrade GFP signals (Ertürk et al., 2012b). Additionally, combining BABB, a refractive index matching solution, with the tetrahydrofuran improved the clearing capacity of spinal cords (Ertürk et al., 2012b). Similar dye quenching effects were observed with alcohol by Schwarz *et al.* (2015) while developing their approach called FluoClearBABB. In their case, they evaluated the use of methanol, 1-propanol, and tert-butanol. They found that the fastest and highest signal loss of enhanced-GFP fluorophores occurred with methanol (Figure 1a). Meanwhile, the dehydrating solutions with higher hydrocarbon content increased fluorescence preservation. Thus, the samples incubated in tert-butanol gave the smallest loss of signal response. While the greatest response occurred with tert-butanol, they still noticed that the signal was quenched after BABB incubation. Thus, increasing the pH to 9.5 helped increase the fluorescence preservation (Figure 1b). Whereas, incubating at 30°C instead of room temperature improved the clearing (Figure 1d) and an increase in the incubation temperature reduced the signal (Figure 1c). As another example, a protocol called 3DISCO replaces the BABB refractive index matching solution with dibenzyl ether (DBE) (Ertürk et al., 2012a). DBE improved transparency (especially with myelinated tissue) and it also increased the preservation of fluorophores like GFP (Ertürk et al., 2012a and Becker, 2012).

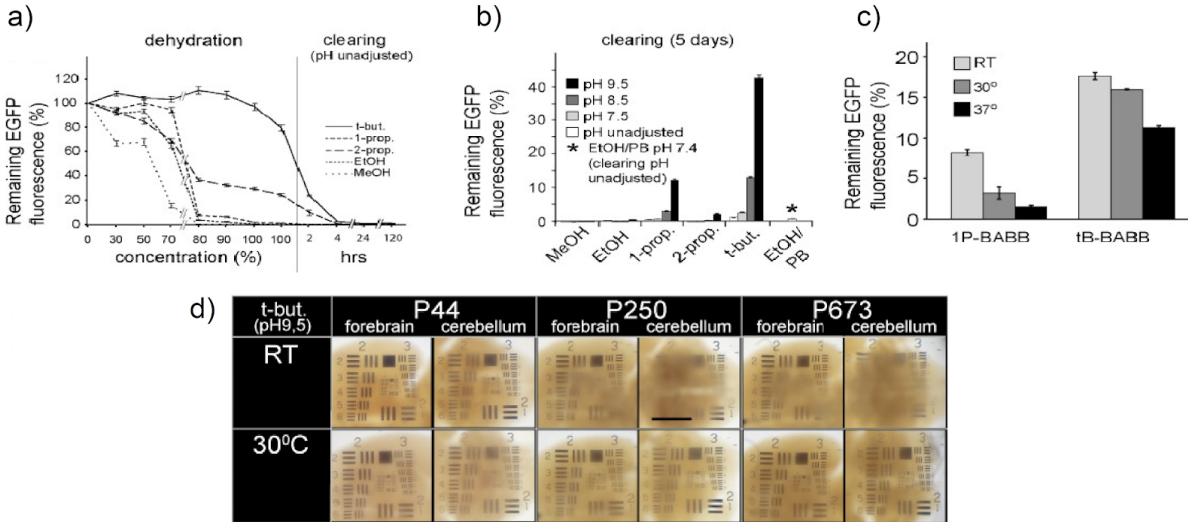


Figure 1. Evaluation of EGFP fluorescence preservation and tissue clearing results based on different incubation parameters. EGFP fluorescence signal preservation in E.coli based on a) dehydrating solutions and incubation parameters: b) pH and c) temperature. d) Changes in clearing quality based on temperature change while using tert-butanol and a pH of 9.5. Observations are made on different parts of the brain on mice of different ages (P44, P250, and P673). (Schwarz *et al.*, 2015, with permission, combination of their Figures 1 and 2).

Till now, we discussed the idea of testing various incubation solutions and parameters to improve fluorescence preservation or clearing results. Interestingly, a reason that causes fluorescent dyes to lose their strength has to do with the formation of peroxides or aldehydes which tend to form in DBE and BABB clearing solutions (Hahn *et al.*, 2019). Many commonly used refractive index matching solutions and dehydrating solutions in hydrophobic clearing protocols form these molecules. These impurities modify chemical behaviors, and they can be hazardous (Jackson *et al.*, 1970). Therefore, it is imperative to avoid the formation of such molecules which can surface when exposed to light, air or water (Hahn *et al.*, 2019, Jackson *et al.*, 1970). More recent protocols have suggested ways to overcome the damage that these molecules can form. We can, for one, embed tissues into resin which allows for long term storage and repetitive imaging since it seems to prevent the access of the peroxides to the sample (Becker *et al.*, 2014). The use of resin can also minimize mechanical damage (Becker *et al.*, 2014). Another option is to use peroxide scavenging solutions or stable solutions that do not form peroxidase. uDISCO (ultimate-DISCO) protocol uses a combination of α -tocopherol antioxidant (vitamin E) and diphenyl ether along with the BABB mixture (Pan *et al.*, 2016). Diphenyl ether, unlike the other 2 refractive index matching solutions, does not have reactive benzylic C-H and C-O bonds which decreases the

probability of the solution to form radicals or other oxidative reactions (Pan et al, 2016). Vitamin E, on the other hand, helps scavenge peroxides (Pan al., 2016, supplement). Thus, using them along with BABB helps reduce fluorescence quenching which allows fluorescence preservation for at least a year. In addition to the changes in the refractive index matching solution, uDISCO protocol utilizes tert-butanol instead of THF. Tert-Butanol is less reactive and more stable to oxidation (Pan al., 2016, supplement). Pan et al.'s uDISCO work gives a brief example of vasculature imaging of the central nervous system of rats using Texas red dextran (Pan et al., 2016). Another study focused on eliminating peroxides and/or aldehydes was performed by Hahn *et al.* (2019) who brought forward the idea of sDISCO (stabilized DISCO). They screen a variety of antioxidants in order to stabilize commonly used dyes for neuronal imaging: EGFP/tdTomato/YFP. From their list of antioxidants, propyl gallate has the greatest peroxide elimination rate compared to other antioxidants including butylhydroxytoluol, butylhydroxyanisol or alpha-tocopherol. It was also found to be a more active hydroxyl radical scavenger compared to alpha-tocopherol or mannitol (Haseloff, 1990). In addition, the use of propyl gallate still allows high-resolution imaging of at least 2.19 um resolution (Hahn et al., 2019). Figure 2 demonstrates the capability of sDISCO to diminish fluorescence quenching. Furthermore, propyl gallate can also keep peroxides from surfacing and preserve fluorescence for solutions stored over a year at 4°C. On a final note, when the solutions are already polluted with fluorescent quenching molecules, it is best to purify them before adding the antioxidant since adding antioxidants without purification will only remove the peroxides while the aldehydes will remain. Aldehydes, which appear in the presence of peroxides, also cause quenching.

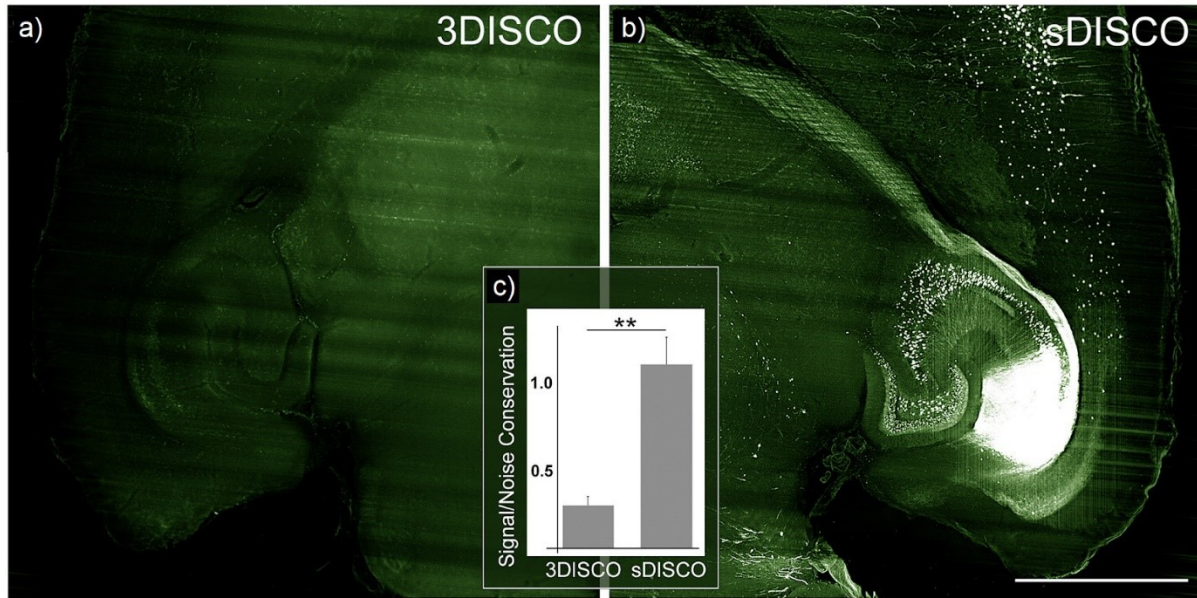


Figure 2. Comparison of EGFP fluorescence preservation between sDISCO and 3DISCO. Demonstration of fluorescence preservation 1 month after staining of mouse brain samples cleared with (a) 3DISCO method and (b) sDISCO method. These are examples of neuronal cells with EGFP fluorescence. (c) The signal-to-noise ratio drops 24% 1 month after clearing with 3DISCO and it stays constant with sDISCO. (Hahn et al., 2019, with permission)

Alternate protocols focused on modifying the incubation conditions. Some examples of such protocols include FDISCO (DISCO with superior fluorescence-preserving capability) and a-uDISCO (alternate-uDISCO) (Qi et al., 2019, Li et al., 2018). FDISCO follows 3DISCO protocol closely. It suggests incubating the tissues in alkaline/4°C condition for THF and at 4°C for DBE. The pH is increased to 9 with triethylamine. With this, they found the fluorescence signal appeared to be stronger with many dyes including the DyLight 649 Lycopersicon esculentum lectin (LEL-DyLight649) used for vascular labeling as well as some of the commonly used dyes such as EGFP, tdTomato, and Cy5 (Figure 3). Qi *et al.* state that 3DISCO clearing procedure generally decreases the fluorophores' signal and that their method had the capability of increasing the signal preservation by over 50%. Figure 3e shows the results of their whole brain vasculature imaging with DyLight 649. They also use Alexa Fluor 647 anti-mouse CD31 antibody for vasculature labeling which did not demonstrate any superior performance. Additionally, FDISCO tends to give a similar level of clearing in the same time period and a similar amount of tissue shrinkage as 3DISCO (Qi et al., 2019). a-uDISCO, on the other hand, aimed to improve uDISCO (Li et al., 2018). They used alkaline incubation conditions. The most effective pH values, without affecting transparency, were found to be 9-9.5 (increased with triethylamine). Li *et al.* state that their method

is ideal for samples that have little fluorescent protein expression, for archiving, or for frequent re-imaging of rare samples (Li et al., 2018). In sum, these papers suggest alkaline incubation conditions to help with longer storage (Qi et al., 2019, Li et al., 2018, Schwarz et al., 2015), and storing samples at 4°C to help with sample revisiting in the long run (Schwarz et al., 2015). It is important to note that incubating the samples at lower temperature may not work for some organic solutions such as tert-butanol which has a melting point of 25-25.5°C (Snyder, 1992). Qi *et al.* (2019) state that 4°C incubations do not impact clearing time. However, Schwarz *et al.* (2015) suggest that clearing at temperatures of 30°C facilitates clearing. Perhaps, the differences in these results are due to the varying selection of organic solutions between the two experiments.

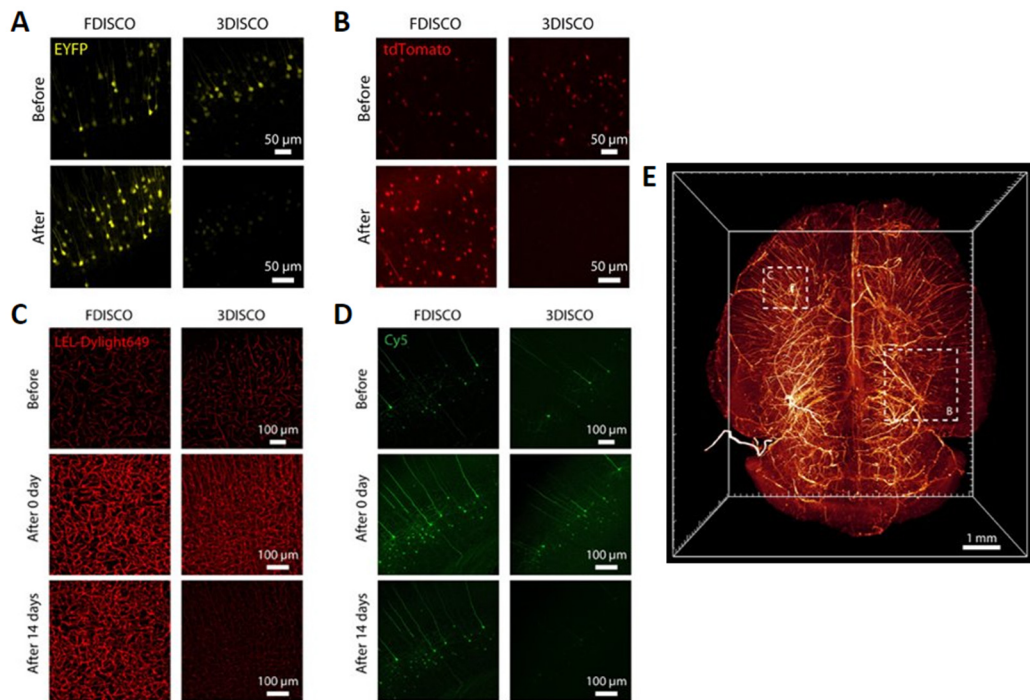


Figure 3. Fluorescence imaging of different dyes with 3DISCO and FDISCO clearing. Fluorescence imaging of 1-mm-thick brain slices of (a) EYFP (Thy1-YFP-H mouse), and (b) tdTomato (Sst-IRES-Cre::Ai14 mouse) before and after FDISCO clearing compared with 3DISCO clearing. Fluorescence imaging of (c) LEL-Dylight 649, and (d), antibody conjugated to Cy5 before clearing (row 1) and 0 days after clearing (row 2) and 14 days after clearing (row 3) with FDISCO and 3DISCO clearing protocols. e) A depiction of brain vascular labeling and FDISCO clearing (injection of CD31-A647 antibody) (Qi et al., 2019, with permission).

Efforts have also been devoted to whole-body clearing. Cai et al. (2019) applied vDISCO where the “v” stands for (variable domain of heavy-chain antibodies). They used nanobodies that can produce rigorous whole-body immunolabeling due to their small molecular weight (Cai et al.,

2019). These nanobodies also improve the fluorescence signal during imaging. Using dyes with a peak emission in the far-red regions can help overcome autofluorescence issues (Cai et al., 2019). Another method is the polyethylene glycol (PEG)-associated solvent system (PEGASOS) which clears whole bodies including hard tissues while preserving fluorescence (Jing et al., 2018). PEG plays a role in protecting endogenous fluorescence (Jing et al., 2018). Beyond the usual 3 steps of dehydration, delipidation, and matching refractive index, both methods (vDISCO and PEGASOS) include additional tissue processing steps. They perform decolorization to reduce background noise from residual blood and they do bone decalcification (Cai et al., 2019, Jing et al., 2018). This allows for detailed subcellular images even through bones.

These organic clearing methods shrink the tissue samples, which can be advantageous for whole organ or body imaging since they will fit under the microscope and provide a smaller data set. When solely looking at an organ, these hydrophobic methods provide an isotropic shrinkage (Pan et al., 2016). However, Jing *et al.* mention that although soft tissue shrinks up to 30-40%, there is no shrinkage in the hard tissues (Jing et al., 2018). Possible distortions during shrinkage can be minimized when the water removal is slow. In other words, it is best if dehydration occurs in a couple of steps with a gradual increase of the dehydrating solution's concentration (Ertürk et al., 2012a).

Renier *et al.* (2014) combine whole-mount immunolabeling methods with 3DISCO and name their protocol iDISCO. They state that with their whole-mount immunolabeling methods, it is no longer essential to preserve endogenous fluorescence proteins (Renier et al., 2014). They achieve a deep diffusion distance with the antibodies even with adult mouse brains. However, unlike clearing techniques from the hydrophilic category, only one round of labeling can be performed since clearing procedures with organic solutions cannot be reversed (Seo et al., 2016). They later changed the THF dehydrating/delipidating solution to methanol and dichloromethane and called it iDISCO+. With this, tissue shrinkage is minimized to 11% (Renier et al., 2016). The clearing performance allowed them to collect consistent signals from c-Fos+ cells up to 6 mm deep into the tissue. iDISCO+ provided a similar clearing performance compared to 3DISCO and iDISCO. Additionally, iDISCO+ gives slightly softer tissues which can allow for further tissue processing (Vigouroux et al., 2017).

For clearing with organic solutions, many studies have been performed to optimize the results. These steps involved screening for chemical compounds that can improve tissue clearing results in terms of transparency, minimizing tissue distortions, and improving fluorescence signal retention.

b. Clearing with aqueous solvents

As in the case of organic solvent-based methods, aqueous-based clearing methods aim to homogenize the refractive index of the elements composing the organ in question. Aqueous cleaning can be categorized into 3 classes of methods: 1) passive immersion in only the refractive index solution, 2) removal of lipids, which reduces the general RI of the tissue, or 3) a combination of both methods with either passive or active measures (Richardson and Lichtman, 2015).

An example of passive immersion is the FRUIT protocol. Here, Hou *et al.* incubate the tissues in increasing concentration of fructose dissolved in distilled water, α -thioglycerol, and urea (Hou et al., 2015). This method does not result in highly transparent tissue. However, it is very cost-efficient. Furthermore, it can be combined with numerous dyes including lipophilic dyes since the process excludes the delipidation step. To be able to keep these advantages at hand, subsequent studies adjusted the protocol in order to give more transparent samples. Hildebrand *et al.* (2020) brought forth hFRUIT. They added non-reducing sugar sucrose to the fructose solution and increased the 1-thioglycerol's concentration (Hildebrand et al., 2020). This provided an enhanced clearing of certain organs relative to the clearing accomplished by FRUIT. Although they did not experiment in blood vessels, they did DiI labeling of myelin from tissues of different species and found the samples could get permeable enough such that dye can be observed 1500 μm into the sample. Another simple immersion system consists of Clear^T or its upgraded version Clear^{T2}. As it does not use detergents or solvents, Clear^{T2} has the capability to preserve lipophilic dyes, fluorescent tracers, immunohistochemical fluorophores, and fluorescent-protein dyes. Kuwakima et al. claim that it takes only 2 days to clear a whole postnatal mouse brain (Kuwajima et al., 2013).

Other protocols with similar concepts include SeeBest (Fumoto, 2020) and MACS (Zhu et al., 2020). Both methods also preserve the lipid ultrastructure. In addition, they demonstrate blood vessel staining and imaging. SeeBest is a pH adjustable tissue clearing solution which is important for dyes that are pH-dependent. Fumoto *et al.* (2020) stain the vasculature using lipophilic

carbocyanine dyes (DiI). They explain that pH alteration can maximize the fluorescence intensity and diminish dye leakage during clearing which may be due to the maintenance of the cell's barrier functions. Their use of polyethylenimine and urea gives enhanced optical clearing. They compared their methods with other protocols such as ScaleA2, CUBIC, and clear^T. They state that SeeBest has comparable results to CUBIC when clearing liver and kidney. However, CUBIC outperforms with brain tissue clearing results. Urea based clearing causes hyperhydration. Thus, dense protein fibers dissolve, which loosens up the solid tissue frameworks (Tainaka et al., 2016). With this, urea leads to RI matching. However, urea has a low RI value and a slow hyperhydration speed. Therefore, Zhu *et al.* (2020) replaced urea with m-xylylenediamine (MXDA) to make MXDA-based Aqueous Clearing System (MACS). They report that MXDA gives good hyperhydration and a high RI value. They show an example of 3D rendering of mouse brain vasculature stained with DiI Figure 4.

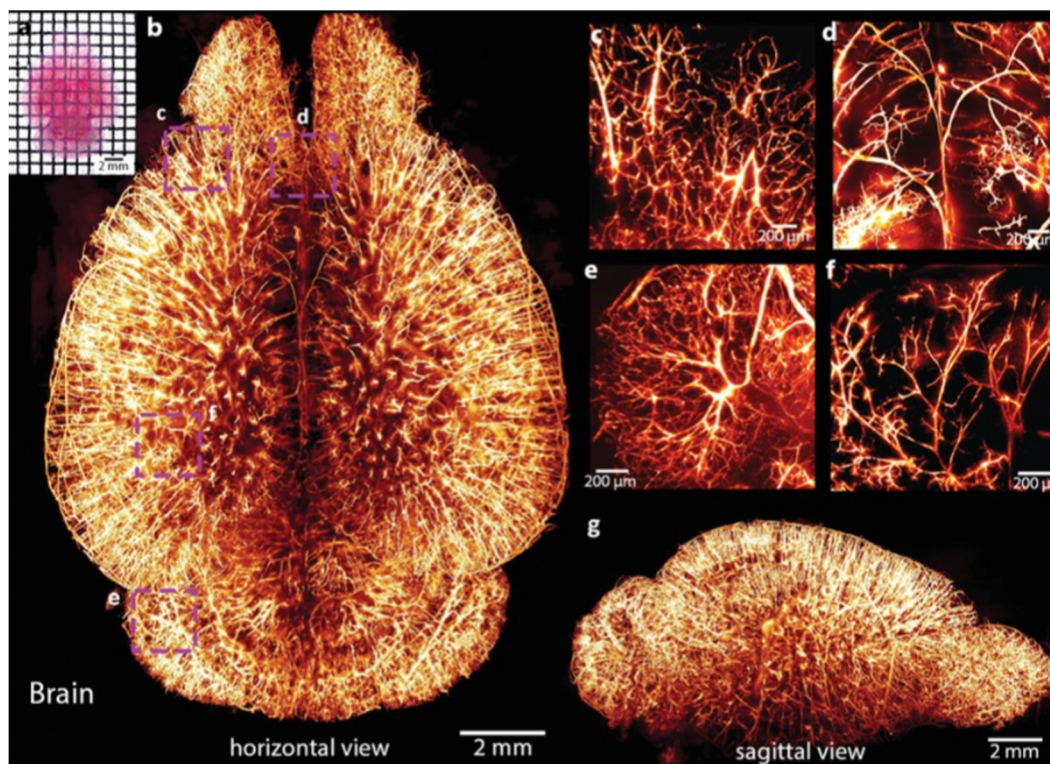


Figure 4. Brain clearing and vessel imaging with MACS. Depiction of a) a dorsal view of a cleared mouse brain and b) of its DiI-stained vasculature. c) - f) zoomed-in views of different regions of the mouse brain from panel a. g) A sagittal view of the mouse brain's vasculature. From (Zhu et al., 2020, with permission).

With most of these methods, the clearing capacity is still limited since light scattering lipid substances remain in the tissue. The aqueous method, CUBIC, is an example of a clearing method

that removes lipids in addition to homogenizing refractive indices. To develop the CUBIC protocol, Susaki *et al.* built on a previous method called *Scale* (Susaki *et al.*, 2015). Susaki *et al.* screened 40 *Scale*-related reagents and came up with *ScaleCUBIC-1* (reagent 1) and *ScaleCUBIC-2* (reagent 2). Both reagents contain urea. With this, they claimed that it takes up to 2 weeks to clear a whole mouse brain (8 weeks old). Figure 5a shows their results (Susaki *et al.*, 2015). Other researchers such as Xu *et al.* based their work on this CUBIC protocol. Xu *et al.* labeled at many structural components in the brain using CUBIC among which is the cerebral vasculature of a 6-week-old mouse (Xu *et al.*, 2019). They used dextran-FITC as their marker (2000kDa, sigma FD2000S). They report that they can reach a maximum imaging depth of 1.2 mm after clearing brain blocks. However, already by 328 μm into the sample, there is a great reduction in the detection of samples (Figure 5b, c).

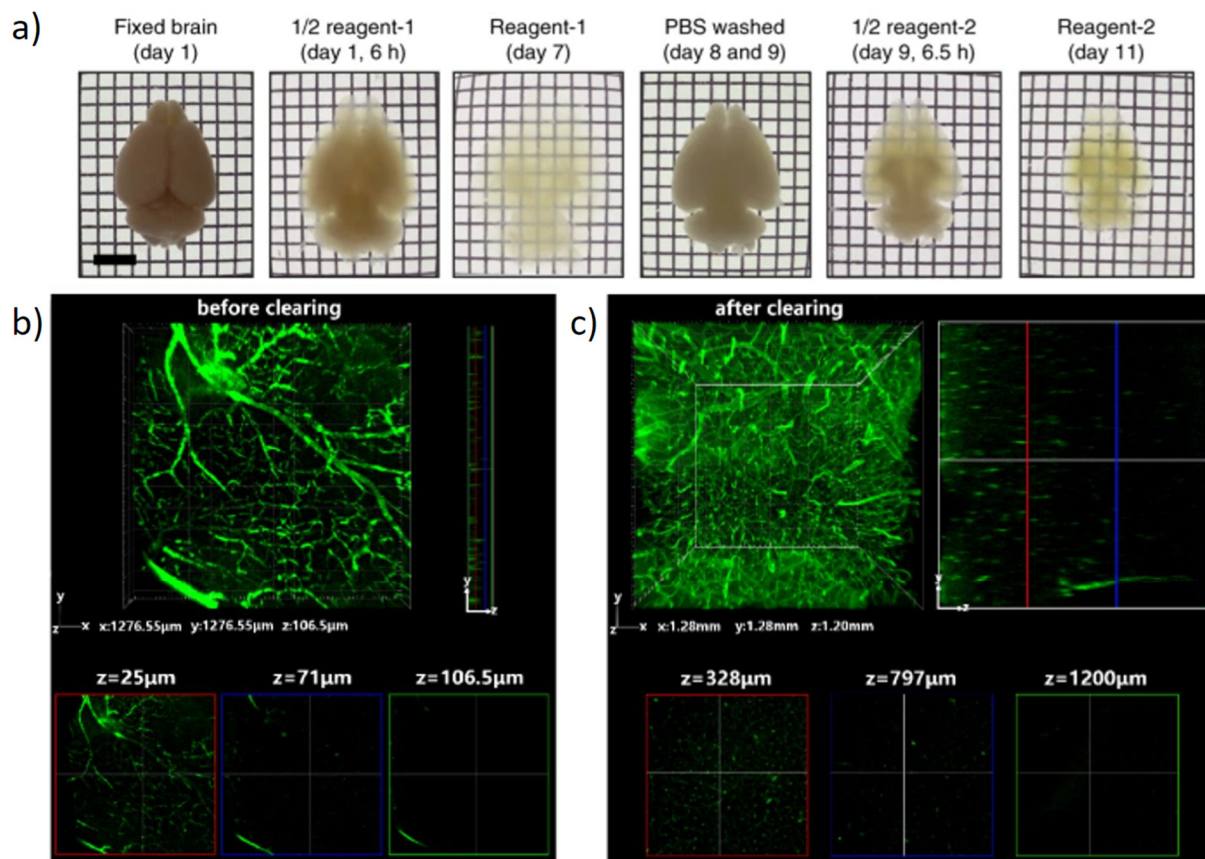


Figure 5. CUBIC clearing progress and imaging of vessels. Demonstration of CUBIC clearing timeline presented by Susaki *et al.* (2015, with permission). Mouse brain blood vessel imaging capabilities at different depths performed b) before and c) after CUBIC clearing (Xu *et al.*, 2019, with permission).

Many other studies also make use of Susaki's CUBIC protocol. Peeters *et al.* (2017) stain 0.35 mm thick rat liver tissue section with IHC. They did this on both non-cleared and cleared samples and found that the imaging depth increased by 3 folds: 50-60 μm and 150-200 μm deep imaging for non-cleared and cleared samples, respectively (Figure 6). Also using staining by immersion, ovarian (Tong *et al.*, 2020) and heart (Yokoyama *et al.*, 2017) vasculature studies have also been conducted. Interestingly, Nehrhoff *et al.* (2017) stained the heart vasculature of an adult mouse with lectin. They do so by *in vivo* administration into the tail vein of mice, followed by an additional round of staining during the terminal perfusion process.

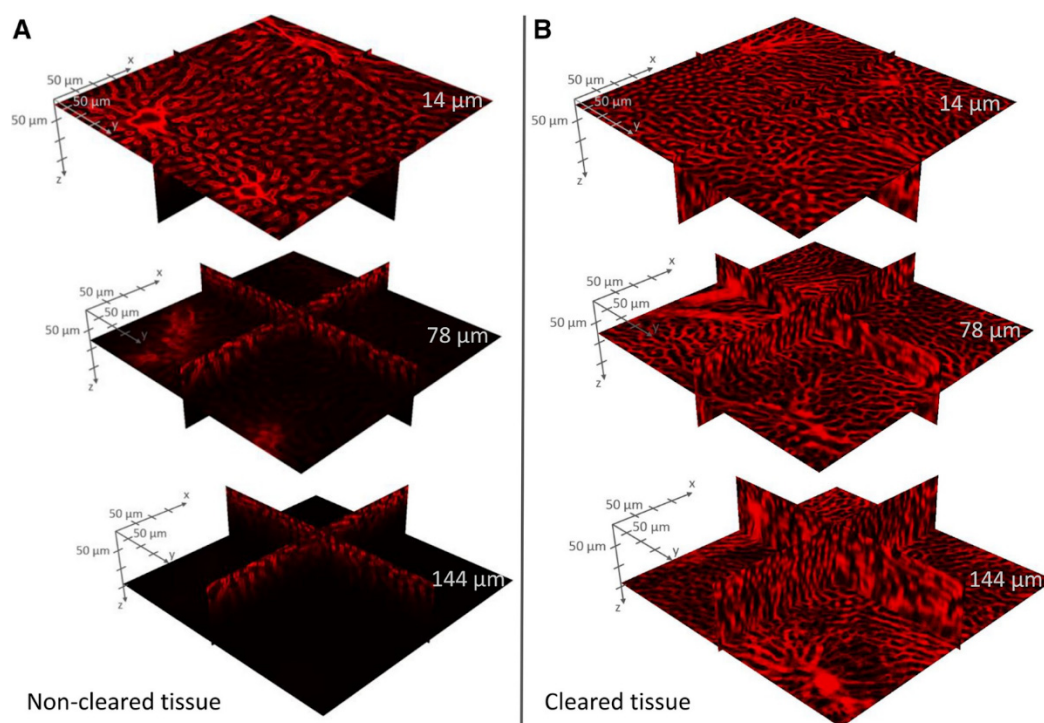


Figure 6. Demonstration of rat liver vasculature intensity obtained with confocal microscope at different imaging depths. Demonstration of rat liver vasculature intensity obtained with confocal microscope at different imaging depths ($z = 14, 78,$ and $144 \mu\text{m}$) of a) non-cleared and b) CUBIC cleared tissue samples (Peeters *et al.*, 2017, with permission)

Tainaka *et al.* (2018) screened over 1600 chemicals and performed a series of tests on potentially useful chemicals that could be used for the CUBIC protocol initially developed by Susaki *et al.* (2015). As a result, Tainaka *et al.* (2018) made a series of CUBIC reagents where each of them improves clearing based on the organ of interest. The list of solvents and the protocol timelines are shown in Figure 7. They find that ideal reagents for delipidation are “salt-free amine with high octanol/water partition-coefficient” (Tainaka *et al.* 2018). For delipidation, they suggest

CUBIC-L. It consists of N-butyldiethanolamine and Triton X-100 in distilled water. For RI matching, Tainaka *et al.* (2018) recommend the use of aromatic amide which have low light absorbance, and high-water solubility and RI value. Thus, they bring forth CUBIC-R. It contains nicotinamide (or N-methylnicotinamide) and antipyrine in distilled water. The pH can also be optionally adjusted with N-butyldiethanolamine.

a)

Name	Role	Components and concentrations
CUBIC-P	Delipidation and rapid decolorization	5 wt% 1-methylimidazole, 10 wt% N-butylidethanolamine (CU#0414), 5 wt% Triton X-100
CUBIC-L	Delipidation and decolorization	10 wt% N-butylidethanolamine (CU#0414), 10 wt% Triton X-100
CUBIC-HL	Rapid delipidation and rapid decolorization	10 wt% 1,3-bis(aminomethyl)cyclohexane (CU#0070), 10 wt% sodium dodecylbenzenesulfonate (CU#0631), pH 12.0 adjusted by p-toluenesulfonic acid
CUBIC-B	Decalcification	10 wt% EDTA, 15 wt% imidazole (CU#1352)
CUBIC-R	RI matching, more cost effective than CUBIC-RA	45 wt% antipyrine (CU#0640), 30 wt% nicotinamide (CU#0855), optionally pH 8-9 adjusted by N-butylidethanolamine (CU#0414)
CUBIC-RA	RI matching, kinder to FP than CUBIC-R	45 wt% antipyrine (CU#0640), 30 wt% N-methylnicotinamide (CU#1283), optionally pH 8-9 adjusted by N-butylidethanolamine (CU#0414)

b)

Protocol Name	Purpose	Protocol
CUBIC protocol I	Mouse organ & body clearing	<p>3 - 7 days, 37°C 2 days 5 - 7 days, 37°C 2 - 4 days, 37°C 2 days</p>
CUBIC protocol II	Tissues including bone clearing	<p>3 - 7 days, 37°C 2 days 7 - 14 days, 37°C or 45°C 2 days 7 - 14 days, 45°C 2 days</p>
CUBIC protocol III	Aggressive organ clearing	<p>7 - 14 days, 37°C or 45°C 2 days 7 - 14 days, 45°C 2 days</p>
CUBIC protocol IV	Human brain clearing	<p>7 - 14 days, 45°C 2 days</p>

Figure 7. List of CUBIC cocktails and protocols. a) A list of CUBIC cocktails with their role and chemical composition. b. A list of CUBIC protocols with their purpose and timeline. (Tainaka et al., 2018, with permission from a portion of their Figure 4)

An additional tissue transformation protocol is tissue transformation clearing. These methods transform the organs of interest into a nanoporous hydrogel-tissue hybrid (Du, 2018). As drawbacks, these methods can be costly, time-consuming (especially with passive clearing options), and complex (especially when electrophoresis is involved) (Du, 2018). Fortunately, they can give highly transparent tissue with minimal distortions and preserve molecular information (Du, 2018). Due to hybridization, chemicals get incorporated into the hydrogel mesh. Therefore, once lipids are removed, the tissues can preserve their molecular or cellular information (Chung, et al. 2013). The different varieties include but are not limited to PACT, mPACT, PARS, CLARITY2, ACT-PRESTO, ETC, and passive clarity (Du, 2018). There is also a method called SWITCH which allows 20 rounds of relabeling and can be interesting for those practicing immunohistochemistry (Murray, et al. 2015).

c. Vasculature Labeling

Besides clearing, we also need to appropriately label our structures of interest. Most methods use modified genetic expressions or immunohistochemistry to study neurons. However, we are interested in vasculature labeling. When labeling vasculatures, important aspects to consider include dye selection and the labeling method.

i. *Dye Selection*

The dye selection will vary based on the clearing method pursued. For instance, lipophilic dye will not work with organic clearing methods and certain aqueous-based methods since the lipid structures in the tissues are lost. We also saw that the use of endogenous fluorophores such as GFP, YFP or tdTomato tend to be unstable in organic clearing solutions. Hence, many researchers brought forward different modifications in tissue clearing protocols to optimize fluorophore preservation. Besides tissue clearing, we also need to select the appropriate dyes. Agents involved in staining microvasculature include dextran, lectins, antibodies, and quantum dots (Wang et al., 2019). Besides endogenous labeling, dextran and lectin conjugated dyes are some of the most common options used.

Dextran is a biopolymer. It is mainly used to test permeability. However, it has also been used amongst clearing protocols since these probes can be conjugated to a wide variety of fluorophores. Among the possible options, we have Texas red dextran which has been used with uDISCO (Pan et al., 2016). Another fluorophore-conjugated dextran, fluorescein isothiocyanate (FITC) dextran has been used for embryo vasculature visualization in combination with a protocol involving methanol/BABB clearing (Bryson et al., 2011). Additionally, it has been combined with non-hydrophobic clearing methods such as X-CLARITY for a human placenta study (Carrillo et al. 2018), and CUBIC and SeeDB for cerebral vasculature imaging (Xu et al., 2019, Steinman et al., 2017). A disadvantage of FITC is that it is a dye with excitation and emission in the green spectrum. At this spectrum, we observe high autofluorescence in the mouse brain (Richardson and Lichtman, 2015, and Ariel, 2017). The background autofluorescence prevails even after tissue clearing (Richardson and Lichtman, 2015). In fact, some studies even make use of this autofluorescence to utilize it as a counterstain and a reference brain (Ariel, 2017).

If we use dyes in the blue-green spectrum, we can find autofluorescence in large biological samples. The autofluorescence can be minimized by using dyes that are in the red or far-red region (Renier et al., 2014). Regardless, work has been conducted to develop fluorescent dyes in the blue range since many structures such as immune cells and pathogens are labeled with dyes from the red and green spectrum. This can be especially useful for multi-labeling. Lee *et al.* brought forth a bright blue fluorescent dextran (HCD-70K1) which can label the blood vessel walls while, simultaneously, diminishing blue fluorophore quenching (Lee et al., 2019). Additionally, the low cell permeability of HCD-70K1 permits its retention within the vasculature. With it, they managed to collect deep in vivo images with two-photon microscopy.

Tomato (*Lycopersicon esculentum*) lectin and wheat germ agglutinin conjugated to dyes are also used for vasculature visualization (Robertson et al. 2015, Qi et al., 2019, and Todorov et al., 2020). These proteins bind to glycoproteins of endothelial cells (Robertson et al. 2015), more specifically to N-acetyl-glucosamine (Kataoka, et al. 2016, Nachbar et al. 1980). Wheat germ agglutinin can also bind to sialic acid. These lectins can be combined with dyes such as DyLight or Alexa Fluor. For one, Alexa Fluor is shown to be a very stable and bright dye compared to dyes of similar spectral analogue such as FITC or Texas Red, as discussed by Panchuk–Voloshina *et al.* and Mahmoudian *et al.* (Panchuk–Voloshina et al. 1999 and Mahmoudian et al. 2011). Similar

to Alexa dyes, DyLight is also a bright and photostable probe (Sarkar, et al., 2010). We can also consider Evans blue dyes. They have a high affinity for serum albumin (Todorov et al., 2020). While it has the possibility of binding to capillaries, Evans blue mainly stains larger vessels (Todorov et al., 2020, Yao et al., 2009).

Another option is vessel painting with DiI (Salehi et al., 2019). DiI has been used to label vascular lumen as they get integrated into the lipid membrane (Salehi et al., 2019). Thus, we cannot combine DiI with organic solvent clearing protocols or with protocols using detergents since these methods will disintegrate lipids (Salehi 2019, Hughes 2014). The use of DiI involves some additional steps as it needs to be heated when dissolved in PBS (phosphate-buffered saline) to avoid precipitations (Salehi et al 2019). Additionally, it seems to label the arterioles/arteries better than venules/veins (Hughes et al., 2014).

There is also the use of fluorescent gels as performed by Steinman *et al* (2017). They used hydrophilic tissue clearing techniques to image deep into the tissue (fructose-cleared). Through comparisons between in vivo and ex vivo imaging. They clear the brain while keeping it inside the skull. They demonstrated that ex vivo cleared tissue images provide deeper imaging in the brain. Shadowing artifacts are eliminated with ex vivo imaging (Steinman et al, 2017). Shadowing artifacts cause the small structures that are below the cortical surface (i.e.: under larger vessels) to be hidden. The depth to which they could image was limited to 2 mm due to the two-photon fluorescent microscope. Di Giovanna, et al. (2018) compare the use of a gel albumin-FITC that fills up the blood vessels to a lectin (lectin-FITC) that stains vasculature walls. For clearing, they use CLARITY. They show that blood vessel lumen staining gives a higher signal-to-noise ratio relative to vessel wall staining. They claim that the gel is retained in the hydrogel matrix during lipid removal since they contain proteins. Moreover, albumin does not cross the blood vessel walls due to its high molecular weight. Therefore, the fluorophores will also remain.

Combining light-sheet microscopy with cleared tissues labeled by dyes in the near-infrared region permits deep imaging with a reduced scattering of light (Wang et al., 2019). Wang et al., show this using PEGylated lead sulfide (PbS)/cadmium sulfide (CdS) core/shell quantum dots (CSQD). The CdS acts as a shell to protect the PbS core from oxidation (Zhang et al., 2018). The combination of quantum dots with near-infra-red imaging can eliminate autofluorescence and

minimize light scattering and absorption (Li et al., 2014, Liu et al., 2020). Furthermore, PEGylated CSQD has a blood circulation half-life of 7 hours (Zhang et al., 2018).

ii. *Labelling methods*

Typically, when it comes to neuronal labeling, most methods either use immunohistochemistry or gene expression. For vasculature labeling, the most common approach is the direct injection of the dyes into the vascular system. Some methods incorporate this step during open-chest perfusion (intracardiac injection) (Li et al., 2008). Others inject a small amount of dye in the caudal or femoral vein and let the dye circulate throughout the body before beginning perfusion (Qi et al., 2019 & Pan et al., 2016).

Open chest perfusion alone has its own set of variables. For one, we need to consider the pressure delivery of the solutions. Salehi et al 2019, compared two methods to study the blood vessels of mice and rat cerebellum. In their first method, they used a nitrogen tank to deliver PBS and PFA under constant pressure and they used a syringe pump to deliver their fluorophore (DiI) dissolved in 50 ml dextrose/PBS with a constant flow rate. For their second method, they did a direct intracardiac injection of the dye (250 μ l in mice, 500 μ l in rat) into the left ventricle of the beating heart before performing the PBS/PFA perfusion. Also, in this case, a peristaltic pump was used instead of the nitrogen tank. With the first method, about 75% of adult mice had heterogenous labeling where not all capillaries were stained. Method 2 demonstrated a higher performance. It is important to note that their evaluations were performed with uncleared tissues and deeper structures evaluations were based on cut sections.

On a similar note, a different study focuses on evaluating different methods of intravenously injecting *Lycopersicon esculentum* agglutinin tomato lectin fluorescent dye to find the most efficient labeling method (Robertson et al., 2015). The different labeling methods involved include injecting the dye in either the jugular vein, the tail vein, or the left ventricle. For the delivery through the left ventricle, the dye was either injected alone (before perfusion) or simultaneously with PBS. They examined the labeling quality with bright field microscopy and electron microscopy. The group of mice with tail vein injection underwent a waiting time of 3 min to 2 days before terminal perfusion. They notice that the labeling decreases with time. In fact, the signal nearly disappears 12 hours post-injection. Figure 8a, shows a fluorescence image of a 50 μ m slice of the forebrain of a mouse with a post-injection survival time of 3-5 minutes. Here, we

see that many small vessels with the possibility of capillaries and a few larger vessels were labeled. When evaluating the labeling of the liver of different dye concentrations the greatest labeling intensity is observed with 100 ug lectin injection, higher than the labeling with 25 ug and 50 ug (figure 8b-d). Figure 5e-h demonstrates the labeling of liver based on the different methods using 100 ug of the lectin. A greater number of vessels were labeled for both the direct tail vein and intracardiac injections compared to the method where the dye and PBS are simultaneously inserted into the heart. However, the labeling intensity was more homogeneous with tail vein rather than direct intracardiac entry. Their results also showed greater variability for labeling homogeneity with the intracardiac injection through the different organs tested.

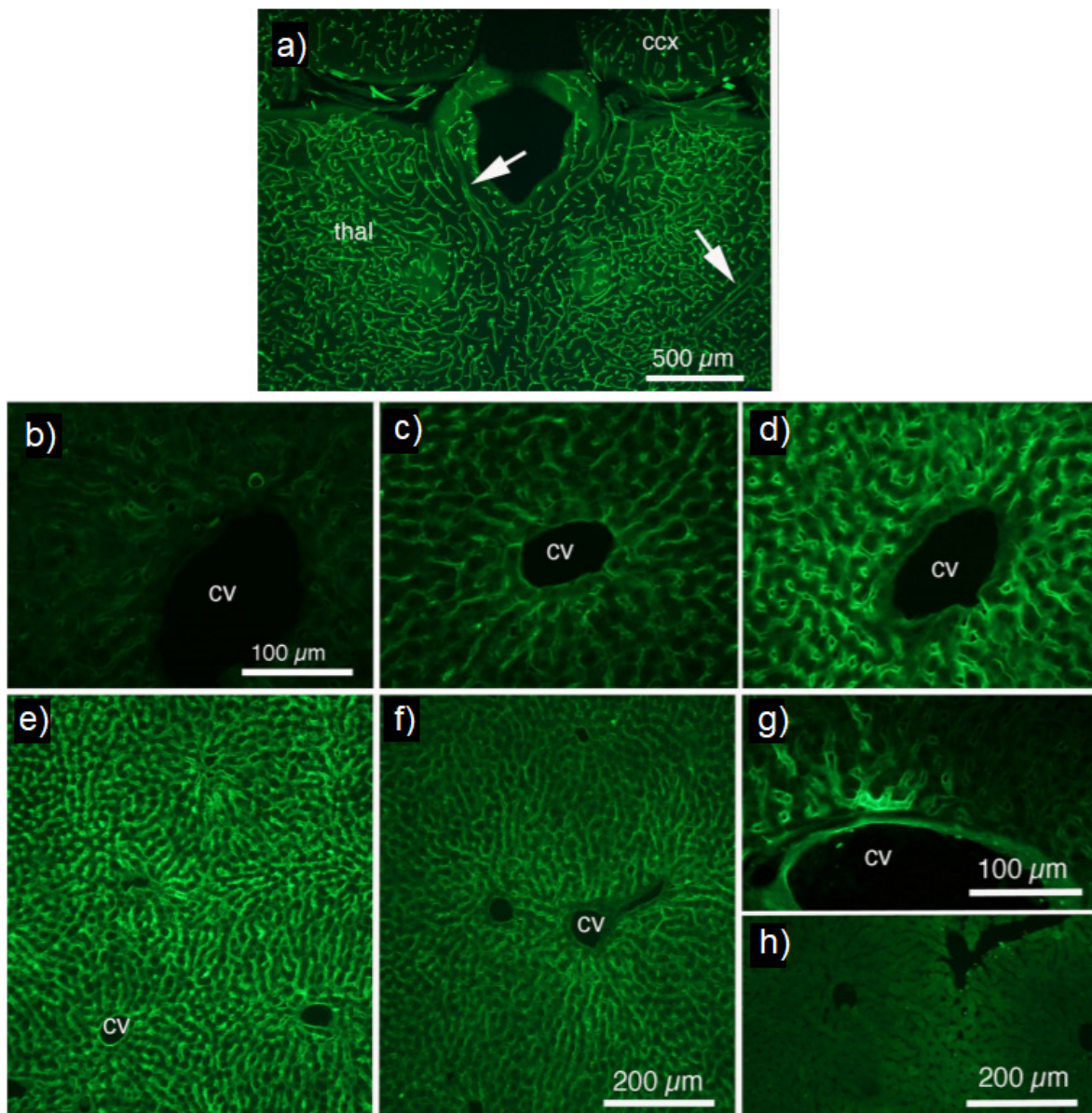


Figure 8. Lectin labeling of brain and liver vasculature. (a) 50 μ m vibratome section image of dorsal diencephalon of the brain with arrows pointing to larger vessels. Vessels labeled with 100 μ g/100 μ l tomato lectin by tail vein injection with 3-5 min post-injection survival time. (b-h) Kidney liver tissue section with vasculature labeled with tomato lectin DyLight. (b-d) test intravenous injection of different quantities of the dye (b) 25 μ g, (c) 50 μ g, and (d) 100 μ g. Labeling with 100 μ g of dye by (e) tail vein injection and 5 min survival and (f) intracardiac injection and 1 min survival. (g) Examples of spotty labeling when performing intracardiac injection and (h) example of the absence of labeling when performing dye-PBS perfusion. *ccx*: cingulate cortex, *thal*: thalamus, *cv*: central venule. (Robertson et al., 2015).

The dye for labeling vasculature needs to circulate through the vessels to get attached to the lumen but also, it needs to remain within the vessels without leakage. Therefore, besides considering the dye selection, we also need to be careful not to rupture the vessels since perfusion flow rate and the form of PFA can cause damage. Such observations are made by Cahill *et al.* (2012). Some perfusion methods cause vessel damage observed by MRI scans as hyperintense rims. Cahill *et al.* found it best to use liquid PFA over laboratory dissolved powdered PFA as the latter may cause blockage followed by vessel rupture due to buildup of pressure. Nonetheless, when the powdered PFA is introduced at low perfusion rates (1 ml/min), the occurrence of perfusion artifacts reduces to 50%. Regardless of the perfusion rate (7 ml/min or 1 ml/min), no artifacts were observed with the liquid PFA. An additional factor to consider is air bubbles. Their presence can form emboli, which impacts the quality of the perfusion (Saltman, *et al.* 2017). It could also risk losing the animal in the process if a dye with air bubbles is injected into the vasculature (Wälchli, *et al.*, 2015).

CHAPTER III – DEVELOPMENT OF METHODOLOGY

In this section, we will present the approaches we took to label the vessels, clear the tissue, image the sample, and visualize it. First, we will give a general overview of our approaches. Next, we will describe the methodology of labeling and perfusion followed by the clearing protocols. Then, we will explain the different setups used to make the comparisons within the experimental designs. Finally, we will present the microscopy methods used and the methods to visualize the samples.

a. Overview

We tested different protocols to stain the cerebral blood vessels of rodents, clear the tissue samples, and image them. In terms of vasculature labeling, we have tested *in vivo* staining as well

as staining by immersion. We have used 3 different dyes including Fluorescein Isothiocyanate-Dextran, wheat germ agglutinin Alexa fluor, and Lycopersicon esculentum (Tomato) lectin DyLight. For clearing, we mainly focused on 3 different methods: CUBIC (clear, unobstructed brain/body imaging cocktails and computational analysis) (Tainaka et al., 2018 and Matsumoto et al., 2019), a modified 3DISCO method (three-dimensional imaging of solvent-cleared organs) (Todorov et al., 2020), and iDISCO+ (Renier et al., 2016). We also varied the volume of Alexa Fluor dye injected in mice and rats. Additionally, we varied the mice's age while keeping a constant fluorophore volume. For comparison between the protocols, we mainly used 2-3 mm thick slabs and imaged the samples with an Opera Phenix microscope. The latter is a spinning disk confocal microscope that allows the screening of multiple tissue samples in one imaging session with the use of multi-well plates. For higher resolution imaging, we used single-point confocal microscopes.

This study was conducted on wild-type mice and rats aged between 2 and 7 months. The rodents were housed at the animal care facility at the Montreal Neurological Institute (MNI). All animal protocols were approved by the Animal Care Committee of the MNI. The mice and rats were housed at $22 \pm 2^\circ\text{C}$ with a 12 h light/12 h dark cycle. The animals were initially anesthetized with 4.5% isoflurane for 3-5 minutes. Next, we injected ketamine, xylazine and acepromazine anesthetic cocktail intraperitoneally. The dose of the anesthetic is administered according to the animal's weight. For mice, we mixed 0.5 ml of ketamine (100 mg/ml), 0.05 ml of xylazine (100 mg/ml), 0.15 ml of acepromazine (10 mg/ml), and 4.3 ml of sterile isotonic saline in a sterile vial. We injected the solution - using 0.1 ml/10g mouse body weight - intraperitoneally. For rats, we used only xylazine (10 mg/kg IP) and ketamine (50 mg/kg IP). A pinch test at the hind- and forepaws was performed to verify an adequate level of anesthesia by the absence of reflexes.

b. Perfusion and staining of the cerebral vasculature

We labeled the vessels using 3 different methods. First, we performed an intracardiac injection. Here, we injected the dye into the left ventricle after opening the chest of the anesthetized mice. Before beginning the terminal perfusion, we let the heart pump the dye throughout the body for 2 and 4 minutes for the Alexa Fluor and the Dextran-FITC, respectively. Second, for tail vein injection, the dye was injected directly into the lateral tail vein. Tail vein injection was mainly used in rats. To localize the vein, we heated it by dipping the tail in warm water. Once again, we allowed

the dye to circulate for 2 minutes before cutting the chest for perfusion. The average time elapsed between the moment we completed the dye injection to the start of the PBS perfusion was 5.89 ± 0.97 minutes. All dye injections were performed slowly in a span of 1 minute. Finally, we also evaluated in vitro vascular labeling. In other words, we carried out the perfusion without prior injection of our dye. After perfusion and brain extraction, we immersed brain slabs into solutions with different concentrations of dyes.

Throughout the perfusion, the head and neck of the rodent were kept flat on the table to prevent any obstruction due to bends within the carotid arteries. We taped the forepaws and hind paws to the table to keep the body as stable as possible, especially at the moment of needle insertion. It is important that the needles get inserted at the left ventricle. It should not pierce through the interventricular septum. Otherwise, the perfusate will be directed to the lungs first. The right atrium was cut during perfusion to allow the blood and perfusate to leave the body. Improper cutting will generate excess pressure in the vascular system causing blood vessels to burst. During the entire process, from anesthetizing the rodents to the end of the perfusion, the animals were kept on a heating pad to prevent the possibility of blood clot formation.

Mice were perfused with 15 ml warm (37°C) heparinized (25U/ml) PBS. Subsequently, we used 15 ml liquid 4% PFA which was dissolved in PBS from 16% PFA (Electron Microscopy Sciences 16% Paraformaldehyde Aqueous Solution from Thermo Fisher Scientific, 50-980-487). For rats, we used 150 ml of each solvent. The perfusion rate was set to 3 ml/min and 12 ml/min for mice and rats respectively. The extracted brains were post-fixed in powder 4% PFA at 4°C. In order to prevent an excess of background fluorescence, the fixation duration was short - 3 hours and 6 hours for mice and rats, respectively. We also tested a post-fixation time duration of 24 hours for rat coronal brain slabs. After post-fixation, I washed the samples with room temperature PBS 3 times for 30 minutes to remove any remaining PFA. The brains were then cut into 2 mm or 3 mm-thick coronal slabs for tissue clearing. The brains were cut such that the corpus callosum was included in the brain slabs. To cut the brain, we used 1 mm stainless steel mouse and rat brain matrices (RWD 68707 and 68709). Bregma is defined as the 'zero' Anterior-Posterior coordinate, just as it is defined in the mouse and rat atlases (Paxinos and Franklin, 2001, and Paxinos and Watson, 2005). All positive coordinates are for areas anterior to the bregma, and all negative coordinates indicate sections posterior to the bregma.

c. Clearing methods

We mainly compared 3 clearing methods: 3DISCO, iDISCO+, and CUBIC. However, we briefly also performed clearing based on other methods: uDISCO and FDISCO. In this section, we will first describe the 3 main methods used. Then, we will give an overview of the others. Throughout the process, samples were kept in the dark until imaging. To evaluate the clearing quality before microscopy imaging, we looked for the presence of any distortions visible by eye, the transparency of the tissue, and the time needed for clearing.

3DISCO

One of the clearing methods we used closely follows the modified 3DISCO clearing protocol presented by Todorov *et al.* (2020). We dehydrated our brain slabs with increasing concentrations of tetrahydrofuran (THF) solution. Namely, we incubated each slab in 50%, 70%, 80%, 90%, and 2 times 100% THF (Sigma Aldrich, 186562) dissolved in distilled water at room temperature. This was followed by a final dehydrating step with 100% tert-butanol (Sigma Aldrich, 24127) at 35°C. A progressive increase in the dehydrating agent's concentration is necessary in order to prevent tissue deformation. Afterwards, we used dichloromethane (DCM) (Sigma Aldrich, 270997) to remove the lipids at room temperature. Finally, we matched the refractive index of the sample with BABB (benzyl alcohol + benzyl benzoate, 1:2, Sigma Aldrich, 305197, and Canadian Med Health Supplies) at room temperature. BABB was mixed with 0.4% of antioxidant DL- α -tocopherol also known as vitamin E (Alfa Aesar, A17039) to prevent the formation of peroxides over time. We renewed the mixture after 24 hours of incubation.

iDISCO+

The second organic solvent clearing method follows closely the clearing protocol of iDISCO+ developed by Renier *et al.* 2016. We dehydrate the tissue with an increasing concentration of methanol (Sigma-Aldrich, 179337) mixed with distilled water (20%, 40%, 60%, 80%, and 100% thrice). This is then followed by delipidation by incubation in a methanol-DCM mixture (1:2), and 100% DCM (twice). Finally, refractive index matching was performed with BABB with the vitamin E addition. The last step differs from iDISCO+ protocol where they had used dibenzyl ether (DBE). All clearing steps were performed on a shaker and inside 15 ml test

tubes made of polypropylene plastic. THF, DCM, and BABB were incompatible with other types of plastic because they melted them.

The incubation times of both mice and rat coronal slabs are shown in Tables 1 and 2 for the 3DISCO and iDISCO+ protocols, respectively. For the rat coronal brain slabs, we performed some additional incubation steps (Tables 1 & 2). The incubation steps and the time of incubation were based on the recommendations from Branch *et al.* 2021. In our preliminary experiments, we used full mouse brains where the incubation times were 12 hours/step (Table 1 & 2). During RI matching, we sometimes saw air bubbles trapped in the sample. For these cases, we used degassing to remove the air. We put our sample into a 50 ml falcon tube and filled it up with 4-5 ml of BABB. The falcon was connected to a suction tube to suck out the air. Air suction was done overnight.

Incubation step	Incubation time		
	Mouse 2-3 mm slabs or whole hemisphere	Rat 2-3 mm slabs	Whole mouse brain
50% THF	overnight	1 hr	12 hrs
70% THF	2 hr	1 hr	12 hrs
80% THF	2 hr	1 hr	12 hrs
90% THF	2 hr	1 hr	12 hrs
100% THF	2 hr	1 hr	12 hrs
100% THF	2 hr	overnight	12 hrs
100% THF	----	3 hrs	---
100% tert-But	2hr	2 hrs	12 hrs
DCM	2hr	1 hr	12 hrs
DCM	----	3 hrs	---
DCM	----	overnight	---
BABB	~ 48 hours	~ 48 hours	~ 48 hours

Table 1. Incubation steps and durations for 3DISCO clearing. The first column represents the clearing steps and the solvents used. The following 3 columns represent the incubation time frames for (1) mouse coronal slabs or whole hemispheres, (2) rat coronal slabs, and (3) whole mouse brains.

Incubation step	Incubation time		
	Mouse 2-3 mm slabs or whole hemisphere	Rat 2-3 mm slabs	Whole mouse brain
20% MeOH	overnight	1 hr	12 hrs
40% MeOH	2 hrs	1 hr	12 hrs
60% MeOH	2 hrs	1 hr	12 hrs
80% MeOH	2 hrs	1 hr	12 hrs
100% MeOH	2 hrs	1 hr	12 hrs
100% MeOH	1 hr	overnight	12 hrs
100% MeOH	1 hr	3 hrs	12 hrs
1 MeOH: 2 DCM	2 hrs	2 hrs	---
100% DCM	0.5 hr	1 hr	12 hrs
100% DCM	0.5 hr	3 hrs	---
100% DCM	----	overnight	---
BABB	~ 48 hrs	~ 48 hrs	~ 48 hrs

Table 2. Incubation steps and durations for iDISCO+ clearing. The first column represents the clearing steps and the solvents used. The following 3 columns represent the incubation time frames for (1) mouse coronal slabs or whole hemispheres, (2) rat coronal slabs, and (3) whole mouse brains.

CUBIC L/R

We also implemented the aqueous-based clearing protocol of CUBIC L/R proposed by Tainaka *et al.* (2018) and Matsumoto *et al.* (2019). The brain slabs were first incubated in 50% CUBIC-L solution for 1 day. We then replaced it with 100% CUBIC-L. We refreshed this solution every 3 days until delipidating process was completed. We tested incubating the slabs at 37°C and at room temperature. The samples were kept on a shaker throughout this whole process. CUBIC-L was made of 10 wt% N-butyldiethanolamine (Sigma Aldrich, 471240) and 10 wt% Titron X-100 (Sigma Aldrich, X100) dissolved in distilled water. Following this step, we repetitively washed the tissue with PBS to remove any trace of CUBIC-L. After overnight washing in PBS, we performed refractive index matching with 50% CUBIC-R+ for 1 day. Finally, we replaced the

solvent with 100% CUBIC-R+. We incubated the samples in CUBIC-R+ at room temperature. CUBIC-R+ consists of 45 wt% antipyrine (Sigma Aldrich, A5882) and 30 wt% nicotinamide (Sigma Aldrich, N3376) in distilled water. We adjusted the pH to 8-9 using N-butyl-diethanolamine.

Prior to these 3 methods, we have additionally performed clearing using other approaches. We have used iDISCO+ where we compared the refractive index matching solutions between DBE and BABB using complete mice hemispheres. We applied the FDISCO (Qi et al., 2019) concept on the iDISCO+ protocol on complete mice hemispheres. Here, we increased the pH of the dehydrating solution with triethanolamine and performed dehydration and RI matching at 4°C. We have also conducted clearing with uDISCO on whole mouse brains where the dehydrating solvent is tert-butanol.

d. Experimental setup for comparing different methods

We compared the results obtained with different protocols in order to optimize the best method to visualize vessels homogeneously throughout the rodent brain. Initial experiments consisted of clearing a whole-brain (or whole hemisphere) at a time. At this time, we compared the use of 2 refractive index matching solutions: BABB and DBE. We also looked at clearing at 4°C and in alkaline conditions relative to room temperature clearing without any pH adjustments. Additionally, we briefly looked at the use of tert-butanol as the dehydrating agent instead of methanol or tetrahydrofuran. Finally, we varied the volume of the solution relative to the air of the test tube in which we incubated our samples.

Following these initial experiments, for which we mainly looked at the clearing, we labeled the vessels and analyzed 2-3 mm thick coronal slabs simultaneously using the Opera Phenix high-content screening system. Table 3 gives an overview of the experiments.

Experiment number	Species type	Aim	Labelling Method	Clearing Method
1	Mice	Comparing DISCO clearing methods	N.A.	iDISCO+ & 3DISCO
2	Mouse	Comparing clearing methods	Intracardiac injection of WGA Alexa Fluor 647	iDISCO+, 3DISCO, & CUBIC
3	Rats	Varying injection volumes and comparing clearing methods	Tail vein injection of WGA Alexa Fluor 647	iDISCO+, 3DISCO, & CUBIC
4	Mice	Varying dye volume	Intracardiac injection of WGA Alexa Fluor 594	iDISCO+ & 3DISCO
5	Mice	Varying mice age and tissue thickness	Intracardiac injection of WGA Alexa Fluor 594	iDISCO+
6	Mice	Varying mice age and tissue thickness	Intracardiac injection of FITC-Dextran	CUBIC
7	Mice	Staining by immersion	Staining before versus after delipidation. Varying dye type and concentration, and incubation parameters	CUBIC

Table 3. Summary of experiments. The Table lists the different experimental designs with the species used, the aim, the labeling methods, and the clearing methods.

Experiment 1: iDISCO+ versus 3DISCO clearing

We compared clearing between iDISCO+ and 3DISCO using 3 mm thick brain slabs from 4 mice (Figure 9a). For 2 of the mice, the anterior brain slabs were cleared with iDISCO+ protocol and the posterior with 3DISCO. For the 2 others, we did the opposite.

Experiment 2: Comparing the 3 clearing methods in mouse

In a final mouse experiment, we compared the 3 clearing methods: iDISCO+, 3DISCO, and CUBIC-L/R+. All the left hemisphere slabs were dedicated to iDISCO+ clearing. As for the right hemisphere, the clearing methods were altered between the 3 methods mentioned above. We used 150 μ l of 5mg/3ml WGA Alexa Fluor 647.

Experiment 3: Comparing the 3 clearing methods and 2 different dye volumes in rat

In all the rat experiments, we compared the 3 clearing methods: iDISCO+, 3DISCO, and CUBIC-L/R+. All the left hemisphere slabs were dedicated to iDISCO+ clearing. As for the right hemisphere, the clearing methods were altered between the 3 methods mentioned above. We used 5mg/3ml WGA Alexa Fluor 647: 0.6 ml for 1 rat and 1.2 ml for 2 rats. For a few rat coronal slabs, we did an overnight post-fixation with PFA.

Experiment 4: Varying Alexa Fluor 594 dye volume

We made a comparison between results obtained with different WGA Alexa Fluor 594 volumes injected intracardially into the vascular system. We used 4 different volumes of 5mg/3ml concentration of dye in 4 different mice: 100ul, 150ul, 200ul, and 250ul. All other perfusion parameters and the mice' ages were kept constant. All coronal brain slabs were 3 mm thick. The clearing protocols we used were iDISCO+ and 3DISCO. Figure 9b demonstrates how we organized the cutting and clearing.

Experiment 5: Varying mice age and slab thickness with iDISCO+ clearing

We evaluated the effect of age on the tissue clearing and labeling using 5 mice of different ages (65, 105, 155, 175, 219 days old) while using a constant volume of WGA Alexa Fluor 594 (150 ul). Moreover, we varied the coronal slab thickness between 2 mm and 3 mm. We cleared using iDISCO+.

Experiment 6: Varying mice age and tissue thickness with CUBIC clearing

We conducted a similar experiment as described above in experiment 5. However, we used 100 ul of FITC-dextran (6 ug/ul) and CUBIC clearing. Figure 9c-d demonstrates how the cutting was done for both experiments 5 and 6.

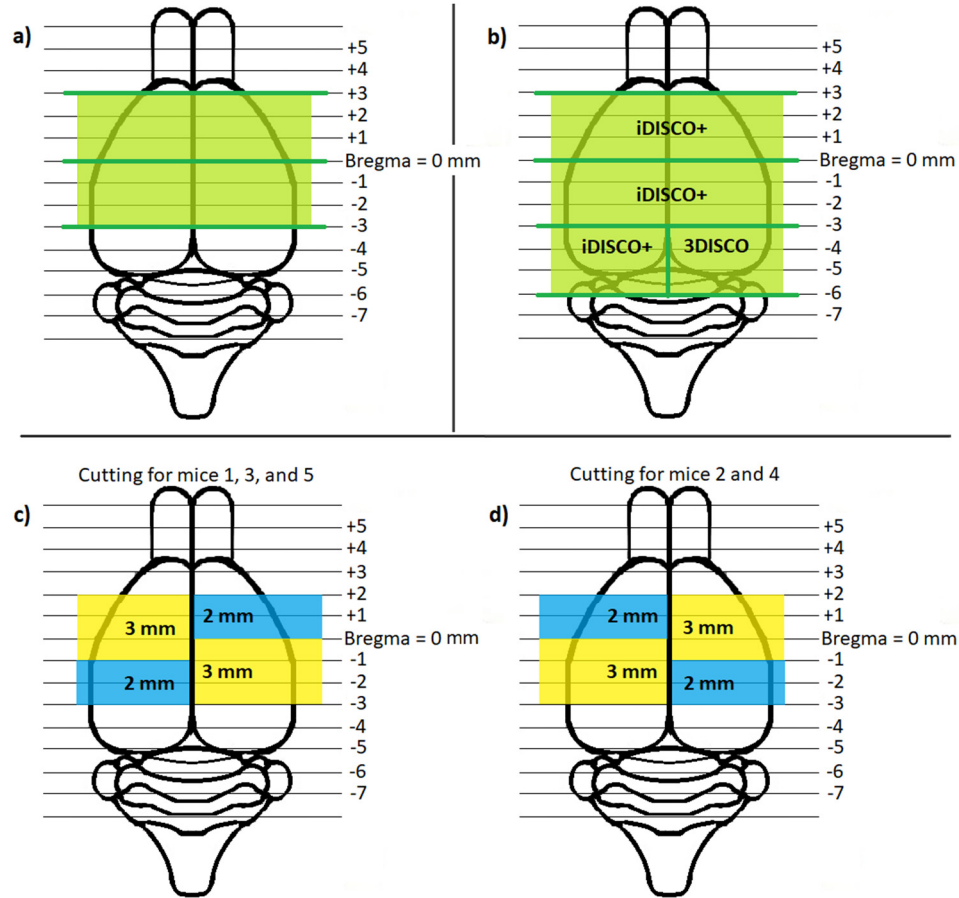


Figure 9. Cutting plan for experiments. a) Shows the 3 mm anterior and posterior sections. The clearing of each of these sections was altered between the slabs and mice. b) Demonstration of how the brain was cut for mice that were stained with different volumes of Alexa Fluor Dye. c-d) Illustration of how the brain was cut for mice of varying ages. The coronal slab thickness was altered within hemispheres and mice. c) Represents mice that were 65, 155, and 219 days old, and d) shows cutting for mice of 105 and 175 days old.

Experiment 7: Staining by immersion with CUBIC clearing

We also tested staining blood vessels by immersing brain slabs into solutions with dyes. We used (1) 0.1mg/ml in LEL Dylight 649, (2) 0.2mg/ml in LEL Dylight 649, (3) 0.1mg/ml in WGA Alexa Fluor 647, and (4) 0.2mg/ml in WGA Alexa Fluor 647. All coronal brain slabs were 2 mm thick. They were incubated in 0.5 ml of the corresponding dye. Table 4 shows how we organized the experiments. A total of 5 mice were used. For 3 of them, we immersed the brain slabs into the dye right after the PBS washing step (before delipidation). For others, they were incubated after the completion of delipidation. Additionally, we varied incubation parameters: (1)

6 hours versus 24 hours PFA post-fixation (2) performing delipidation at room temperature versus 37°C (Table 5).

Coronal slab information	Dye & concentration
LEFT HEMISPHERE ANTERIOR	LEL DyLight 647 & 0.2 mg/ml
LEFT HEMISPHERE POSTERIOR	LEL DyLight 647 & 0.1 mg/ml
RIGHT HEMISPHERE ANTERIOR	WGA Alexa Fluor 649 & 0.2 mg/ml
RIGHT HEMISPHERE POSTERIOR	WGA Alexa Fluor 649 & 0.1 mg/ml

Table 4. Indication of dye type and concentration used for each coronal slab.

Experiment number	Staining time point	PFA post fixation time	Staining conditions	Delipidation conditions
Mouse 1	Before delipidation	3 hours	37°C	37°C
Mouse 2	Before delipidation	3 hours	Room Temperature	Room Temperature
Mouse 3	Before delipidation	24 hours	37°C	37°C
Mouse 4	After delipidation	24 hours	Room Temperature	Room Temperature
Mouse 5	After delipidation	24 hours	Room Temperature	Room Temperature

Table 5. Experimental design for labeling by immersion applied 5 mouse brains. 3 mice were stained before the start of delipidation. The PFA post-fixation time was either 3 hours or 24 hours. The staining and delipidation were done either at room temperature or at 37°C. 2 other mouse brains were stained after the completion of delipidation. The post-fixation time was 24 hours and incubation was done at room temperature.

e. Imaging the brain slabs

The data shown in this thesis were obtained using Opera Phenix High-Content Screening microscope (PerkinElmer) and from a Zeiss LSM-880 with AiryScan detector microscope (Zeiss). The Opera Phenix and the LSM-880 use the eHarmony and Zen software packages, respectively. We performed data collection with 16-bit images.

i. *The Opera Phenix High-Content Screening Microscope*

For experiments involving a comparison between methods, I mainly used the Opera microscope from the Advanced BioImaging Facility (ABIF) of McGill University to image multiple samples in one session using 24 well plates (ibidi, 82426) or 12 well plates (Cellvis, P12-1.5H-N). We placed each tissue slab in the center of a well. We surrounded the sample with cleared agarose blocks to keep the tissue still during imaging. The agarose blocks were cleared by dehydration (methanol) and refractive index matching (BABB with 0.4% with an addition of vitamin E). We next filled up the wells with the appropriate clearing solution until the tissue slab was fully covered. The well plates from Cellvis are not made with polypropylene plastic. Therefore, it should not be used with organic solvents since this solvent melted the material of the well walls. We used the 12 well Cellvis plates only for rat coronal brain slabs cleared with CUBIC because they did not fit in the 24 well plates.

We obtained data by first performing a pre-scan using 5x/0.16 NA air objectives (PerkinElmer, HH14000402) and by imaging 5 different planes with a step size of approximately 500 μm in the Z direction. For the 5x objective, we used a XY-pixel size of 1.196 $\mu\text{m}/\text{pixel}$. With this data, we then set up an online job with the *image analysis* feature in the *eHarmony* software. With the online job, we identified the edges of the samples. Therefore, once we performed imaging at higher magnification, only the sample was imaged instead of a whole rectangular region with ‘void’ space. Thus, for our online job, we first carried out a maximum projection of our 5x data. Next, we filtered our image. We chose a Gaussian filter of width 3 to filter out the noise. Then, to localize the region of interest, we performed absolute thresholding. In other words, all pixels with an intensity value above the threshold were a part of our region of interest. This value may need to be changed between experiments in order to correctly localize the region of interest. Next, we can also inform the system that we want our surface area to be greater than a certain value. By doing so, the possibility of imaging dust particles is reduced. With this, we have obtained our online job. We next proceeded to image with 10x/0.3 NA air objectives (PerkinElmer, HH14000403). The XY-pixel size was 0.598 $\mu\text{m}/\text{pixel}$.

We used a tile overlap of 10% for all 5x and 10x images. The laser power used was 80% for all experiments except for 10x imaging of the experiment where we used different volumes of

WGA Alexa Fluor 594 to stain the vasculature. For this experiment, we used 75%, because with 80%, there were many saturated pixels. The exposure time was set to 200 ms for all the scans. The excitation lasers used were the 488 nm laser for FITC-dextran (490/520), 561 nm for Alexa Fluor 594 (590/618), and 640 nm for both Alexa Fluor 647 (650/671) and DyLight 649 (655/670). The light absorption spectrums for the 488 nm, 561 nm, and 640 nm lasers were 500-550 nm, 570-630 nm, and 650-760 nm, respectively.

The Opera Phenix microscope also gives the ability to perform autofocus. We selected the “one peak” option which searches for the bottom of the imaging plate only. “Two peaks” would look at the bottom and the top surface of the imaging plate. We chose “one peak” since at 10x the system cannot locate the top surface of the plate for clearing solutions that have an RI greater than 1.5. The microscope also gives binning options. We chose binning 1 as it gives the smallest pixel size. Binning 2 would combine 2 by 2 pixels into 1 pixel. This reduces the resolution, gives brighter results, and a shorter acquisition time.

ii. Zeiss LSM-880 with AiryScan detector microscope

We also used the LSM-880 microscope (Zeiss Axio Observer.Z1 inverted microscope) of the Montreal Neurological Institute’s microscopy facility. The tissue slabs were placed flat on a 35 mm μ -Dish (81156, ibidi). Again, we placed cleared agarose blocks around the sample to keep it in place. We then filled up the dish with BABB such that the sample was submerged in the solution. We used a Plan-Apo 10x/0.45NA objective. The XY-pixel size of the images was 1.99 $\mu\text{m}/\text{pixel}$. The step size was 1.99 μm and we imaged approximately 1.2 mm in the z-range. The pixel dwell time was 1.02 μsec . The laser power was set to 1.5%. The pinhole size followed Zeiss software’s recommendation of 89.8 (2.33 airy units \cong 16.4 μm). The pinhole prevents scattered lights from passing through to the detectors. We mainly used the LSM-880 microscope with slabs labeled by Alexa Fluor 647. We used a solid-state 633 nm laser to excite the fluorophores. The emission filter range for the recorded fluorescence was 638-756 nm. Bi-directional imaging was used. The system used a photon multiplier tube detector where the gain was set to 700V. This detector converts photon values to a voltage output. It can support the amplification of the signal.

f. Visualization of data

The microscopy data were saved as .tiff files. Each image represented one tile in the X-Y mosaic and the Z-plane. Therefore, in order to visualize the data, we had to stitch these tiles

together. This task was accomplished by using *Imaris Converter* to convert .tiff files to .ims files. Next, we utilized the *Imaris stitcher* to stitch the tiles together. Finally, we visualized and saved the images as tiff with *Imaris*. Further processing was done with FIJI (Fiji Is Just ImageJ). In order to perform a comparison within an experiment, image processing was applied in a similar manner to all the images. As such, we used 2%-pixel saturation. We used the red color to show data stained with red dyes and the green color for the dextran-FITC.

To demonstrate the data obtained by immersion staining, we found very bright signals in the white matter. This hindered the visualization of possible capillaries. Thus, we performed further processing. We blurred our raw stitched image using Gaussian blur ($\sigma = 50$). We then took the inverse of this image. This result was multiplied by the original raw stitched image. Next, we used 1%-pixel saturation.

As the illumination of the laser was uneven between the center of a tile to its periphery, when stitching, it created grid artifacts between tiles. In order to eliminate these artifacts, we additionally scanned the same dye (dissolved in PBS) that stained our blood vessels (initially, we also tried to perform the correction using BABB or food coloring dissolved in CUBIC instead of our dyes). We found that the dye gave a better removal of the grid artifact. Then, we used FIJI to apply the correction to our original data before proceeding with the stitching. As such, we first took an average intensity projection of the individual control tiles from the equivalent plane (I_{avg}). We next took the average pixel intensity value from I_{avg} ($pixel_{I_{avg}}$). Finally, we divided each tile of our data with the average intensity projection followed by multiplication with the $pixel_{I_{avg}}$. Initially, we were not aware of this correction process. Therefore, we began collecting these control data only after a certain timepoint. From the set of data shown in this work, the experiment that did not have grid correction is the experiment where we performed the Alexa Fluor 594 volume variation.

g. Quantitative analysis

We calculated the signal-to-background ratio of WGA Alexa Fluor by collecting intensity values from capillaries and its adjacent background signals. We performed the signal-to-background ratio evaluation on results that compare injection of different dye volumes between the mice injected with 100 μ l ($n = 1$), 200 μ l ($n = 1$), and 250 μ l ($n = 1$) where n represents the

number of rodents used (experiment #4). I used one iDISCO+ cleared 3 mm thick full coronal brain slab per animal (spanning from 0 to -3 mm from bregma). I looked at the middle cortical layer from 5 different regions of interest which was consistent between all slabs and used plane Z = 1200 μ m counting from the most anterior side (0 mm from bregma). A total of 100 data points were collected for each slab representing a different volume (20 pairs from each ROI, 10 from signal and 10 from background).

We also performed signal-to-background ratio evaluation for experiment #3 between the rats injected with 0.6 ml (n = 1) and 1.2 ml (n = 1). Once more, I looked at 1 iDISCO+ cleared brain slabs per animal (left hemisphere spanning from -5 to -7 mm from bregma). I used plane Z= 800 μ m. We collected data points from a straight line along the cortical depth (Figure 10). We used 7 lines from the somatosensory region. The data collection process was performed with the contralateral right hemisphere brain slabs cleared with 3DISCO. We used plane Z = 600 μ m to adjust for the tissue shrinkage. We also compared the signal-to-background ratio for iDISCO+ clearing vs 3DISCO clearing with the same data points using the contralateral brain slabs of the same rats: 1) the rat injected with 0.6 ml and 2) the rat injected with 1.2 ml (Z= 800 and 600 μ m for iDISCO+ and 3DISCO respectively from slab located at -5 to -7 mm from bregma). We also collected data for the comparison of clearing methods from the mouse of experiment #2 stained with 150 μ l of dye (Z= 800 and 600 μ m for iDISCO+ and 3DISCO respectively from slab located at +1 to -1 mm from bregma).

We performed one-way analysis of variance (ANOVA) when comparing multiple groups (e.g., different volumes) to determine if there is a statistical difference between the means of the groups. If there was a difference, we used Tukey Kramer's multiple comparisons to determine which of the paired group comparisons contain(s) a significant difference. When we compared only 2 groups of data, we used the two-tail student t-test. The null hypothesis was that there were no statistically significant differences between the means.

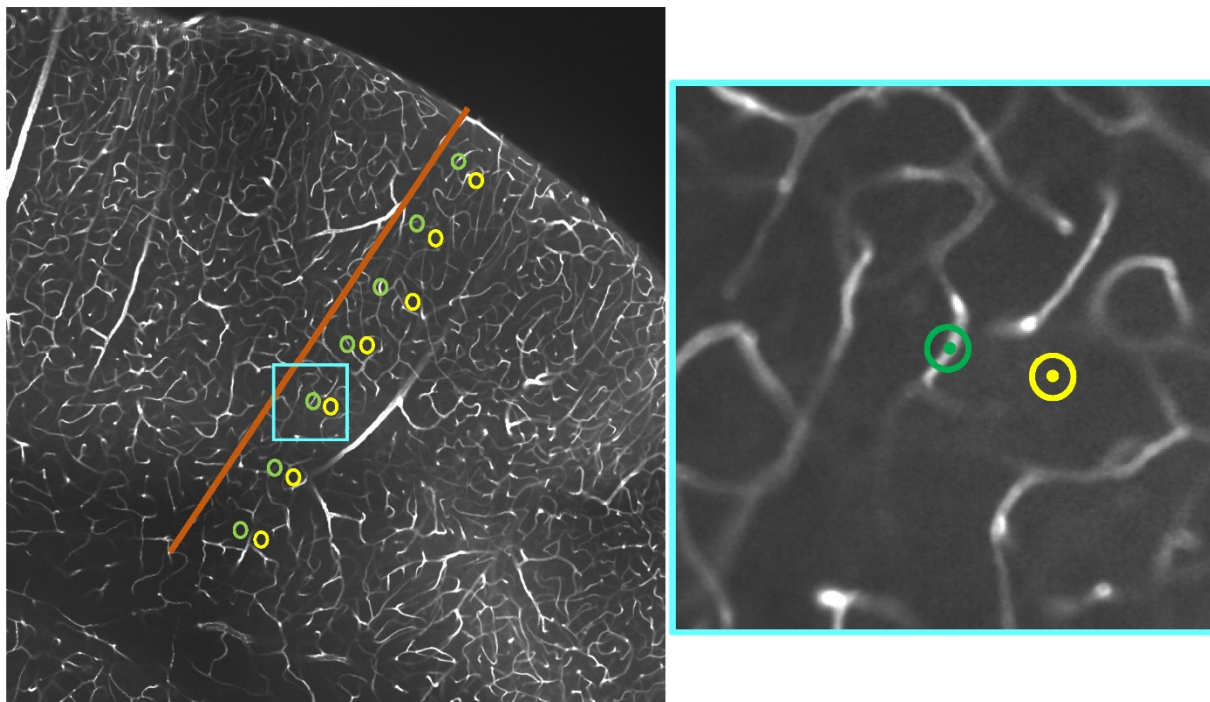


Figure 10. Example of capillary and background signal sampling across the cortical depths. We collected 7 data points from the capillaries (green circles) and 7 data points from the background adjacent to each sampled capillary (yellow circles) along the cortical depths orthogonal to the cortical surface (dark orange line). The distance between each point is approximately the same. If at a certain depth there were no capillaries, then we sampled the signal and the background from the background. A zoomed-in view of the blue cyan rectangle is shown on the right, to illustrate more precisely how the sampling was done.

CHAPTER IV - RESEARCH FINDINGS

a. Preliminary clearing results of whole brains & hemispheres

In the initial stages, we used complete mouse brains or whole hemispheres to evaluate clearing protocols. As one of the first evaluations, we followed the iDISCO+ clearing protocol and compared the refractive index matching solutions. We used BABB and DBE. The clearing quality remained similar with both refractive indices. Another initial evaluation included clearing our samples at 4°C and in alkaline conditions while using the iDISCO+ protocol. The clearing solvents were methanol, dichloromethane and dibenzyl ether. We used triethanolamine to increase the pH to 9-9.5. We saw clearly that the samples incubated at these conditions became more opaque compared to the samples cleared at room temperature and normal pH (Figure 11). Therefore, for our subsequent studies, we abandoned the clearing at colder temperatures and higher pH.

Additionally, as clearing results were similar between BABB and DBE, we proceeded with Todorov et al.'s (2020) recommendation to use BABB.

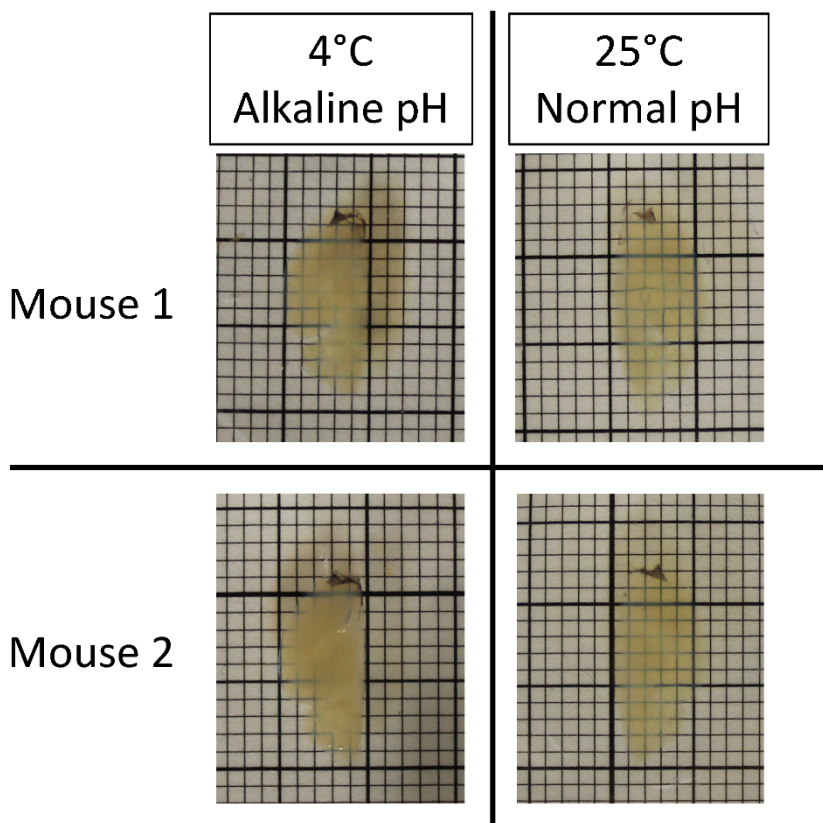


Figure 11. Comparison of clearing results based on different incubation conditions. Rows 1 and 2 demonstrate clearing examples of 2 different mice. The left hemisphere (first column) was cleared at 4°C and with alkaline pH. The right hemisphere (second column) is cleared at room temperature with normal pH.

As part of our preliminary studies, we also cleared the whole mouse brain. We performed uDISCO, 3DISCO, and iDISCO+ clearing. Figure 12 a-b demonstrates uDISCO clearing. Even though we used the same protocol for the 2 mice brains, we noticed a difference in the results. From panel b, we see that the cleared brain was relatively darker in color. Next, we cleared with the modified 3DISCO protocol as recommended in Todorov et al (2020) (Figure 12 c-e). The first 3 samples were incubated in 10 ml solvent volumes (panels a-c) in 15 ml test tubes. We noticed that the cleared brains had a dark amber appearance. Following troubleshooting recommendations from iDISCO, I understood that the dark amber color may be related to the fact that the samples were exposed to too much air. Thus, we varied the volume of the incubation solutions relative to the air-filled space of the 15 ml test tubes. Brain samples in panel c), d), and e) were incubated in

10ml, 14 ml, and 5 ml volumes respectively. We expected to see the brain incubation in 5 ml solutions to be the darkest. Instead, we noticed that it was the one incubated in 10 ml. Despite the troubleshooting recommendations, a clear trend of transparency was not observed between these 3 cleared brains. Thus, after a closer look, I realized the perfusion of the brain from panel c) was unsuccessful since, during perfusion, the pressure of the perfusate entering the heart was too high relative to the pressure leaving. Notably, we can look back at the difference in clearing results from panels a and b which followed the same uDISCO protocol. In b), the perfusion was also unsuccessful, and we noticed a darker sample. Finally, we also demonstrate a comparison between the 3DISCO (f) and the iDISCO+ (g) protocols. In panel g), the dehydrating solution was switched to methanol. As a result, we noticed a more transparent brain. As a whole, we found that iDISCO+ clearing gave greater optically cleared brain samples and that poor perfusion directly affects the quality of the clearing.

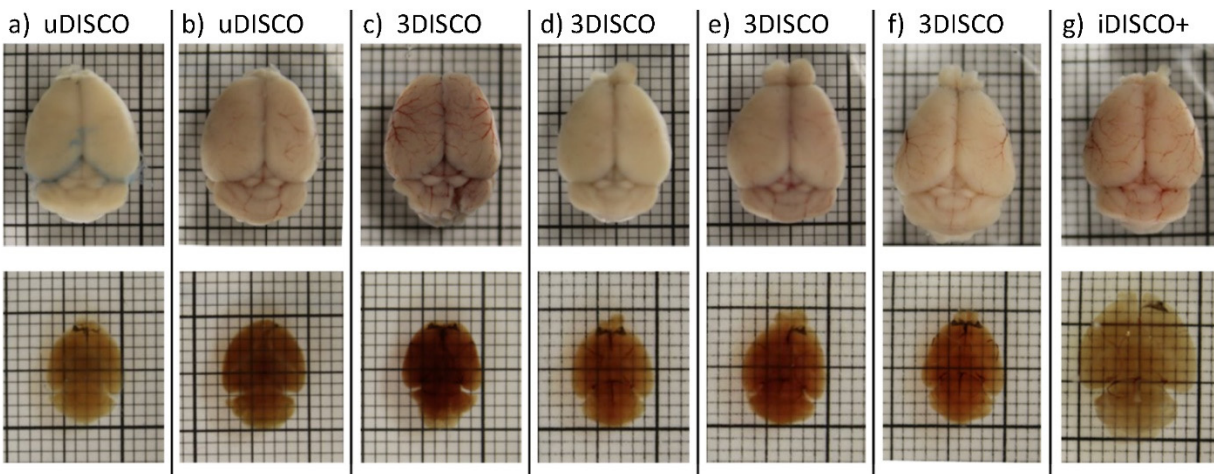


Figure 12: Demonstration of whole-brain clearing performance using different organic solvent protocols. The top and bottom rows represent images of mouse brains taken before and after clearing respectively. Both brains in columns a) and b) were cleared using uDISCO solvents and they were injected only with Evans blue dye. Columns c) to f) show 3DISCO clearing as described by Todorov et al. Alexa fluor and Evans Blue staining are used for columns c) to e) only. The solvent incubation volumes are 10 ml in c) 14 ml in d), and 5 ml in e). Only Alexa fluor is used for f) and g). Finally, iDISCO+ clearing is shown in column g).

Finally, we performed CUBIC clearing on a whole mouse brain following the recommendation time stamps of Tainaka *et al.* (2018) and Matsumoto *et al.* (2019). Figure 13 demonstrates the clearing progress. The sample was delipidated for a total of 5 days at 37°C. After being transferred to the RI solution, the clearing was insufficient as the sample was not transparent.

Therefore, for our subsequent CUBIC tissue clearing of coronal brain slabs, we performed delipidation for longer periods in order to get a complete clearing of our samples.

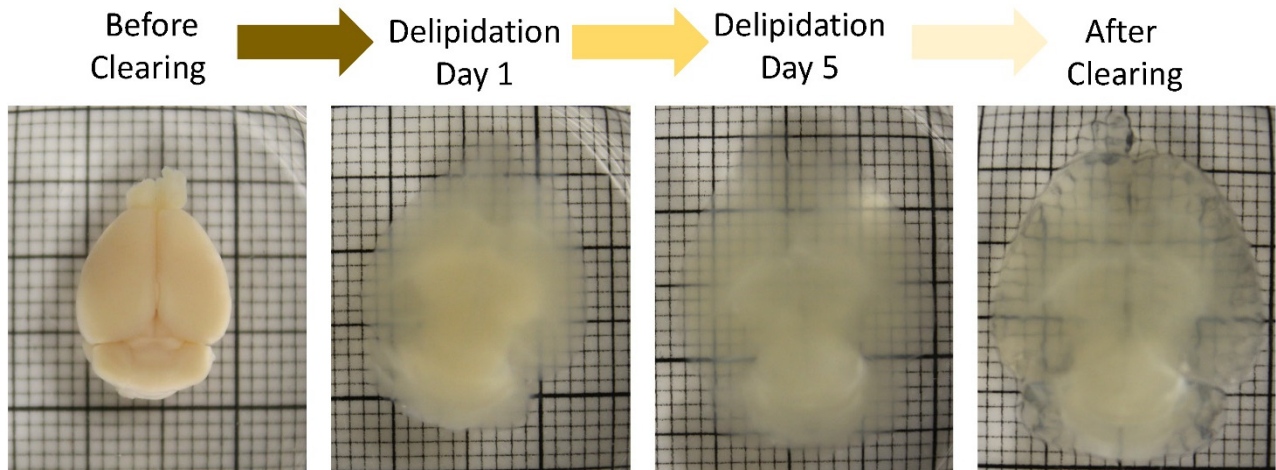


Figure 13: Example of CUBIC clearing progress of a whole brain. From left to right, images represent the clearing progress of a whole mouse brain: before clearing (in PBS), days 1 and 5 from the start of delipidation (in CUBIC-L), and after refractive index matching (CUBIC-R).

b. Comparison of clearing protocols: 3DISCO, iDISCO+, and CUBIC: Experiments 1-3

We switched to using coronal slabs in order to increase the speed of the optimization and application of our protocol. For microscopy imaging, we used the Phenix Opera High Content Screening System which is a spinning disc confocal microscope. It has the capability to scan multiple samples in one imaging session.

i. *Clearing results in mice: Experiment 1*

Figure 14 shows images from tissue slabs cleared with the organic solvent methods using 4 different mice. The brains were cut into 2 coronal slabs of 3 mm thickness. The slabs from the top row of each panel were cleared with iDISCO+ and the bottom row with modified 3DISCO. We looked at the possibility of tissue deformation by taking pictures of the coronal slabs in air before and after clearing. Two views are shown: a dorsal view and a coronal view. We noticed that with iDISCO+ clearing, the samples remained relatively the same size with no visible distortions. Meanwhile, 3DISCO clearing decreased the sample's size about 20-30%. The last column of the figure demonstrates the clearing capacity. All tissue slabs were transparent after RI matching.

In general, both organic solvent methods cleared the coronal slabs: the grid underneath the samples became visible. Additional comparison of both organic solvent clearing methods is shown in Figure 15. Once again, each panel represents a different mouse. The right hemispheres (3 mm thick slabs) were cleared with 3DISCO. The contralateral left hemispheres were cleared with iDISCO+. We noticed that, with iDISCO+, the coronal slabs achieved a higher RI matching with the surrounding BABB compared to the 3DISCO cleared samples. That is, they become more transparent. We also always refreshed the clearing solution after one day of BABB incubation to help increase transparency. We noticed that the transparency of the slabs increased slightly after 2 days of clearing. In fact, it became difficult to localize the edges of the iDISCO+ samples after refreshing our BABB solution.

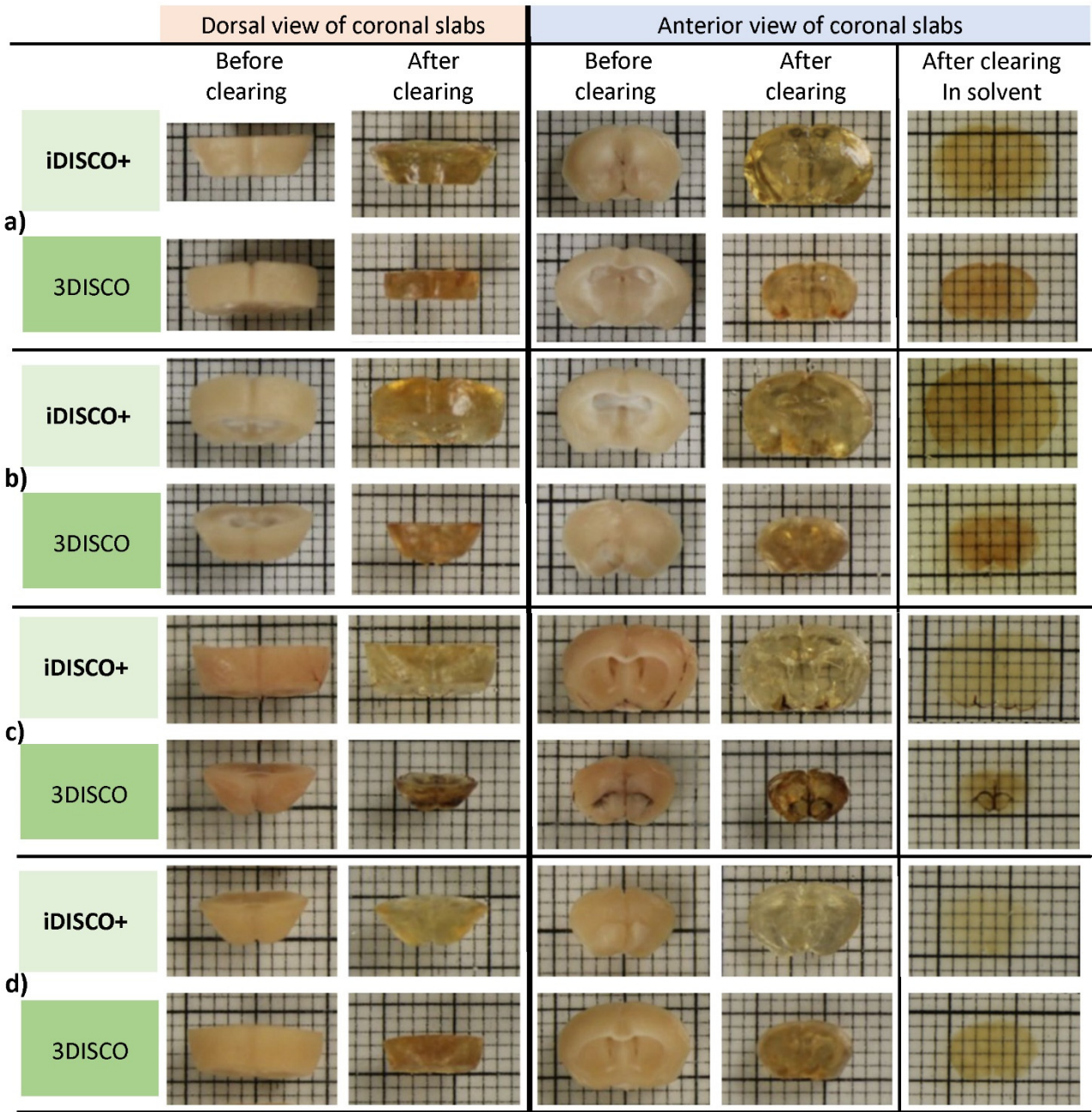


Figure 14. Clearing results from 3 mm thick coronal brain slabs using iDISCO+ and 3DISCO. A depiction of volume before and after clearing of coronal brain slabs of 4 different mice. There is one panel for each mouse (a-d). The top row of each panel illustrates iDISCO+ clearing and the bottom shows modified 3DISCO clearing. The first 2 columns show a dorsal view of the coronal slabs in air. The remaining columns show the anterior view. The slabs are immersed in BABB in the last column.

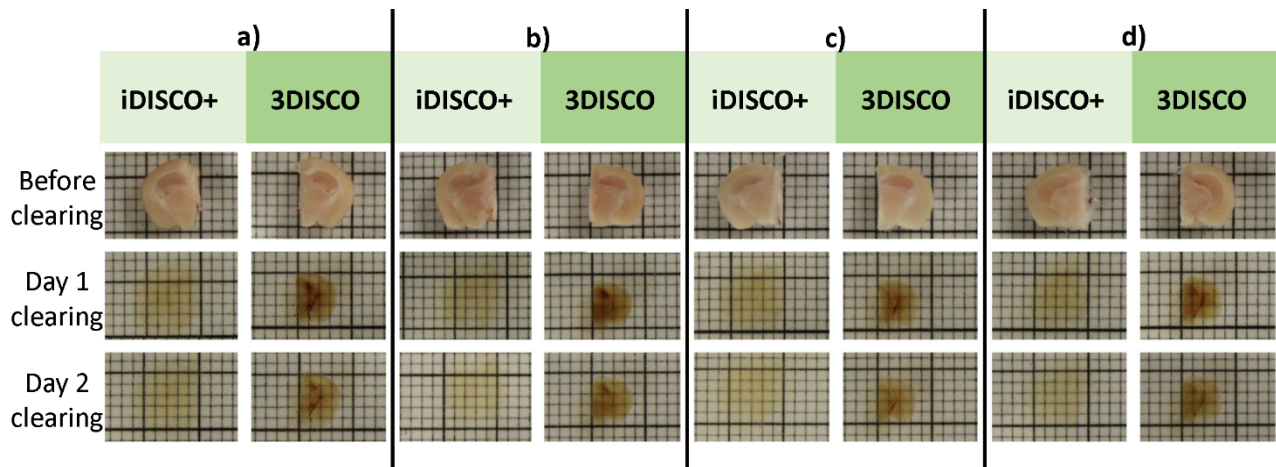


Figure 15. Comparison of iDISCO+ and 3DISCO clearing after 1 and 2 days of refractive index matching. Panels a) to d) depict the anterior view of coronal brain slabs from 4 different mice. All right hemispheres are cleared with iDISCO+ and the left hemispheres with modified 3DISCO. Images of the slabs before the clearing process, 1 day after RI matching, and 2 days after RI matching are shown in rows 1 through 3 respectively.

Although, in general, there were no major distortions caused by the clearing, sometimes certain slabs were slightly bent after clearing (data not shown). Additionally, the clearing protocol amplified any minor artifact that occurred during brain extraction or tissue cutting (Figure 16).

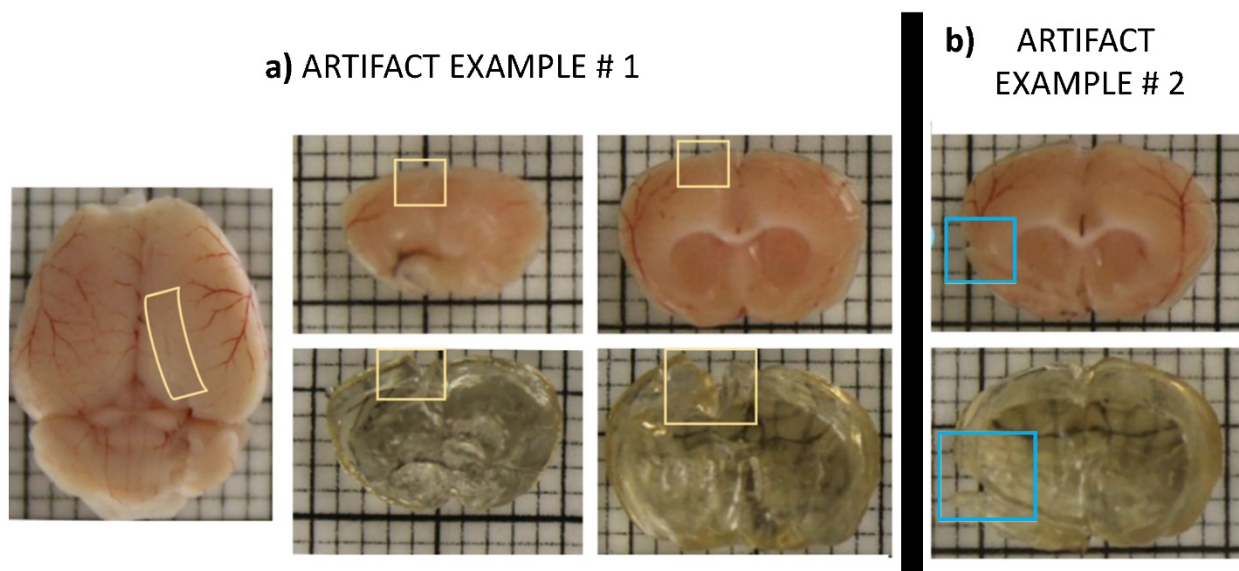


Figure 16. Depiction of clearing artifacts. In a) a thin line of cut occurred during brain extraction. The cut shown by the yellow boxes is barely visible before clearing the sample. After clearing (bottom row), the cut artifact is amplified. b) A second example of a cut that occurred on the lateral side of the slab. It was also increased in size after clearing (blue boxes). The coronal sections were placed such that the anterior side of the slabs faced the camera.

ii. Clearing results in the rat: Experiment 3

We also performed experiments on rat brains. All the rat coronal slabs were 2 mm thick. All the slabs from the left hemisphere were cleared with the iDISCO+ protocol (Figure 17b). The contralateral right hemispheres were cleared with CUBIC, 3DISCO, or iDISCO+ (Figure 17a). The right hemisphere coronal slabs centered at 0 mm and at -4 mm from bregma were cleared with CUBIC. Those centered at +2 mm and -6 mm from bregma were cleared with 3DISCO. Similar to the mouse brains, 3DISCO clearing resulted in a darker color relative to the slab's contralateral counterparts which were cleared with iDISCO+. The right hemisphere slab centered at -2 mm from bregma was cleared with iDISCO+. They all yielded transparent samples such that the millimetric grid remained completely visible. Therefore, all clearing methods have the capability to yield transparent samples.

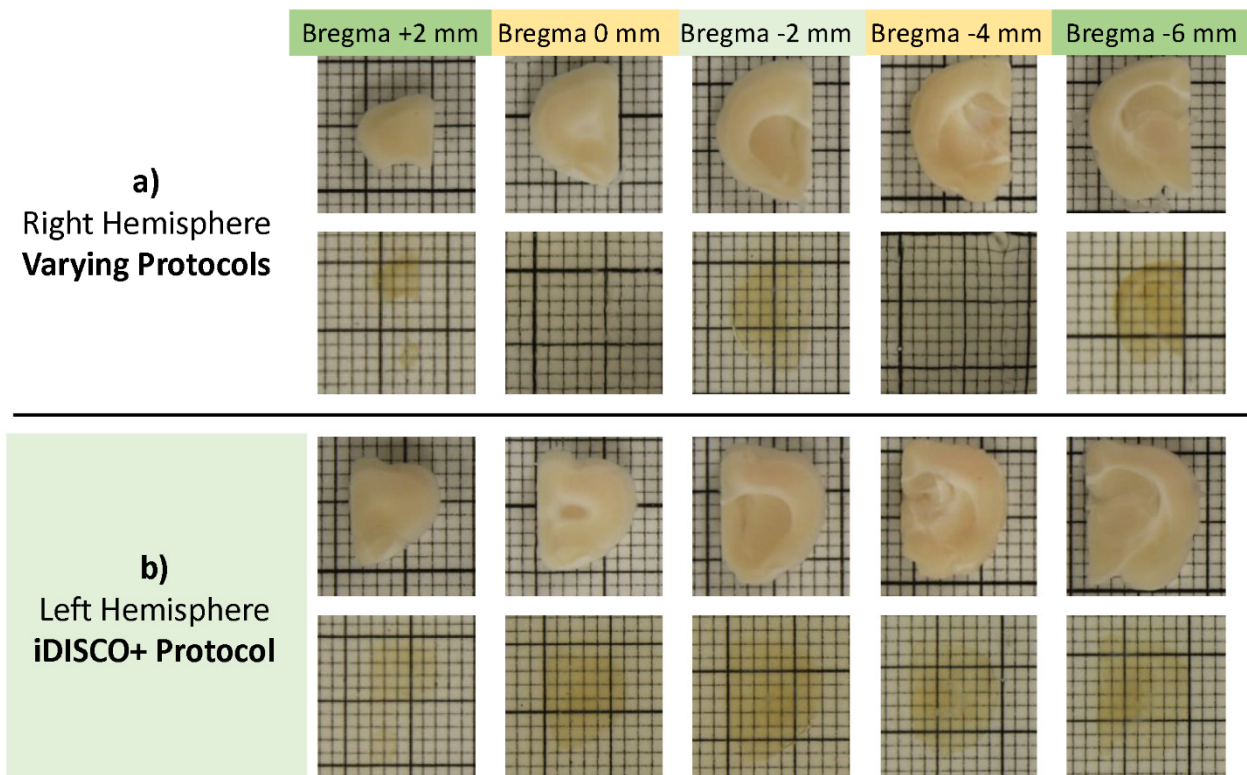


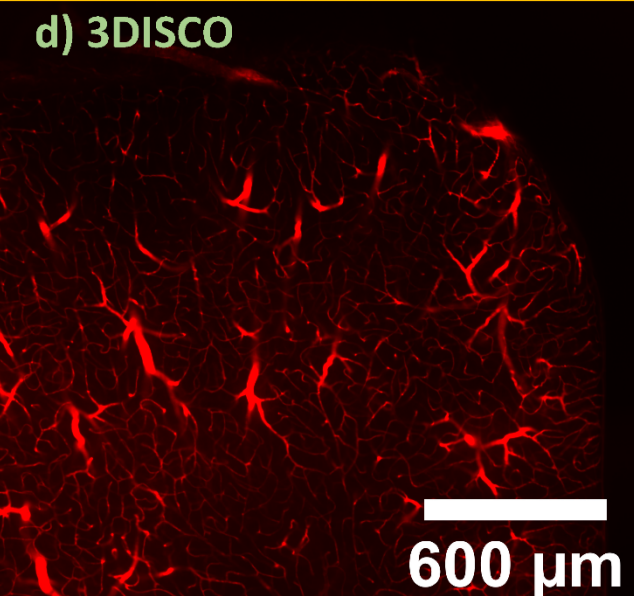
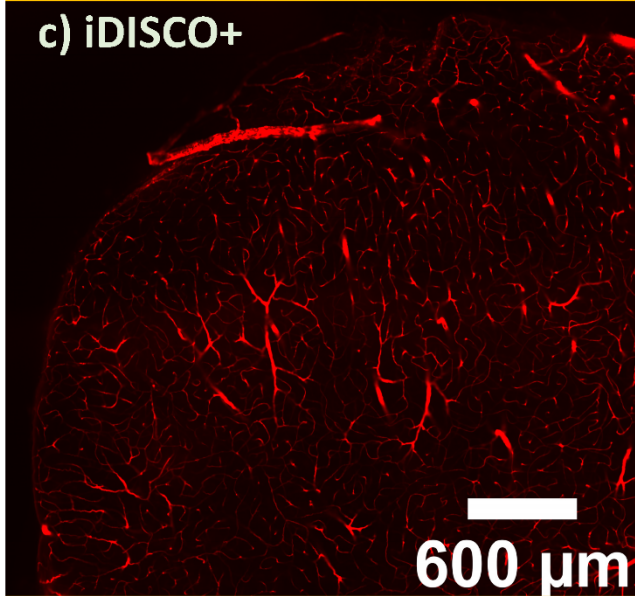
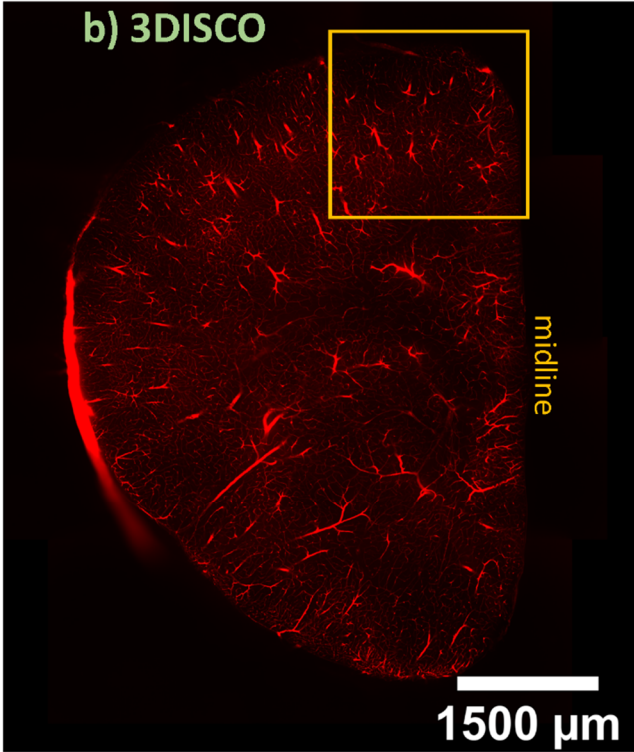
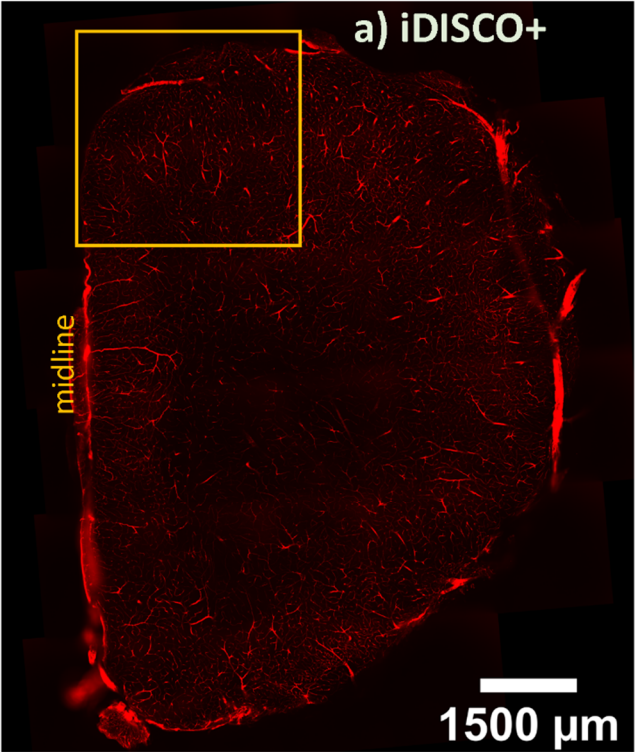
Figure 17. Demonstration of final clearing results from rat coronal brain slabs using 3 different clearing methods. Before and after clearing images are shown of five 2 mm thick rat coronal brain slabs. a) The right hemispheres are cleared with different protocols. They are cleared with modified 3DISCO, CUBIC, and iDISCO+ for coronal slabs centered at +2 mm and -6 mm from bregma, at 0 mm and at -4 mm from bregma, and at -2 mm from bregma, respectively. b) The left hemispheres are cleared with iDISCO+ protocol for all the slabs.

iii. Imaging results in mice: Experiment 2

A comparison of the 3 clearing methods in terms of vascular imaging is shown in Figures 17 and 18. The mouse was intracardially labeled with 150 μl of Alexa Fluor 649. We see that there is homogenous labeling throughout the cortical layers from all brain slabs demonstrated. In Figure 17, we looked at 2 mm thick contralateral brain slabs of similar depth considering tissue shrinkage caused by 3DISCO ($z = 800 \mu\text{m}$ and $600 \mu\text{m}$ for iDISCO+ and 3DISCO). The left and right hemisphere were cleared with iDISCO+ and 3DISCO, respectively (Figure 18a, b). A magnified view of the brain coronal slabs is also shown in Figure 18c and d. It is important to note that 3DISCO clearing shrinks the samples by about 20-30% which explains the difference in the scale bar size.

In order to evaluate the performance of each of the clearing protocols, we compared the signal-to-background ratio between contralateral slabs cleared with iDISCO+ and 3DISCO. The mean signal-to-background ratio were 3.514 ± 2.117 and 2.299 ± 0.708 , respectively (Figure 18e). The standard deviation of the ratio with iDISCO+ is relatively large. However, the difference in the means was statistically significant ($\alpha=0.001$, $\text{DOF} = 60$, $t_{\text{stat}} > t_{\text{crit}} \rightarrow 3.810 > 3.460$). To better understand the reasons for the different signal-to-background ratios, we computed the mean fluorescence levels at the capillary and background separately (Figure 18f). The iDISCO+ background intensity was lower than 3DISCO's background (6448 ± 1485 and 8300 ± 2144 , respectively) with a statistically significant difference ($\alpha=0.001$, $\text{DOF} = 80$, $t_{\text{stat}} > t_{\text{crit}} \rightarrow 4.918 > 3.416$). In addition, the iDISCO+ mean signal intensity in the capillaries was higher than 3DISCO's (22058 ± 12492 , and 18425 ± 5603 respectively). Thus, we observed an increase in signal-to-background ratio. However, we see that the capillary signals with iDISCO+ varied a lot throughout the ROIs as seen by the large standard deviation. With this, the confidence level for the significant difference in the mean capillary intensity was 90% ($\alpha=0.1$, $\text{DOF} = 60$, $t_{\text{stat}} > t_{\text{crit}} \rightarrow 1.838 > 1.671$).

The CUBIC cleared slab was centered at +2 mm from the bregma (figure 19). We noticed higher background signal with the CUBIC clearing in general. Additionally, the distance between the vessels was larger than the distance observed with the DISCO protocols. We applied a grid correction protocol as described in the methods section. However, the grid pattern still remained with the CUBIC samples.



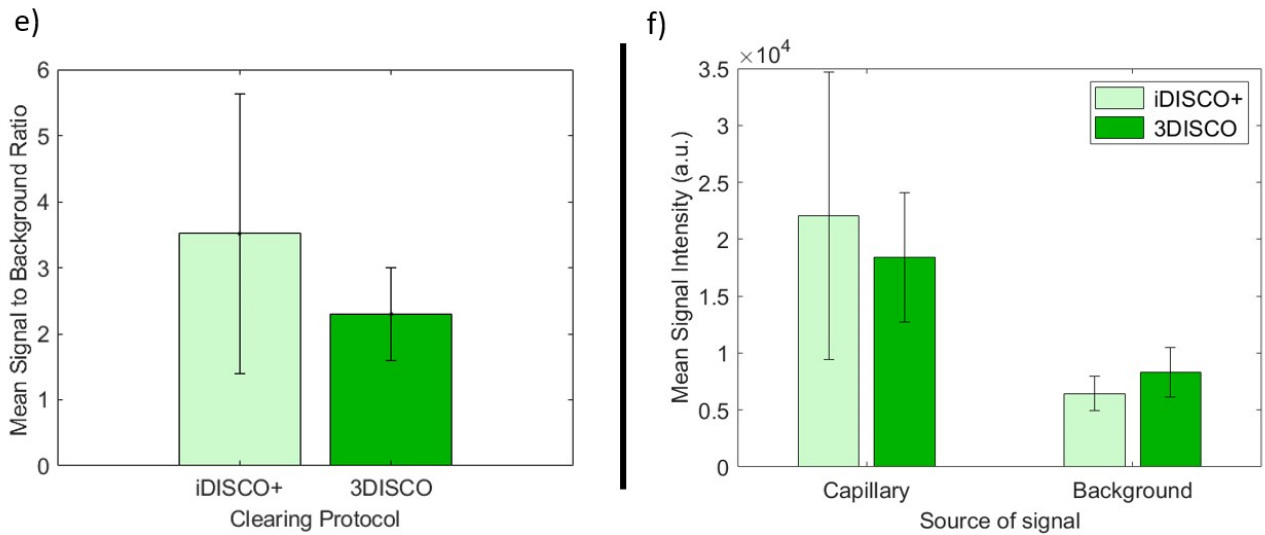


Figure 18. Depiction of vascular staining results using DISCO clearing methods in a mouse. A demonstration of vascular staining is shown from 2 mm thick homologous coronal slabs from the same mouse. The a) left hemisphere is cleared with iDISCO+ and the b) right hemisphere is cleared with modified 3DISCO. A zoomed-in view of the orange rectangle depicting the cortical layers is shown of both c) the iDISCO+ slab and d) the modified 3DISCO slab. The mouse was stained with 150 ul Alexa Fluor 647. A depiction of e) signal-to-background ratio with standard deviations and f) capillary and background signal intensity with standard deviations for both iDISCO+ and 3DISCO protocols.

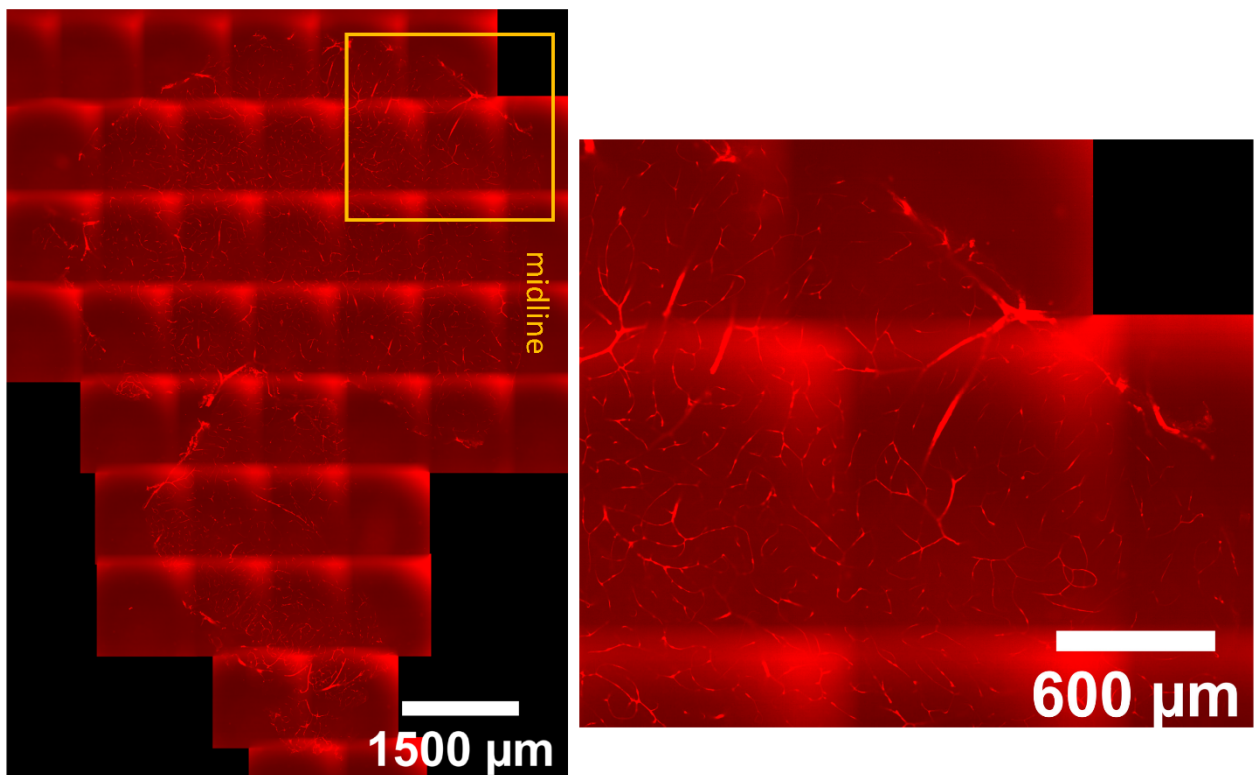


Figure 19. Depiction of blood vessel images from a CUBIC cleared mouse coronal slab. An overview

of a coronal slab cleared with CUBIC is shown on the left with a magnified view of the orange square on the right.

iv. Imaging results in the rat: Experiment 3

In the rat experiments, we injected the dye through the tail vein with volumes of 1.2 ml (Figure 20a, c) and 0.6 ml (Figure 20b, d) with 5mg/3ml WGA Alexa fluor 647. We first used 1.2 ml of dye. We based our decision to use this volume on the fixed dye volume we used in mice (150 μ l) which was suggested by Todorov *et al.* (2020). We performed a cross-product calculation of the blood volume in mice and rats, and the dye volume we used for mice blood vessel labeling. This gave us the dye volume we used in rats. We additionally tested 0.6 ml to see if using less dye could still yield good results. The left hemisphere demonstrates an example with iDISCO+ clearing and the right hemisphere shows an image of a 3DISCO cleared sample. The rat brain's vascular labeling through tail vein injection demonstrates homogenous labeling. There are no dark areas that show a lack of labeling. In Figure 20, we can spot many ascending venules/penetrating arterioles. We can especially distinguish the cortex from the white matter. Mainly from the coronal slabs injected with 1.2 ml of the dye, we can also identify the inner, middle, and outer cortical layers as shown by the green, yellow, and red rectangles respectively. These separate regions were not as visible in the rat coronal slabs injected with 0.6 ml Alexa Fluor. The background around the blood vessels in 3DISCO cleared sample was not as defined with the 1.2 ml injection compared to 0.6 ml. The imaging results from the CUBIC clearing were poor (data not shown) since most of the slabs had no signal in the vasculature.

We compared the signal-to-background ratio of iDISCO+ to 3DISCO cleared samples for samples stained with 1.2 ml and 0.6 ml of WGA Alexa Fluor 647 (Figure 21). The mean signal-to-background ratio for the labeling with 1.2 ml volume were 4.387 ± 1.650 and 2.295 ± 0.596 for iDISCO+ and 3DISCO, respectively. The means for the 0.6 ml were 2.829 ± 0.833 and 1.853 ± 0.411 for iDISCO+ and 3DISCO, respectively. We can see the ratio is greater with both iDISCO+ clearing examples. Although the standard deviation is higher with iDISCO+, we still get a statistically significant difference in the means using student t-test with a 99.9% confidence level ($\alpha=0.001$, for iDISCO+ vs. 3DISCO with 1.2 ml: $t_{\text{stat}} > t_{\text{crit}} \rightarrow 8.347 > 3.46$, DOF=60; and with 0.6 ml: $t_{\text{stat}} > t_{\text{crit}} \rightarrow 7.354 > 3.416$, DOF=80). In addition, we directly compared the capillary intensities and the background intensity values. The mean capillary signals obtained with iDISCO+ cleared samples (43167 ± 16517 for 1.2ml and 43830 ± 12589 for 0.6ml) was higher relative to

the mean capillary signals obtained with 3DISCO (27903 ± 10887 for 1.2 ml and 40883 ± 12521 for 0.6 ml). Conversely, there was a lower background signal with iDISCO+ clearing. The background signals for 1.2 ml dye volume were 9850 ± 1423 for iDISCO+ and 12141 ± 3091 for 3DISCO. The background signals from 0.6 ml dye injection were 15580 ± 2385 for iDISCO+ and 22055 ± 4619 for 3DISCO. Thus, both the higher capillary signal and the lower background fluorescence contributed to the higher signal-to-background ratio demonstrated by the iDISCO+ protocol.

Interestingly, when comparing the signals between the clearing protocols, we found a statistically significant difference between the background signals. The background signal was lower in iDISCO+ cleared samples compared to the 3DISCO cleared samples, with 99.9% confidence level ($\alpha=0.001$, with 1.2 ml: $t_{\text{stat}} > t_{\text{crit}} \rightarrow 4.665 > 3.460$, DOF=60, and for 0.6ml: $t_{\text{stat}} > t_{\text{crit}} \rightarrow 8.630 > 3.416$, DOF=80). However, the capillary signals obtained with the two methods following the injection of the 0.6 ml dye solution did not show a statistically significant difference ($\alpha=0.3$, $t_{\text{stat}} > t_{\text{crit}} \rightarrow 1.150 > 1.042$, DOF=100). In contrast, after injecting the higher volume (1.2 ml), there was a significant difference in the mean capillary signals with a 99.9% confidence level ($\alpha=0.001$, $t_{\text{stat}} > t_{\text{crit}} \rightarrow 5.346 > 3.416$, DOF=80).

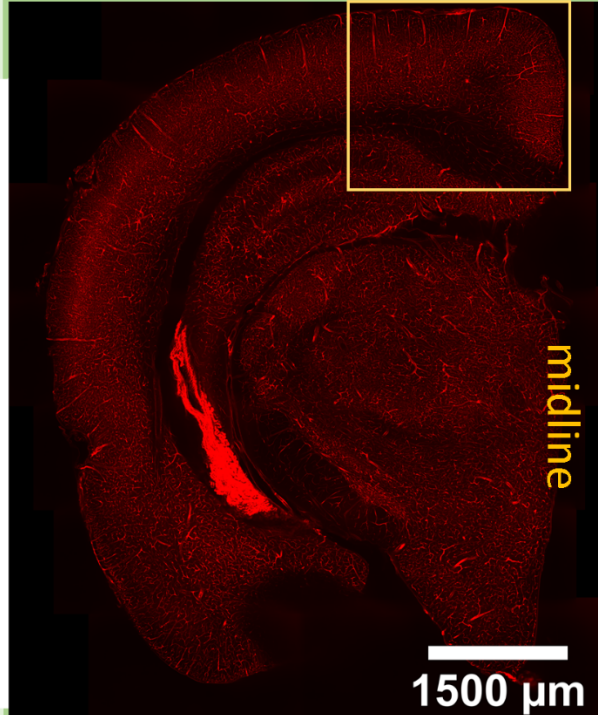
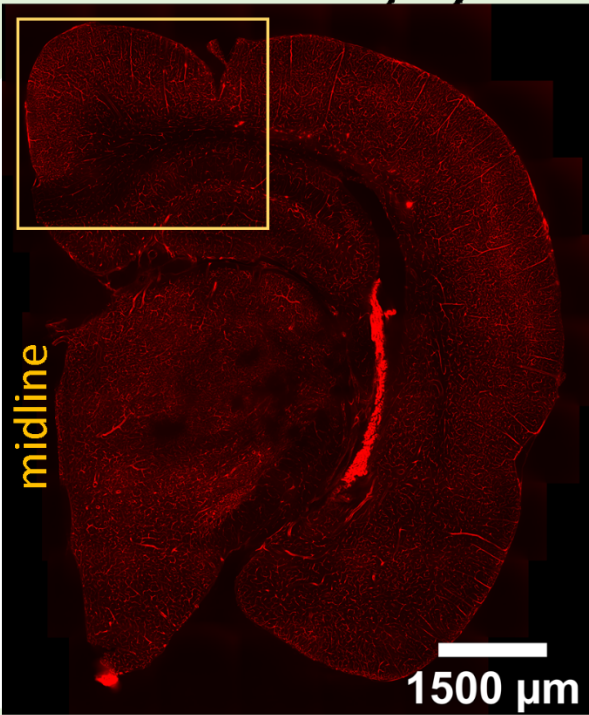
We also performed a direct comparison between the signal-to-background ratio of 1.2 ml to 0.6 ml Alexa Fluor staining (Figure 22). We observed a statistically significant difference in the signal-to-background ratio ($\alpha=0.001$, DOF=80, with iDISCO+: $t_{\text{stat}} > t_{\text{crit}} \rightarrow 5.900 > 3.416$; and for 3DISCO: $t_{\text{stat}} > t_{\text{crit}} \rightarrow 4.269 > 3.416$). For comparing the signal-to-background ratios obtained with injections of 1.2 ml and 0.6 ml dye and iDISCO+ clearing, the difference in the mean capillary signals was relatively small, such that the null hypothesis could not be rejected ($\alpha=0.5$, DOF=80, $t_{\text{stat}} = 0.221$ and $> t_{\text{crit}} = 0.678$). The main factor that led to the difference in signal-to-background ratio was the difference in the background signal. Here, this difference was statistically significant ($\alpha=0.001$, DOF=80, $t_{\text{stat}} > t_{\text{crit}} \rightarrow 14.289 > 3.416$). In contrast, comparing the signal-to-background ratios obtained with injections of 0.6 ml and 1.2 ml dyes and 3DISCO clearing, there were significant differences in both the capillary and the background signals ($\alpha=0.001$, for capillary: $t_{\text{stat}} > t_{\text{crit}} \rightarrow 5.4198 > 3.390$, DOF=100; for background $t_{\text{stat}} > t_{\text{crit}} \rightarrow 12.359 > 3.416$, DOF=80).

Finally, we typically used 3 hours of PFA post-fixation in mice and 6 hours in rats. We incubated several slabs for 24 hours to see if overnight fixation would impact the autofluorescence of the sample. We did not observe a difference (Figure 23).

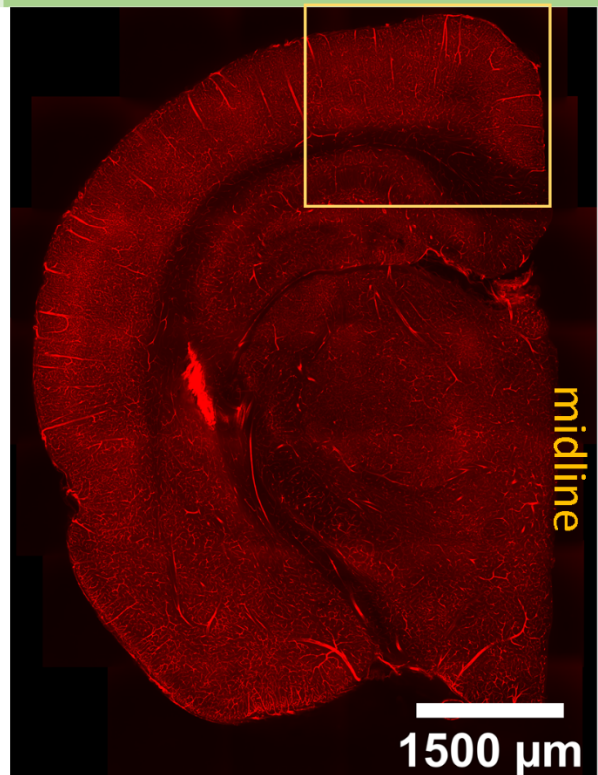
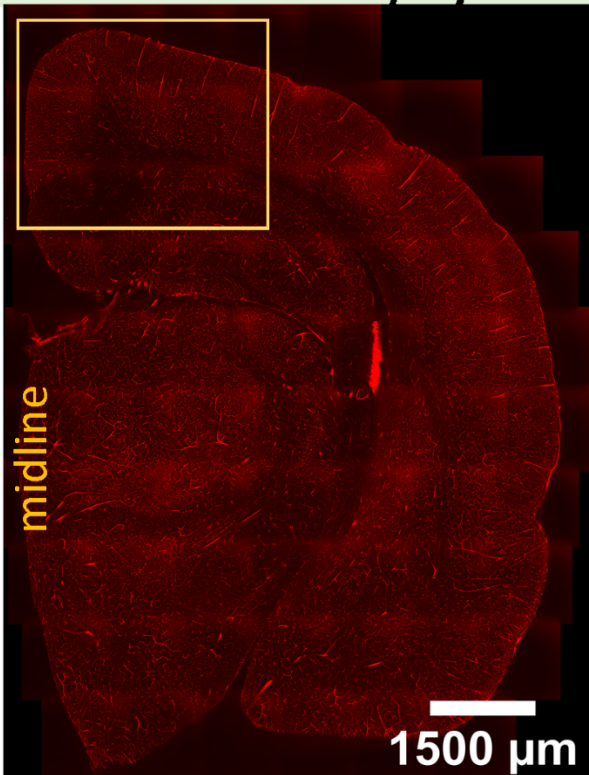
iDISCO+ Left Hemisphere

3DISCO Right Hemisphere

a) Dye Volume: 1.2 ml



b) Dye Volume: 0.6 ml



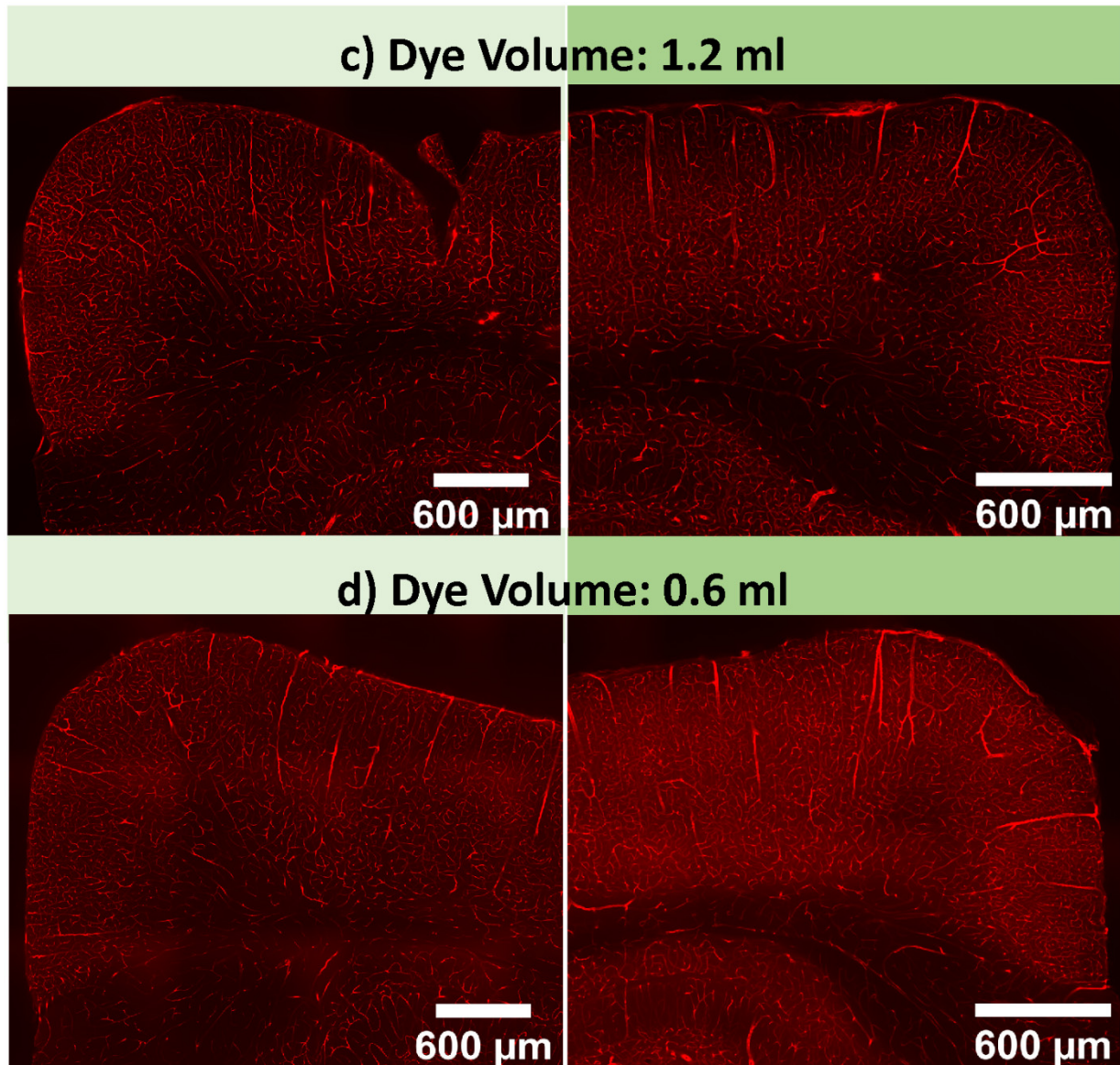
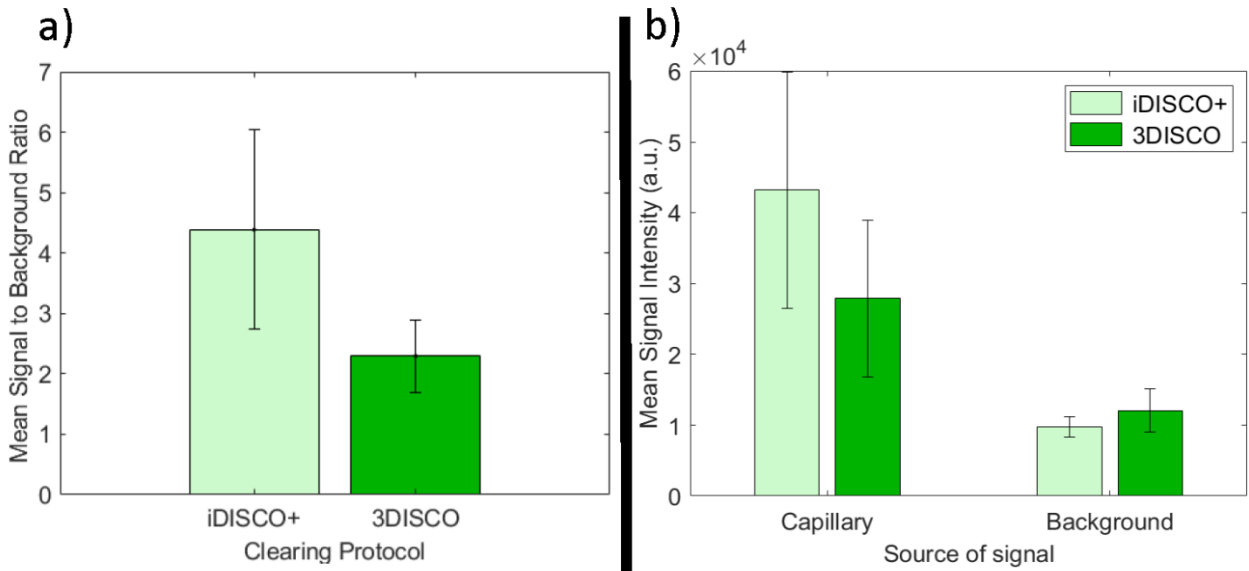


Figure 20. Depiction of vascular labeling results using DISCO clearing methods in a rat. A demonstration of vascular labeling is shown from 2 mm thick homologous (each slab from one hemisphere contralateral to the other slab) coronal slabs from a rat injected with a) 1.2 ml and b) 0.6 ml of Alexa Fluor 649. The injection was done through the tail vein. The images on the left show clearing of the left hemisphere with iDISCO+. The images on the right show clearing of the right hemisphere with modified 3DISCO. Panels c) and d) show zoomed-in views of the orange rectangles depicting the cortical layers from the rat brain labeled with 1.2 ml and 0.6 ml volume of dye, respectively.

1.2 ml of WGA Alexa Fluor 647



0.6 ml of WGA Alexa Fluor 647

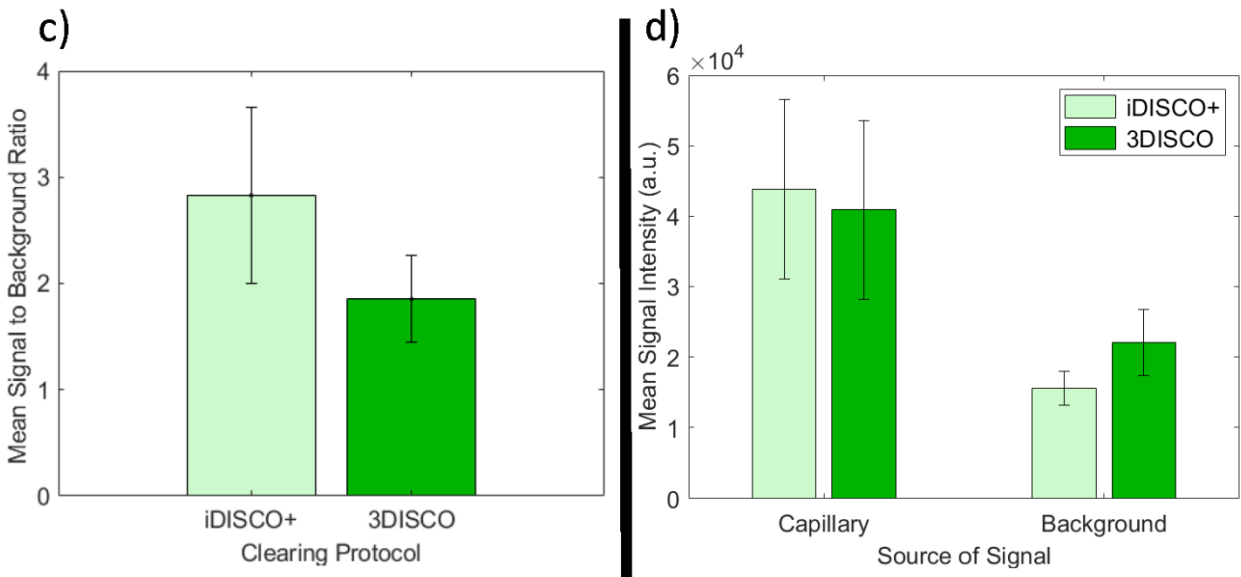


Figure 21. Comparison of signal-to-background ratio and signal and background intensities between clearing protocols. Depiction of a) signal-to-background ratio with standard deviations and b) capillary and background signal intensity with standard deviations for both iDISCO+ and 3DISCO protocols using 1.2 ml of WGA Alexa Fluor 647. Depiction of c) signal-to-background ratio with standard deviations and d) capillary and background signal intensity with standard deviations for both iDISCO+ and 3DISCO protocols using 0.6 ml of WGA Alexa Fluor 647.

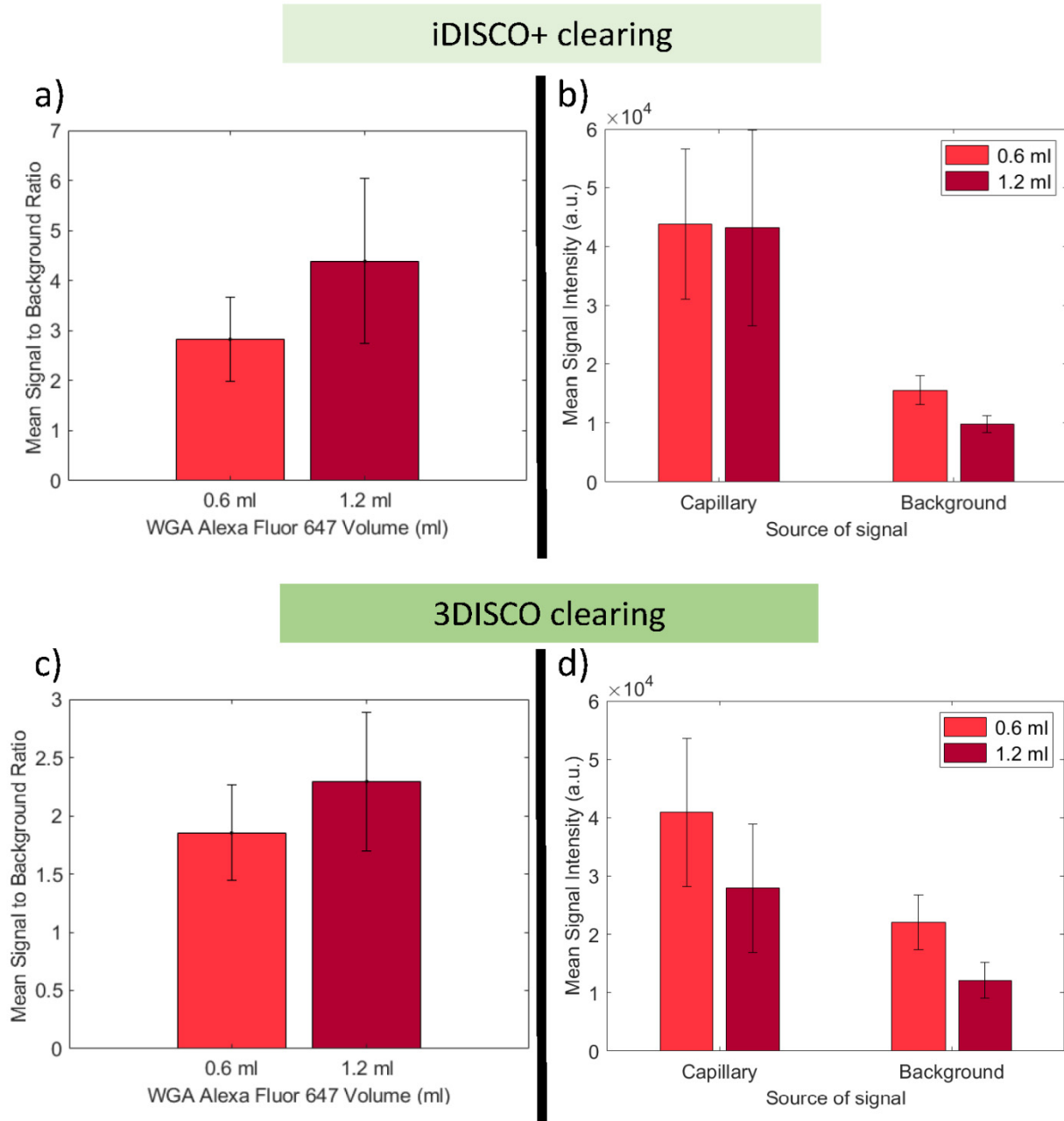
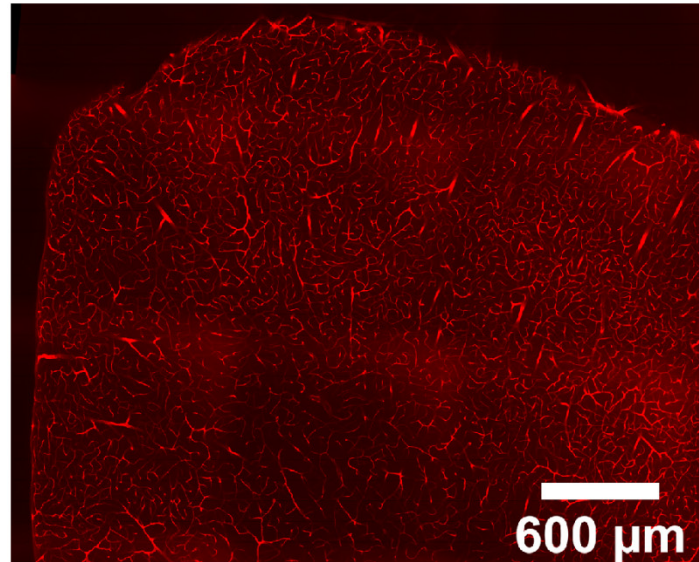
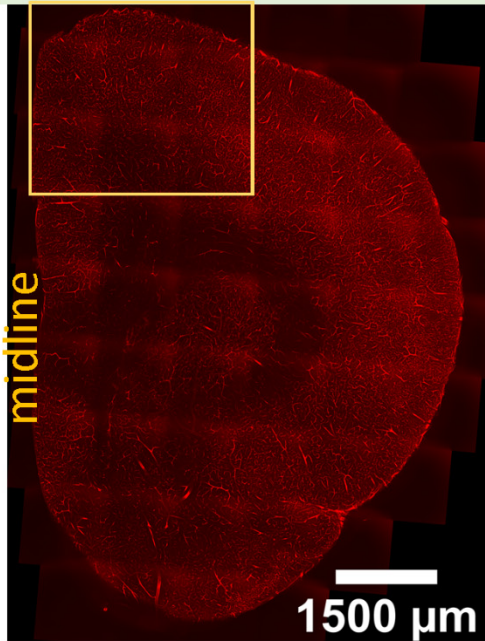


Figure 22. Comparison of signal-to-background ratio and signal and background intensities between different dye volumes. Depiction of a) signal-to-background ratio with standard deviations and b) capillary and background signal intensity with standard deviations for labeling with both 1.2 ml and 0.6 ml WGA Alexa Fluor 647 and iDISCO+ clearing. Depiction of c) signal-to-background ratio with standard deviations and d) capillary and background signal intensity with standard deviations for labeling with both 1.2 ml and 0.6 ml WGA Alexa Fluor 647 and 3DISCO+ clearing

a) iDISCO+
6 hours PFA post-fixation



b) iDISCO+
24 hours PFA post-fixation

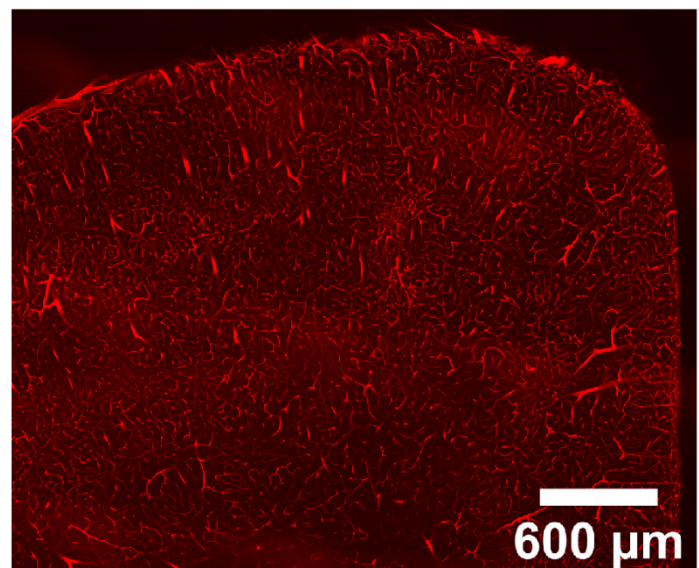
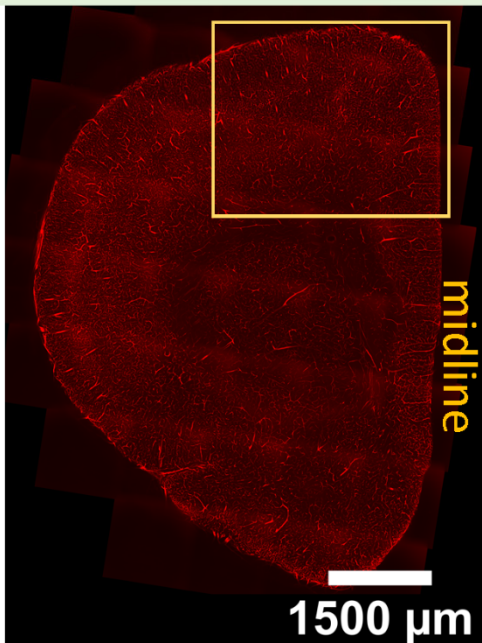


Figure 23. Depiction of vascular labeling results using the iDISCO+ clearing method in a rat. A demonstration of vascular labeling is shown from 2 mm thick contra-lateral coronal slabs from a rat injected with 1.2 ml of Alexa Fluor 649 through the tail vein. The PFA post-fixation duration after brain extraction

was varied between these two brain slabs. a) The left hemisphere was post-fixed for 6 hours and b) the right hemisphere for 24 hours. In both cases, the samples were cleared with iDISCO+. A zoomed-in view of the orange rectangles depicting the cortical- depth-dependent labeling from the rat brain is shown on the right-hand side.

Figure 24 demonstrates data obtained from a single point confocal LSM880 microscope. The images show data from a 2 mm slab obtained from the rat injected with 1.2 ml of WGA Alexa Fluor 647. The slab was centered at -2 mm from bregma, and it was cleared with iDISCO+. The slab was placed on the imaging dish such that its posterior side was facing the laser and the objective (both located below the sample). The figure shows the intensity projection of 10 planes from each of the following depth ranges: 200 μm to 220 μm (a), 300 μm to 320 μm (b), and 400 μm to 420 μm (c) into the samples. The step size between the planes is 2 μm . At these planes, we can identify the cortex as shown by the yellow arrows and the white matter underneath (blue arrows) (Figure 24a, b). We use panel C as an example to show the cortical layers. The red-orange, orange-yellow, yellow-green, green-blue, and blue-purple lines show an approximate delineation of layer 1, layers 2/3, layer 4, layer 5, and layer 6 respectively, in the somatosensory area (Sotero et al., 2015).

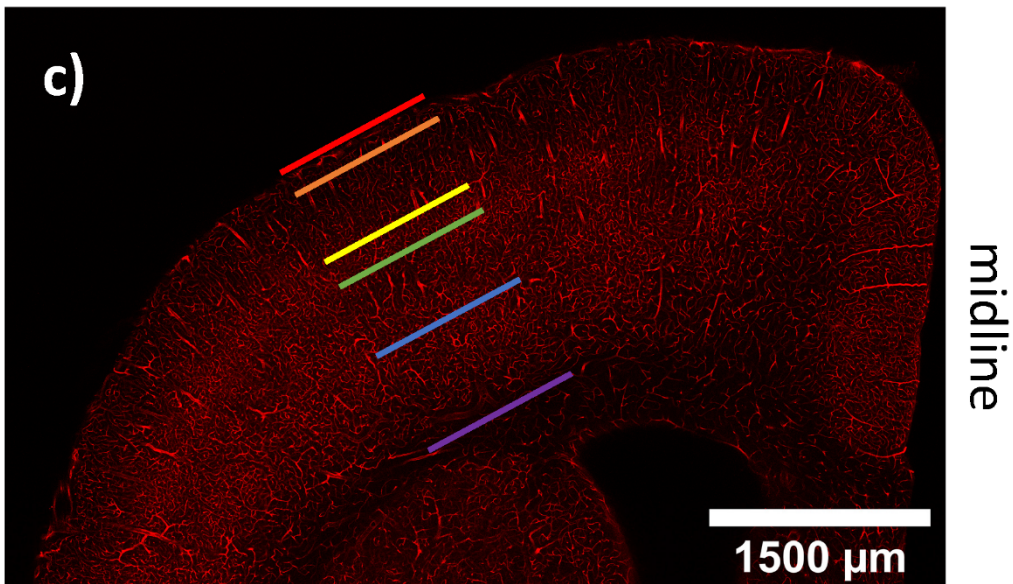
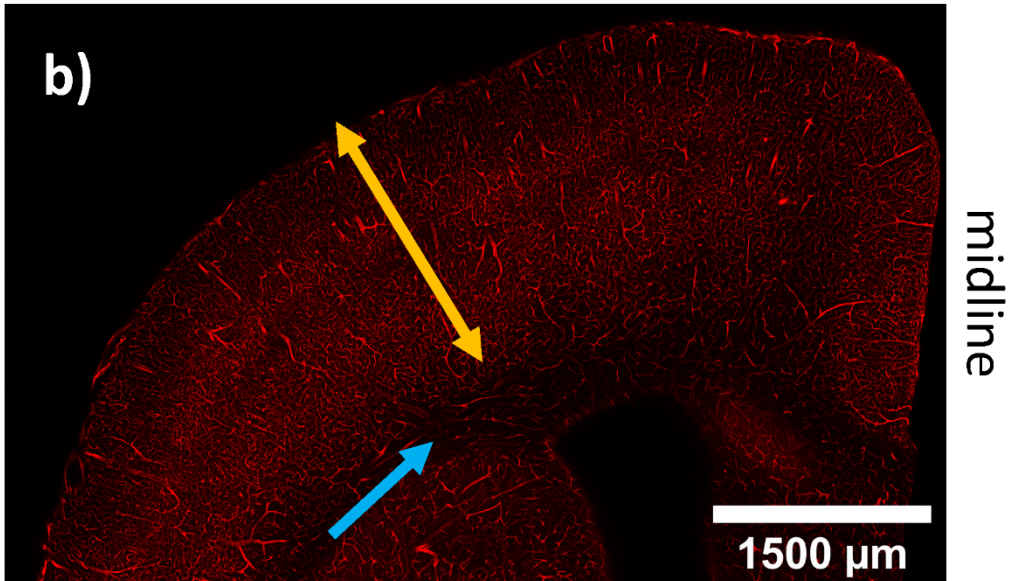
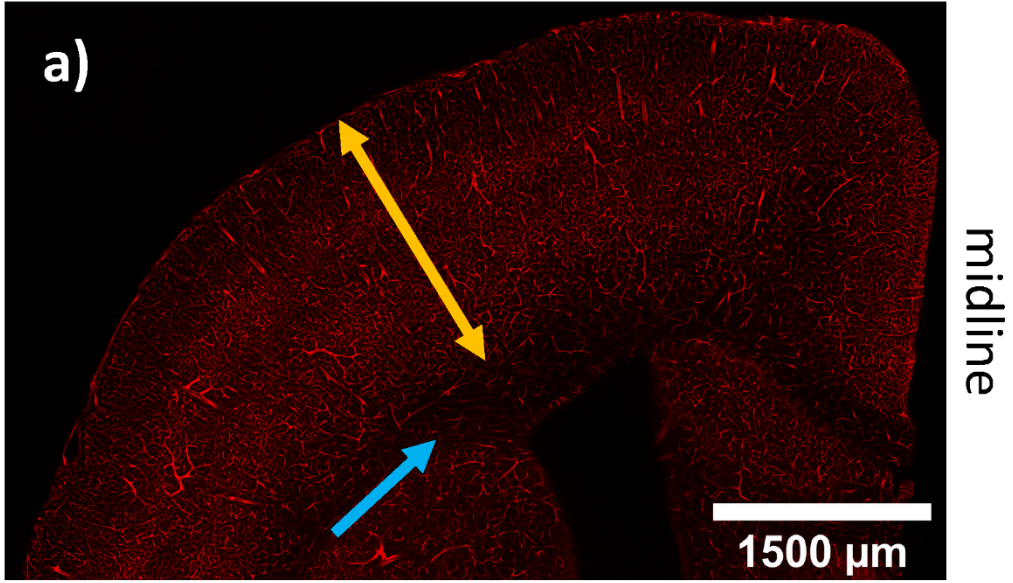


Figure 24. Average intensity z-projection of 10 planes using a single point confocal microscope (LSM880) from a 2 mm thick rat coronal brain slab. An average intensity projection of 10 planes is shown where the step size between the planes is 2 μm . In a) there is a z-projection from z-plane 200 μm to 220 μm , in b) from 300 μm to 320 μm , and in c) from 400 μm to 420 μm . The axis of increasing cortical depth is shown with the yellow arrows. The white matter approximately overlaps with the dark area underneath (blue arrow) as shown in a) and b). The labeling shows cortical depth-dependent variations, as demonstrated in c). The red-orange, orange-yellow, yellow-green, green-blue, and blue-purple lines approximately mark layer 1, layers 2/3, layer 4, layer 5, and layer 6 respectively in the somatosensory area (Sotero et al., 2015).

c. Dye volume selection: Experiment 4

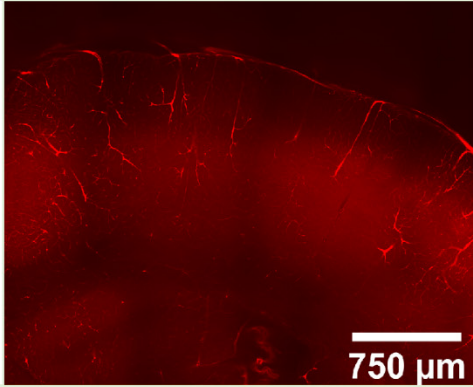
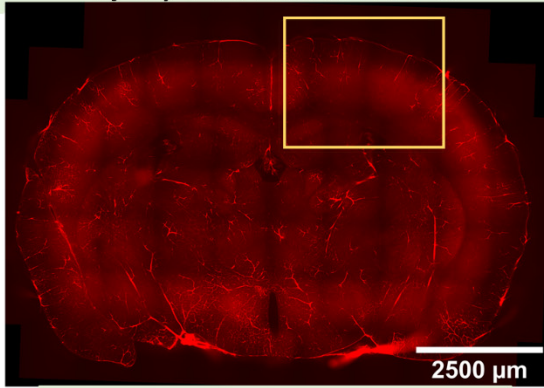
We varied the amount of dye that was injected into the vascular system to search for an optimal volume. With a concentration of 1.67 mg/ml, we tested intracardiac injections of 250 μl , 200 μl , 150 μl , and 100 μl in 4 different mice. Figure 25 shows complete 3 mm-thick coronal slabs that span from bregma (0 mm) to -3 mm from bregma. They were all cleared with iDISCO+. For all 4 mice, the perfusion had seemed to go well. However, the mice injected with 150 μl of the dye had patchy staining (Figure 25b). There were dark areas without vessels. In general, for all samples, we can identify venules/arterioles spanning the cortical depth perpendicularly to the cortical surface. Looking at the regions of interest more closely, we see that the capillaries were less visible for the mouse stained with 100 μl of the dye (Figure 25a): the signal to background ratio seemed lower. The coronal slabs with 200 μl and 250 μl gave the best signal-to-background ratio in terms of capillaries (Figure 25c, d). We evaluated quantitatively the signal-to-background ratio of the mice stained with 100 μl , 200 μl , and 250 μl . The data from the mouse stained with 150 μl were omitted from the calculation since the labeling was unsuccessful and it had regions with no data. We looked at the middle cortical layer from 5 different regions of interest (figure 26a). The mean signal-to-background ratio for each mouse from each region of interest is shown in Figure 26b. Table 6 includes the mean and the standard deviation values. The mice stained with 100 μl gave the lowest ratio in all 5 cases. However, in certain ROIs, the difference was more prominent. We did not notice a significant difference between the 200 μl and 250 μl .

Region of interests	Mice labeled with different volumes of WGA Alexa Fluor 594		
	100 μ l	200 μ l	250 μ l
# 1	1.389 \pm 0.128	1.671 \pm 0.211	1.614 \pm 0.335
# 2	1.500 \pm 0.246	1.566 \pm 0.192	2.014 \pm 0.564
# 3	1.543 \pm 0.299	1.579 \pm 0.234	1.589 \pm 0.194
# 4	1.383 \pm 0.159	1.587 \pm 0.236	1.561 \pm 0.182
# 5	1.330 \pm 0.087	1.362 \pm 0.153	1.471 \pm 0.219

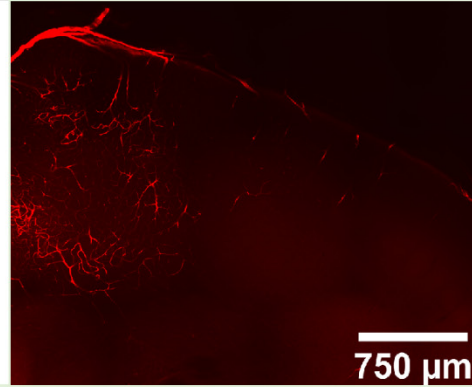
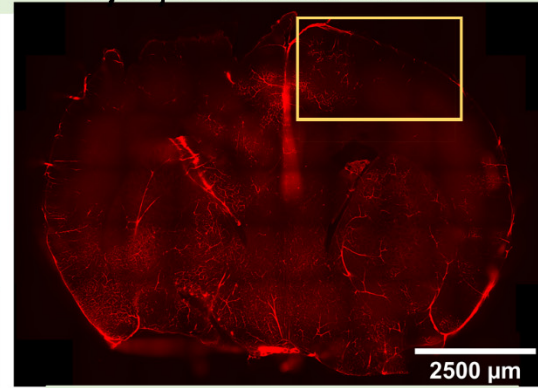
Table 6. Mean and standard deviation values of the signal-to-background ratios for each mouse from each region of interest. The rows represent the 5 different regions of interest. The columns represent the mice labeled with 100 μ l, 200 μ l, and 250 μ l of WGA Alexa Fluor 594.

To test the differences statistically, we performed a one-way ANOVA statistical test of the capillary signals from all the regions between the 3 mice ($n=50$ / mouse). The F test statistic (84.4) is greater than the F critical value ($F=7.3211$, $\alpha = 0.001$). Thus, we concluded that there was a statistical difference between the 3 means of the capillary signals (39679 ± 7656 for 100 μ l, 32382 ± 7232 for 200 μ l, 33743 ± 9771 for 250 μ l). We also evaluated the background signal ($n=50$ / mouse) with one-way ANOVA. Again, we found a statistical difference ($F_{\text{test}}=131$, $F=7.3211$, $\alpha=0.001$) between the 3 means (27770 ± 3478 for 100 μ l, 21043 ± 4365 for 200 μ l, 20431 ± 3454 for 250 μ l). With the Tukey Kramer multiple comparison test, we found that there was a significant difference in the capillary signals between 100 μ l versus 200 μ l ($Q_u=5.211$, $\alpha=0.001$) and 100 μ l versus 250 μ l ($Q_u=4.523$, $\alpha=0.005$). For the background signal, we found a statistical difference between 100 μ l versus 200 μ l ($Q_u=5.211$, $\alpha=0.001$) and 100 μ l versus 250 μ l ($Q_u=5.211$, $\alpha=0.001$). There was no significant difference between the two capillary mean signals and the two background mean signals when comparing 200 μ l vs 250 μ l injections ($\alpha=0.1$).

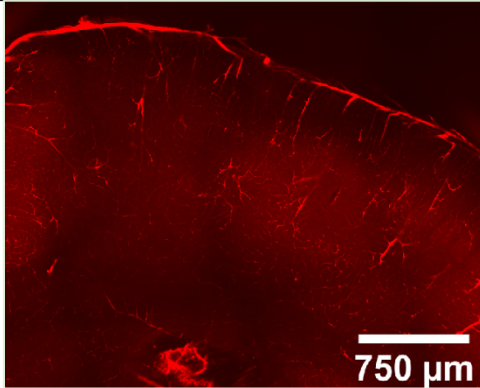
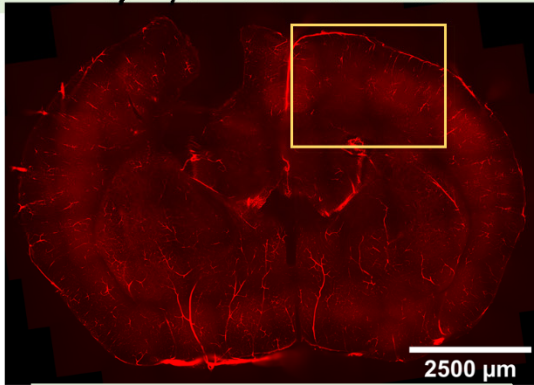
a) Dye Volume: 100 ul



b) Dye Volume: 150 ul



c) Dye Volume: 200 ul



d) Dye Volume: 250 ul

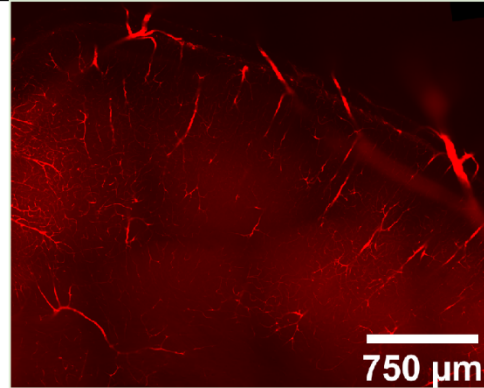
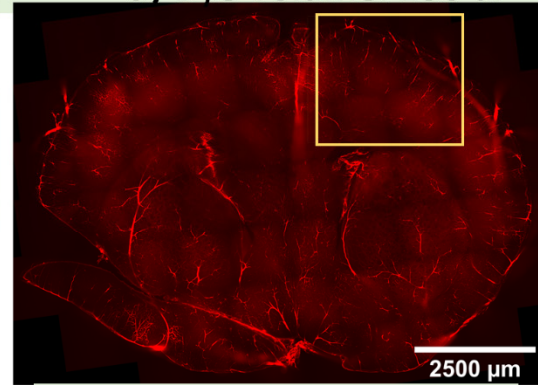


Figure 25. Vascular imaging results from 4 mice injected with different volumes of Alexa Fluor 594. The complete coronal slabs and magnified views of the orange rectangles show the cortical depth-dependent labeling. The images were obtained from 4 mice injected with a) 100 ul, b) 150 ul, c) 200 ul, and d) 250 ul of Alexa Fluor.

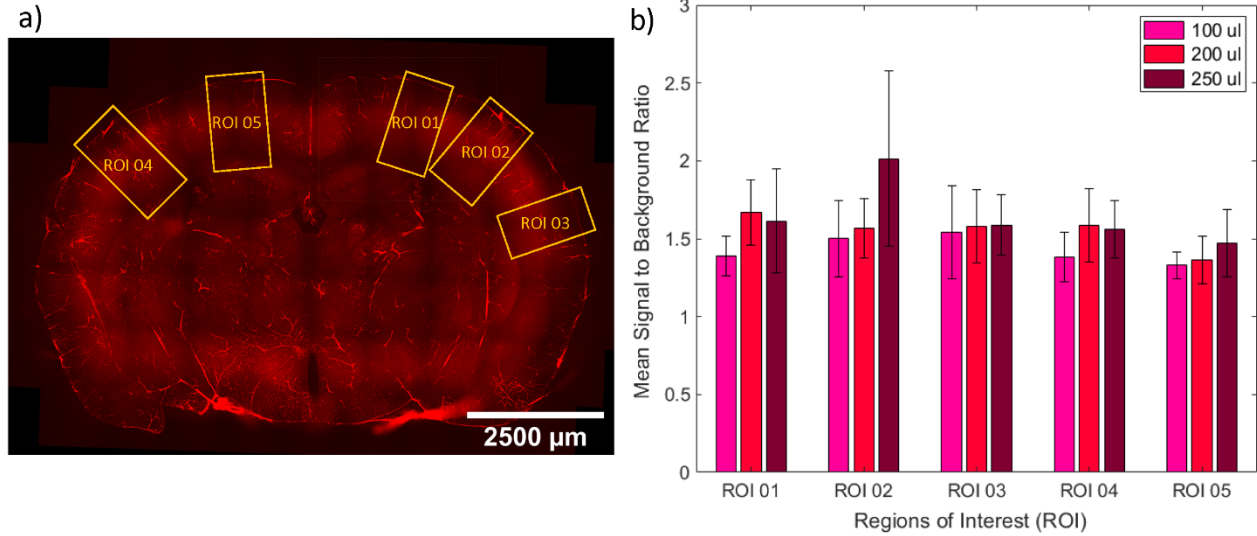


Figure 26. Signal to background ratio from 5 different regions of interest (ROI) in mouse brains. Signal to background ratio was evaluated from the middle cortical layer of 5 different ROI around the somatosensory area. a). The example shown in panel a is from a coronal slab of a mouse injected with 100 ul of WGA Alexa Fluor 594. The intensity was sampled from twenty points (10 points from capillaries and 10 from the background adjacent to the selected capillaries) per region of interest. b) The bar graph demonstrates the mean and the standard deviation of the signal-to-background ratio from each region and from mice stained with 100 ul (magenta bars), 200 ul (red bars), 250 ul (dark red bars) of WGA Alexa Fluor 594.

From the same set of mice, we also compared iDISCO+ vs 3DISCO cleared slabs (Figure 27). In each mouse, we used a 3 mm-thick coronal slab located from -3 mm to -6 mm from the bregma. The right and left hemispheres were cleared with iDISCO+ and modified 3DISCO, respectively. Again, we noticed inhomogeneous labeling in the slabs from the mouse that received with 150 μ l. It was particularly the neocortical areas that were not properly labeled (Figure 27b). We obtained the most homogenous labeling and best signal-to-background ratio with the samples stained with 200 μ l (Figure 27c). However, there was a structural distortion artifact that occurred during the clearing due to a cut made during brain extraction. Although the right hemisphere of the coronal section stained with 250 μ l gave a good signal, we noticed a lack of vascular labeling within the left hemisphere that was cleared with 3DISCO (Figure 27d).

For both iDISCO+ and 3DISCO cleared slabs, the images were processed the same way. Following stitching, a 2% percent pixel saturation was applied on the images. The 3DISCO cleared

samples resulted in bright images such that the signal-to-background ratio was reduced. Further data processing techniques would be necessary here.

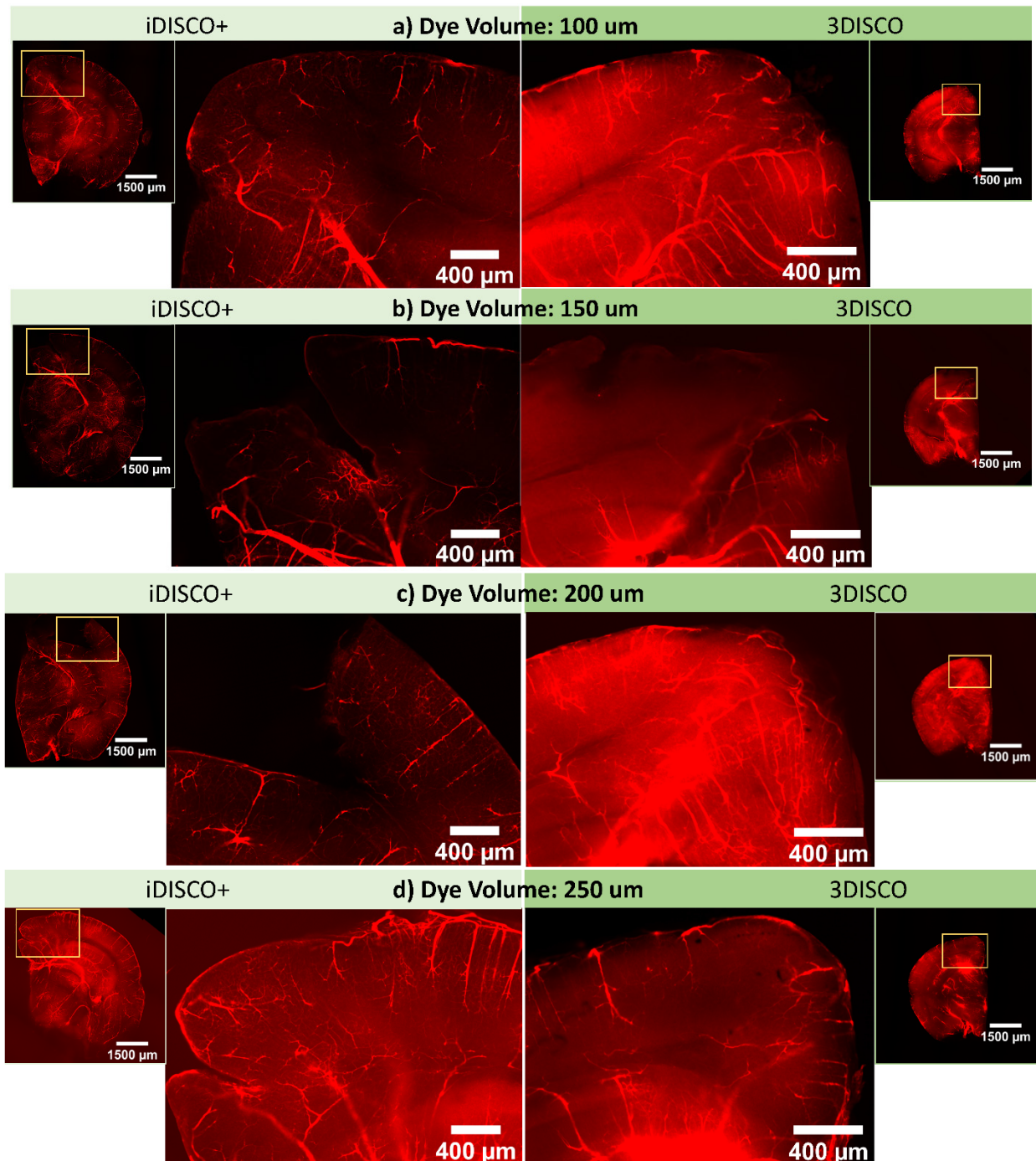


Figure 27. Imaging results obtained from iDISCO+ and 3DISCO clearing and labeling with 4 different volumes of WGA Alexa Fluor 594. A comparison between iDISCO+ and 3DISCO clearing of contralateral coronal brain slabs cut from the same region along the anterior-posterior axis. The left-hand side and right-hand side of the figure present images obtained with iDISCO+ and 3DISCO, respectively.

For each, a general view of the coronal slabs and a magnified view of the orange rectangles is shown. The panels show imaging results from 4 different mice labeled with a) 100 ul, b) 150 ul, c) 200 ul, and d) 250 ul volume of Alexa Fluor.

d. Effects of clearing on age and tissue thickness: Experiments 5 and 6

We varied the ages of the mice to test if there was an optimal mouse age for labeling the capillaries. We also varied the slab thickness, to test the effect of the thickness on the clearing result. We performed 2 experiments of this type. In the first experiment, all samples were cleared with iDISCO+. In the second experiment, they were cleared with CUBIC. The 5 different ages used were approximately 65, 115, 165, 185, and 229 days old. The 2 different slab thicknesses used were 2 mm and 3 mm.

i. Clearing results using the iDISCO+ protocol: Experiment 5

Figure 28 represents posterior slabs of 5 different mouse brains of varying ages. Panels a) and b) demonstrate clearing of the 3 mm and 2 mm thick slabs respectively. In terms of age, there was no noticeable change in the clearing quality. However, the tissue thickness did influence transparency. The homogeneity between the 2 mm thick coronal slabs and the surrounding BABB is higher relative to the 3 mm slabs. However, we noticed an outlier. The clearing 2 mm slab of the 65 days old mouse turned out darker than its 3 mm counterpart. Regardless of the “improvement” with the 2 mm slabs, all samples yielded optically transparent tissues in the same time frame (4 days).

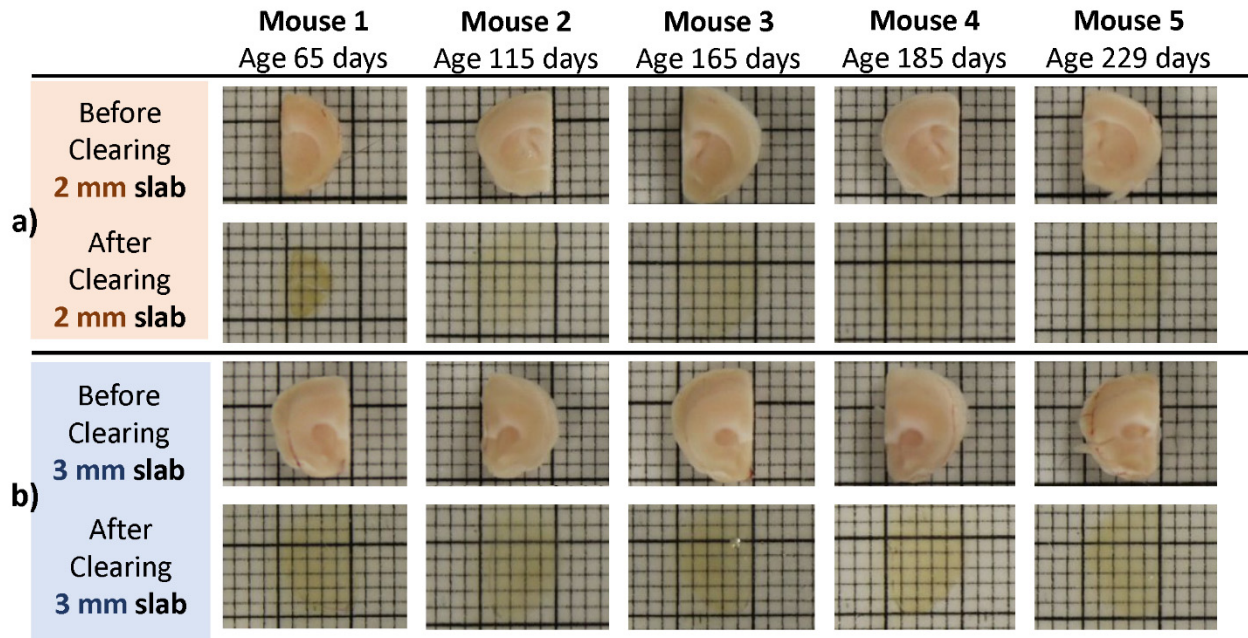


Figure 28. Comparison of clearing between different coronal slab thicknesses from mice of different ages. Depiction of iDISCO+ clearing of (a) 3 mm thick and (b) 2 mm thick coronal brain slabs. Columns 1 through 5 show results from 65, 115, 165, 185, 229 days old mice respectively.

ii. Imaging results from iDISCO+ protocol: Experiment 5

All 5 mice were stained intracardially with 150 ul of WGA Alexa Fluor 594. The perfusions of the mice of age 115 and 219 days did not go well. Consequently, the vasculature labeling of these 2 mice was inhomogeneous (Figure 29). The yellow arrows point at areas that have minimal to no vessels. Interestingly, even though the perfusion of the 65 days old mouse went well it also had areas with no labeled vessels (Figure 29). Mice of age 165 and 185 days old demonstrated vessel and capillary labeling throughout the cortex (Figure 30). However, we noticed some inconsistencies in the signal-to-background ratio between the left and right hemispheres in both mice. The capillary signals were dimmer in the right hemispheres.

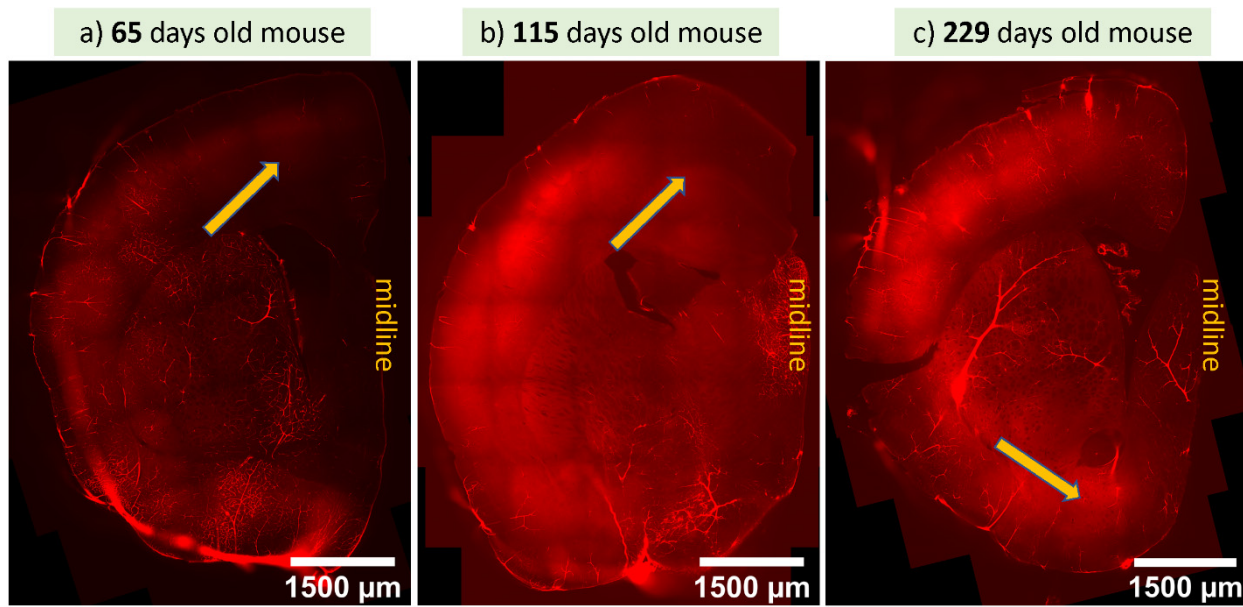


Figure 29. Observation of inhomogeneous labeling. Examples of inhomogeneous labeling are demonstrated in coronal brain slabs from 3 different mice of varying ages: a), b), and c) present images obtained from 65 days-, 115 days-, and 229 days old mice, respectively. All slabs were cleared with the iDISCO+ protocol. The slabs are from the right hemisphere and span from 0 mm to -3 mm from bregma for the 65 and 229 days old mice, and from -1 mm to -3 mm from bregma for the 115 days old mouse. Images are shown from a depth of 1200 µm in the z-plane. Orange arrows illustrate areas of little to no blood vessel labeling.

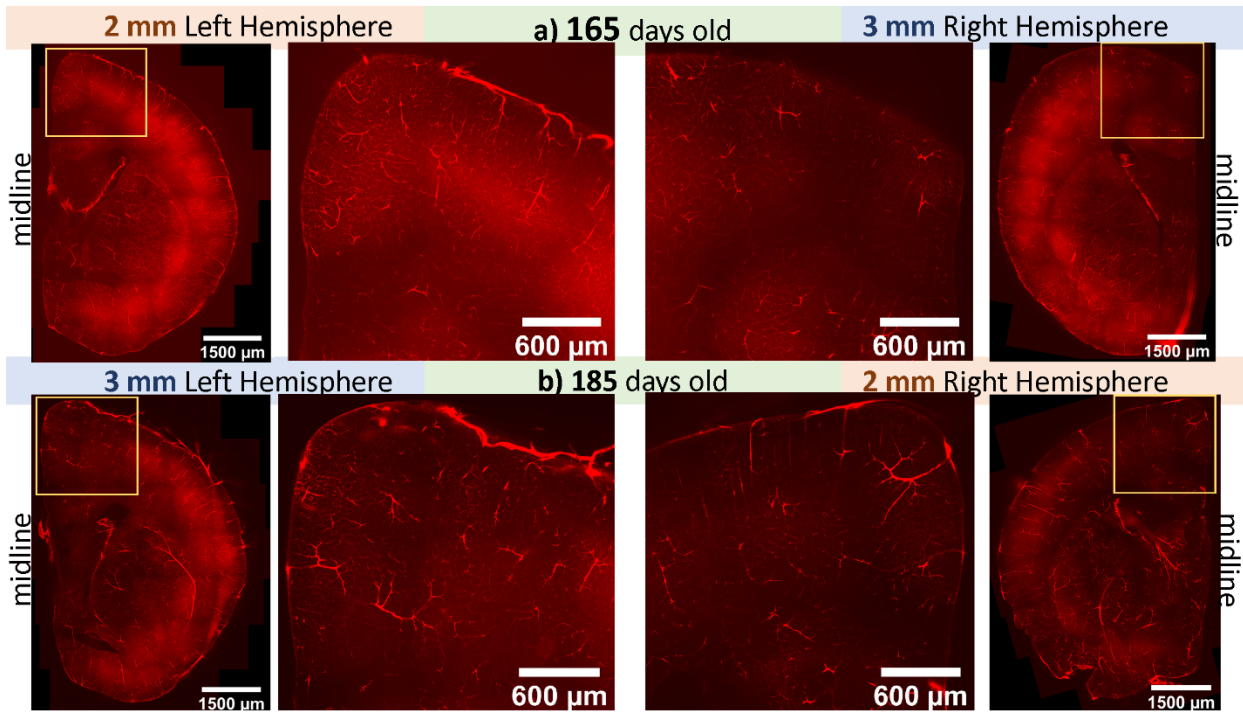


Figure 30. Imaging the vasculature in slabs with different thicknesses obtained from 2 mice of different ages. a) Blood vessels labeling of a 2 mm thick coronal slab (left hemisphere) and 3 mm thick coronal slab (right hemisphere) obtained from a 165 day old mouse. B) Labeling of a 3 mm thick coronal

slab (left hemisphere) and a 2 mm thick coronal slab (right hemisphere) obtained from a 185-day old mouse. Each mouse was injected with 150 ul Alexa Fluor 594.

iii. Clearing results from CUBIC protocol: Experiment 6

We performed a similar experiment with the CUBIC protocols (Figure 31). In general, with CUBIC, it took a few weeks to clear the coronal slabs. The longest part of the CUBIC clearing was the delipidation process. The brain slabs from the younger mice showed a higher delipidation rate relative to the older ones. This difference was most apparent in coronal slabs of 3 mm thick (blue rectangle). On day 28, the 3 mm thick coronal slab of the 219 day old mouse was cloudier in appearance relative to that of the 65 day old mouse. We also noticed that the rate of delipidation was slower with thicker brain slabs (orange rectangle). On day 37, the 3 mm slabs were more opaque compared to the 2 mm slabs. The longest time to delipidate was about 43 days, recorded for a 3 mm thick posterior slab of the 219 days old mouse. The shortest number of days to delipidated was 16 days, recorded for 2 mm thick anterior slabs of 65 and 115 days old mice. We performed the clearing process for this set of mice at room temperature. After refractive index matching, we found that all samples gave optically transparent tissues and about a 40% increase in volume.

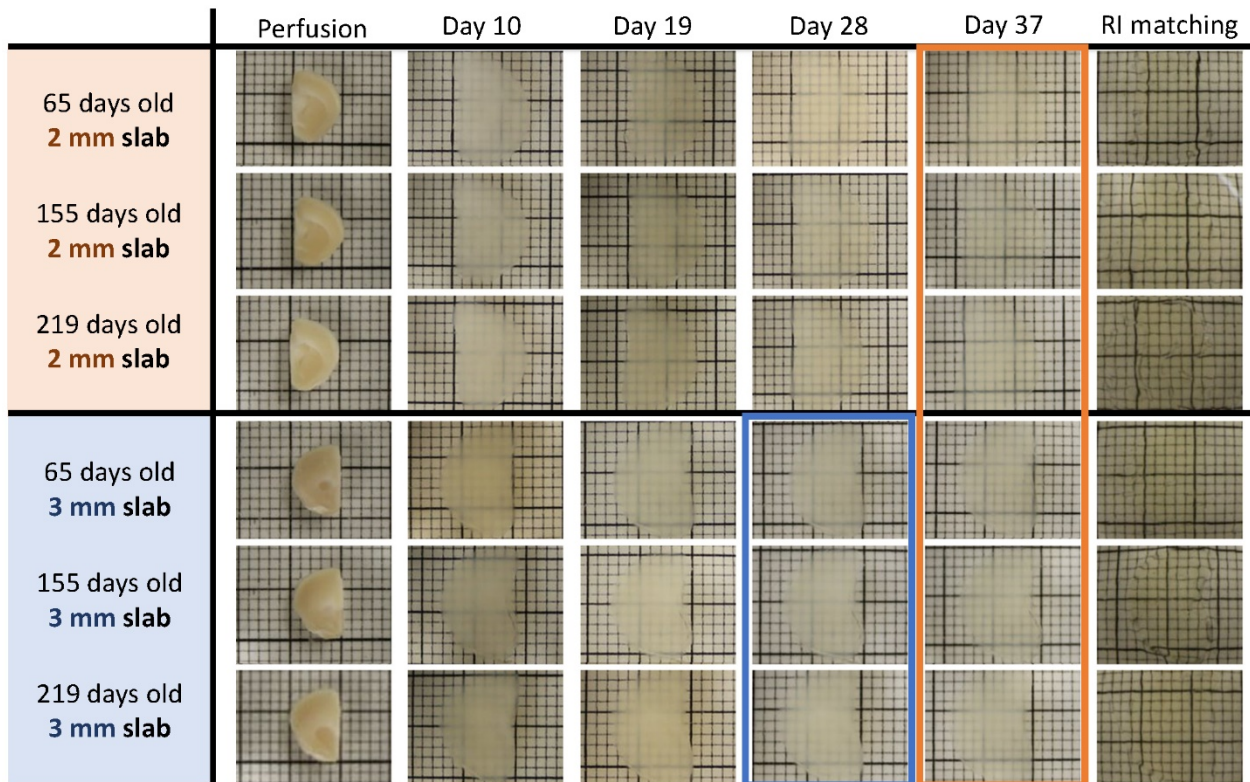


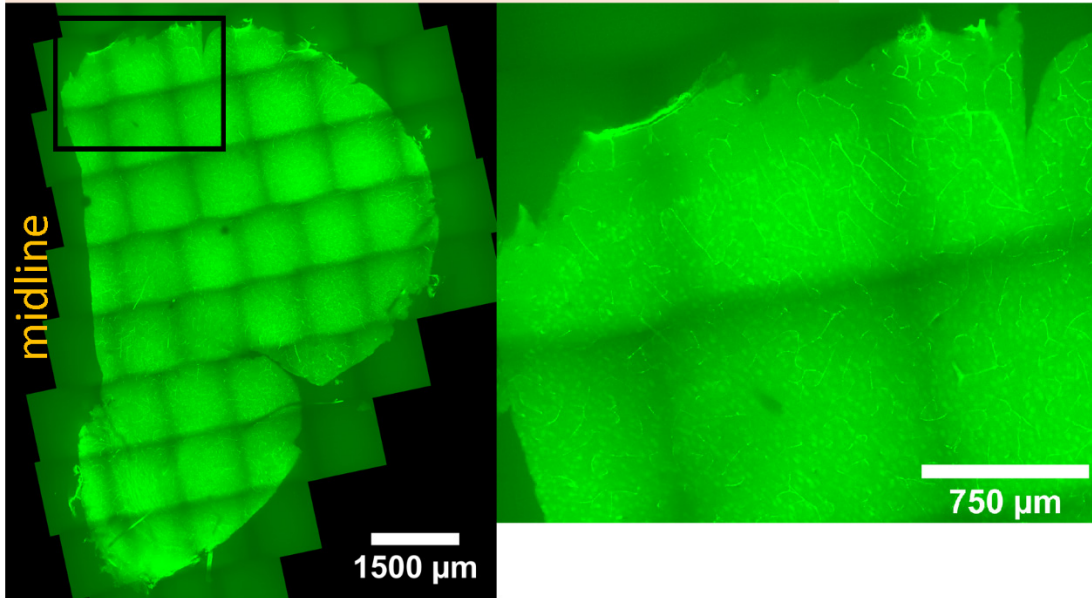
Figure 31. Depiction of the progress of CUBIC clearing applied to coronal slabs of different

thicknesses from mice of varying ages. In chronological order, the columns represent images of the progress of clearing after perfusion, delipidation for 10, 19, 28, and 37 days, and refractive index matching. The top 3 rows (marked in orange) show 2 mm coronal slabs of 65, 155, and 219 days old mice from top to bottom. Similarly, the bottom 3 rows demonstrate results from 3 mm thick slabs obtained from the same mice. The blue frame highlights small differences in the delipidation rates in mice of different age. The orange box highlights differences in the delipidation rate of 2 mm versus 3 mm thick brain slabs.

iv. Imaging results from CUBIC protocol: Experiment 6

For all 5 mice, the perfusions were performed without issues. We used 100 ul of dextran-FITC (6 ug/ul) to stain. We observed poor labeling in 4 out of the 5 mice. Barely any vessels were visible in the microscopy images. Solely, the slabs from the 105 days old mouse showed labeling signals in blood vessels. Figure 32 shows an example of homologous labeling of coronal slabs: 2 mm thick coronal slab (+2 mm to 0 mm from bregma) and 3 mm thick coronal slab (+2 mm to -1 mm from bregma). We can observe some blood vessels more clearly by looking at the magnified images in Figure 32. However, in addition to the vasculature, we noticed other cellular components that were labeled as well. Finally, during clearing, the extremities of the tissues lost their integrity. This can be seen by looking at the tissues' edges.

a) 105 days old mouse - 2 mm slab



b) 105 days old mouse - 3 mm slab

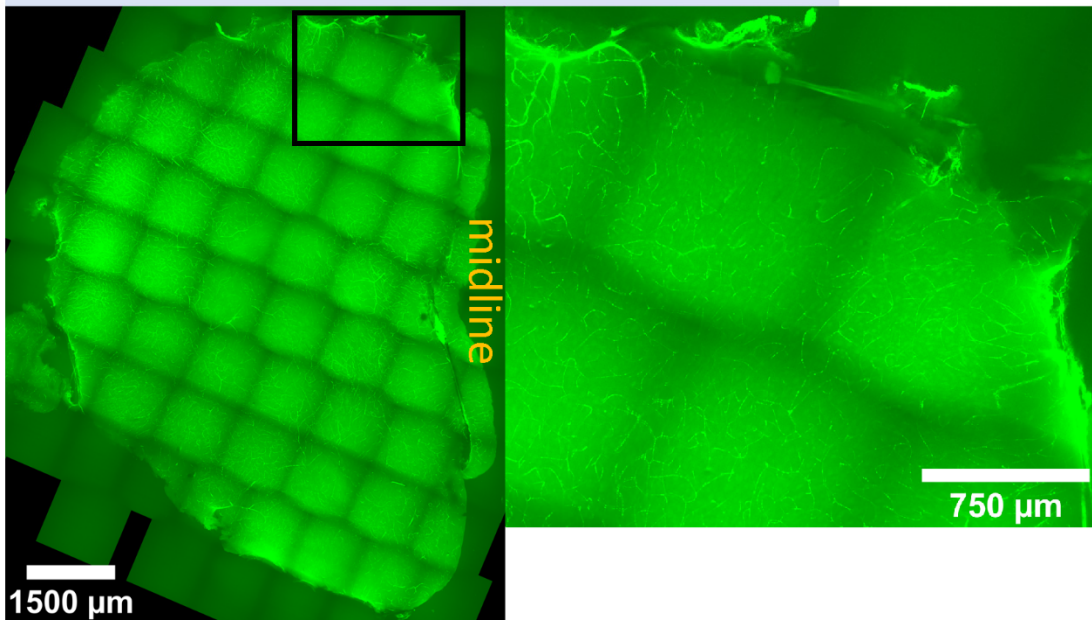


Figure 32. Demonstration of blood vessels labeling with dextran-FITC and CUBIC clearing. a) A 2 mm and b) a 3 mm thick homologous coronal brain slabs from a 115 days old mouse are shown. The 2 mm slab from the left hemisphere spans from +2 mm to 0 mm of the bregma. The 3 mm slab from the right hemisphere spans from +2 mm to -1 mm of the bregma. A zoomed-in view of the black square is shown on the right-hand side of each slab.

e. Staining by immersion: Experiment 7

We further attempted to label the vasculature by immersing 2 mm thick coronal brain slabs in 0.5 ml of the fluorophores for 14 days while on a shaker. The clearing of all the mouse brain slabs was performed with CUBIC. For 3 mice, the staining was performed after the PBS wash. In other words, before we started the delipidation. We varied the tissue PFA post-fixation time and the incubation temperature between these 3 mice. For an additional 2 mice, the vessels were stained after the end of the delipidation at room temperature. All left hemispheres were used for DyLight staining and all the right hemispheres for Alexa Fluor staining.

Examples of the delipidation progress are shown in Figure 33. Panels a) and b) show the delipidation progress of slabs cleared at room temperature. We saw that the rate of delipidation was relatively faster for the mouse brain slabs of panel b). This mouse was half the age of the mouse whose slab delipidation is presented in panel b). Looking at panel b) and c), the mice were of the same age. However, the brain slabs were cleared at 37°C in panel c). The delipidation rate was faster at 37°C compared to delipidation at room temperature. We can observe pale blue colors in the initial stages of the delipidation of the right hemisphere (panel c). Here, the immersion staining was performed prior to the removal of the lipids. Although generally, the CUBIC cleared samples increase in size, we noticed an outlier with the slabs of the mouse in panel b). Here, the brain slabs did not increase in size.

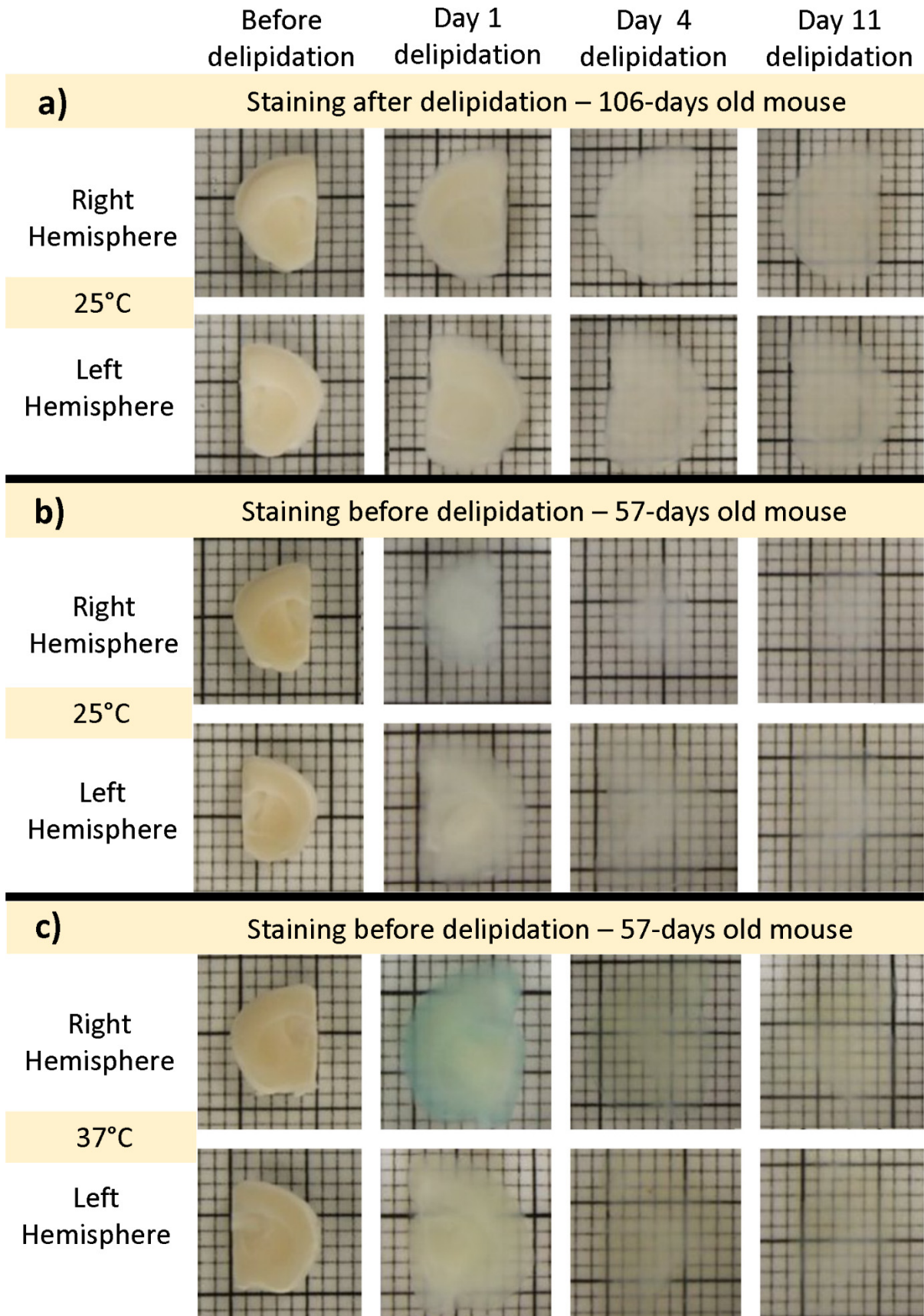


Figure 33. CUBIC delipidation progress of 3 different mice brains used for labeling by immersion. The delipidation of slabs from a) 106 days old and b) 57 days old mice was done at room temperature. c) The delipidation of a slab from a 57-day old mouse was done at 37°C. From left to right, we present images of the coronal slabs before delipidation, and 1 day, 4 days, and 11 days after the initiation of the delipidation process. The immersion in the dye was done after delipidation for the mouse in a) and prior to the initiation of delipidation for the mice in b) and c). The examples shown are from 2 mm contra-lateral coronal brain slabs centered on the same A-P coordinate. The slabs from the right and left hemispheres were immersed in Alexa Fluor 647 and DyLight 649, respectively.

The labeling by immersion was performed with 2 different dyes: WGA Alexa Fluor 647 and LEL DyLight 649. All the right hemisphere slabs were dedicated to WGA Alexa Fluor 647 labeling. For this dye, we found that there was no vascular labeling regardless of the protocols we tried (Figure 34a). All the left hemispheres were labeled with LEL DyLight 647. We incubated the anterior and posterior slabs in 500 μ l of the dye with 0.2 mg/ml and 0.1 mg/ml concentrations respectively. In 3 mice, we labeled the vessels prior to delipidation (Figure 34b-d). For both dye concentrations and the 3 incubation conditions, the results were similar. We observed minimal vascular labeling. However, there was an improvement when applying 37°C during the incubation as we could observe some larger penetrating vessels (Figure 34b, c).

Figure 35 shows labeling examples performed following the delipidation. We can see the capillaries. However, we can also see other cellular structures that were labeled. Notably, this method additionally labeled the white matter. The white matter labeling was very bright. In order to reduce its impact and improve the viewing of capillaries, we pre-processed the images. We blurred the image and took its inverse. This result was in turn multiplied by the original image. The bright white matter area became dark, enabling us to visualize capillaries. Panels a and b show the labeling of the slabs incubated in 0.2 mg/ml and 0.1 mg/ml of the fluorophore, respectively. The mouse brain slabs incubated in 0.2 mg/ml of LEL DyLight 647 span from +1 mm to -1 mm from bregma and the brain slabs incubated in 0.1 mg/ml span from -1 mm to -3 mm from bregma. We noticed an improved signal-to-background ratio with 0.1 mg/ml labeling and less labeling of additional cellular compounds such as microglia.

Once more, we noticed that the samples that were cleared with CUBIC lost their integrity at their edges (Figure 34, 35).

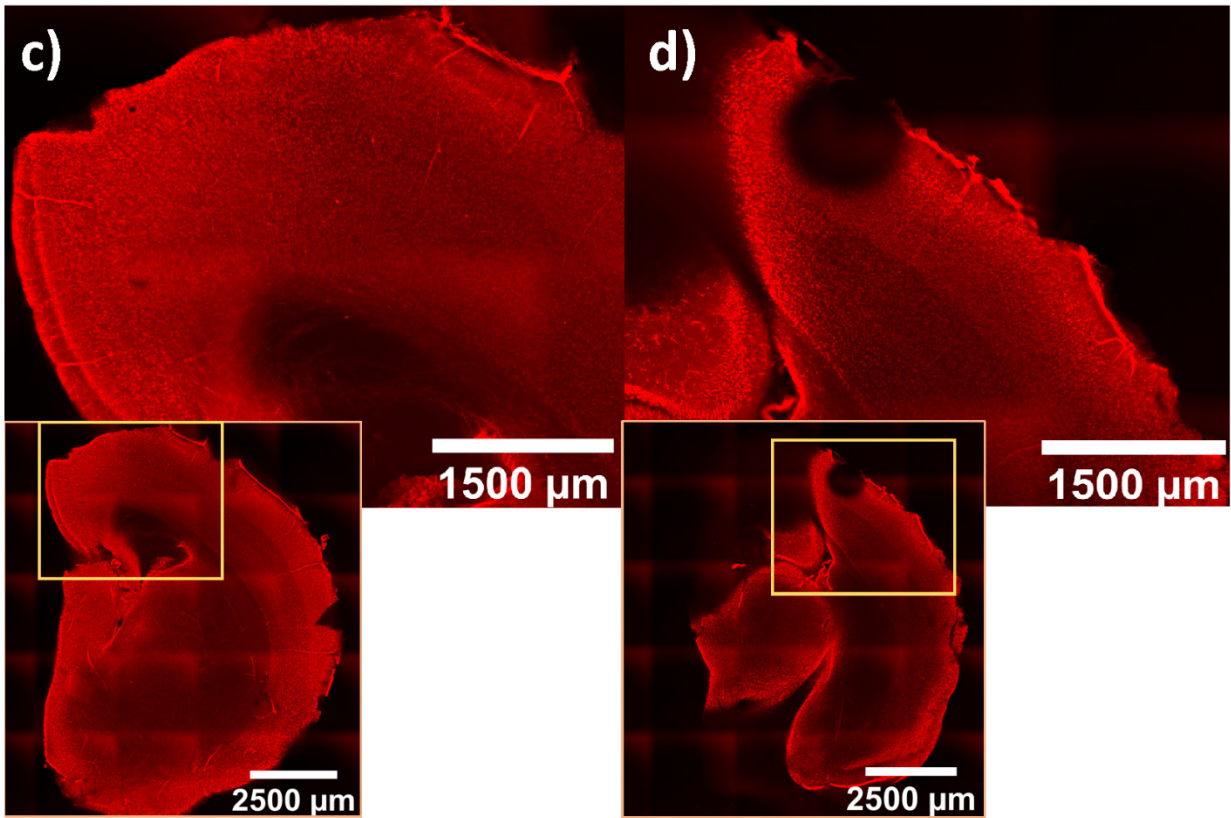
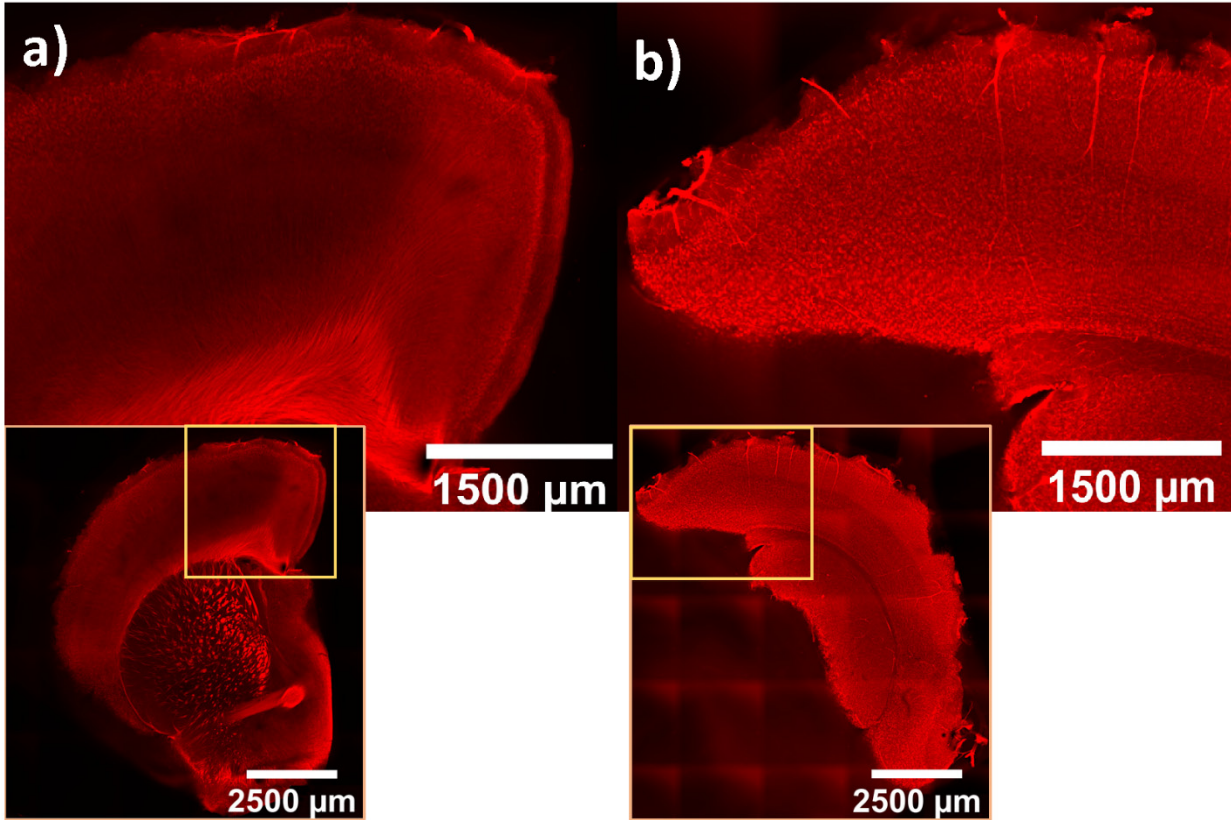
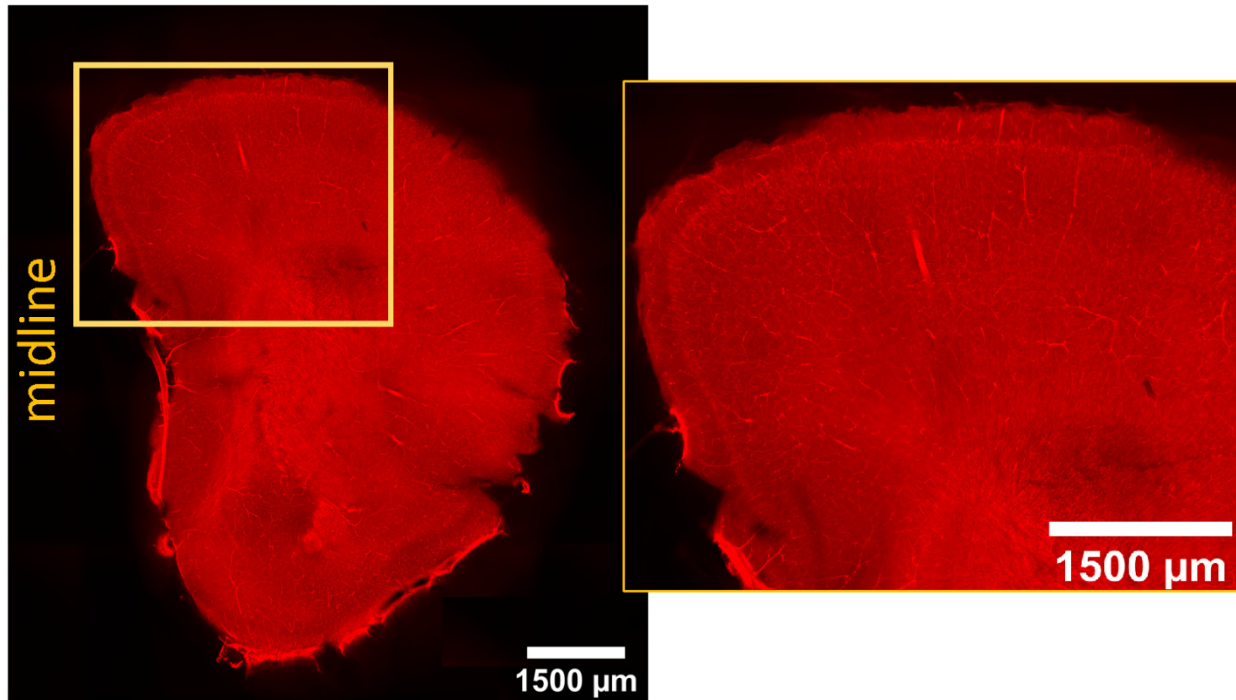


Figure 34. Labeling by immersion with 4 different protocols. a) Shows an example of labeling the vasculature by immersion with Alexa Fluor 647. The slab was stained and cleared at room temperature after the delipidation process. The PFA post-fixation time was 24 hours. b)-d) Show an example of labeling the vasculature with DyLight 649 before the start of the delipidation process. In b) the coronal slab was stained and cleared at 37°C. The PFA post-fixation time was 24 hours. In c) the coronal slab was stained and cleared at 37°C. The PFA post-fixation time was 3 hours. In d) the coronal slab was stained and cleared at room temperature. The PFA post-fixation time was 3 hours. A zoomed-in view of the orange square is shown for each example, to illustrate the cortical depth-dependent labeling

a) 0.2 mg/ml DyLight



b) 0.1 mg/ml DyLight

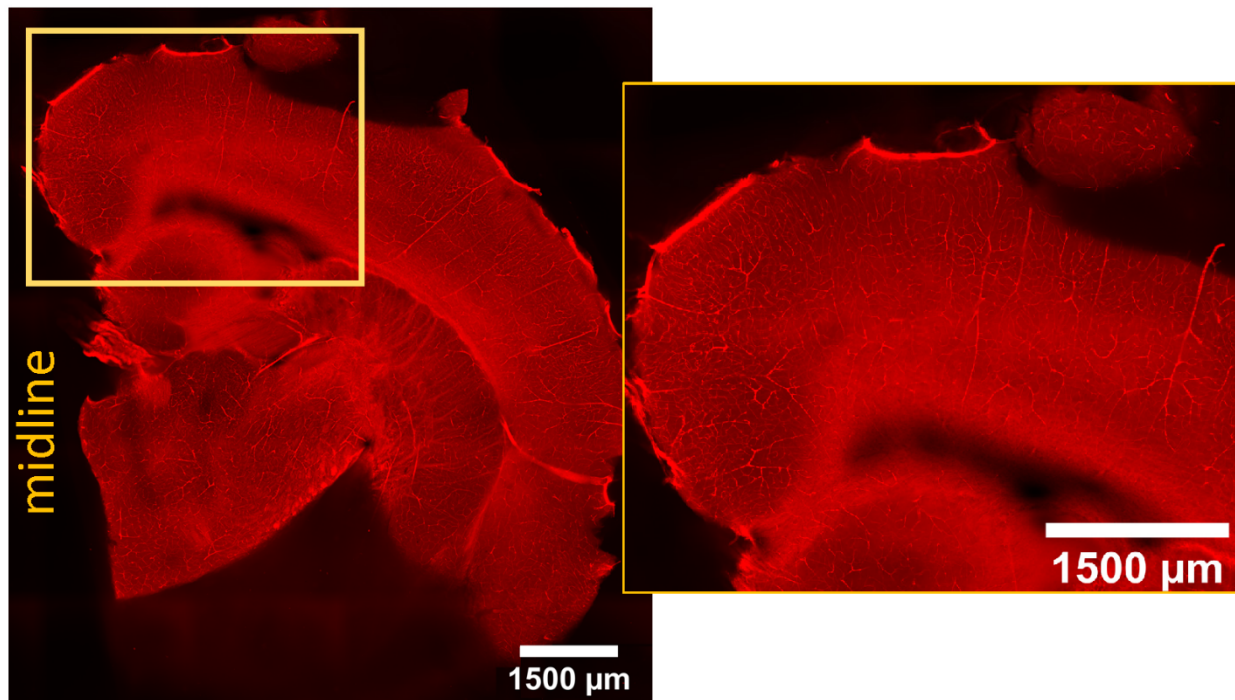


Figure 35. Labeling by immersion with DyLight 649 performed after delipidation. A) Blood vessel labeling of a 2 mm slab that was immersed in 0.2 mg/ml of DyLight 649. The slab was centered on the bregma. **b)** Vasculature of the same mouse brain imaged from a 2 mm slab that was immersed in 0.1 mg/ml

of DyLight 649. This slab was centered at -2 mm posterior to the bregma. The slabs were cleared with CUBIC. A zoomed-in view of the orange square is shown on the right-hand side of each of panels a) and b), illustrating the cortical-depth dependence of the labeling.

CHAPTER V – DISCUSSION

Summary of the findings

In this study, we compared different methods for labeling blood vessels and clearing brain samples. We aim to optimize our protocol to get high-resolution images of neocortical vessels in mice and rats. In short, we used different parameters to label the vasculature and we varied the clearing protocol among brain slabs. We obtain transparent brain slabs with all the clearing protocols used. However, DISCO protocols are relatively more rapid. They clear the tissue slabs within a few days and the rate is not influenced by the mouse age. A thinner slab provides higher transparency. For CUBIC, it takes a few weeks to clear 2-3 mm brain slabs. The clearing rate varies between slabs of different thicknesses and between mice of different ages. We find that intracardiac injection of Alexa Fluor in mice can give homogenous labeling of vessels. However, the results are not consistent. We varied the different volumes of 1.67 mg/ml Alexa Fluor 594 injected in mice (100 μ l, 150 μ l, 200 μ l, and 250 μ l) and saw a statistically significant difference, with a higher signal-to-background ratio for mice labeled with 200 μ l and 250 μ l compared to 100 μ l. Similarly, we compared the dye volume of Alexa Fluor 647 (1.67 mg/ml) in rats. We found that labeling with 1.2 ml gave a higher signal-to-background ratio compared to 0.6 ml. iDISCO+ provided a greater signal-to-background ratio compared to 3DISCO and CUBIC. Finally, immersion staining does not work with the WGA Alexa Fluor dye. It is only successful with LEL DyLight and after the samples are delipidated. However, other structures such as the white matter also get stained, and it requires more image processing to view the vasculature. Of the different methods and parameters that we applied, intravenous blood vessel injection of 1.2 ml WGA Alexa Fluor 647 (1.67 mg/ml) in rats yielded the best results: homogeneous labeling of the cortex, fine cortical depth-dependent variation, and differences between the gray matter and white matter.

Selection of refractive index matching solution

There is debate in the literature on whether DBE or BABB would act as a better RI matching solution (Ertürk et al., 2012a, Pan et al., 2016, and Becker et al., 2014). Thus, as part of

the preliminary work done in the lab, we looked at both solutions and found inconclusive results. They both had, in general, good clearing capabilities. However, DBE and benzyl alcohol (BA) are prone to form peroxides. Thus, similar to Todorov et al. (2020)'s choice of replacing DBE with BABB in their modified 3DISCO protocol, we selected BABB with the addition of vitamin E antioxidant which helps prevent the formation of peroxides.

Retaining fluorescence signal during clearing

Another part of our preliminary work evaluates DISCO clearing with different incubation parameters. FDISCO was expected to improve fluorescence preservation of substances such as fluorescent proteins and chemical fluorescent tracers by using alkaline pH and lower temperature incubations. Moreover, using these parameters was not expected to lengthen the clearing duration (Qi et al., 2019). In our hands, the clearing time is longer under these conditions since the samples came out opaque. However, we used methanol instead of THF. The goal of Qi et al.'s is to support the preservation of fluorophores. Nonetheless, we find that simply using fresh chemicals from well-sealed containers (Ertürk et al., 2012a), checking for peroxides with Quantofix peroxide strips before use (Hahn et al., 2019), and adding vitamin E in BABB (Pan et al., 2016) suffice for preserving the signal of our dyes. In addition, we carry out long-term storage at 4°C (Schwarz et al., 2015). In fact, we imaged some of our samples about 1.5 months following the initial imaging session and obtained strong signals. The use of strong fluorophores also helps in preserving the signal.

Improper perfusion's effects on clearing and imaging

As a final part of our preliminary work, we performed whole-brain clearing. One of the two mouse brains we cleared with uDISCO was darker in color relative to the other sample. The grid underneath was less visible. This was followed by a 3DISCO clearing procedure that gave an even more pronounced amber color. We found through iDISCO troubleshooting recommendations that this is the result of excess air exposure (Renier et al., 2016). They suggest filling test tubes more than halfway or to the top. Our initial incubations were done in 10 ml solution inside 15 ml falcon tubes. To test this concept, we cleared 2 other brains in 5 ml and 15 ml of the solvents. We expected to see a trend where incubating the sample in 15 ml would yield improved transparency relative to incubating in 10 ml and 5 ml. However, we observed that the 10 ml option yielded the worst results. After a second look, I noticed that both the uDISCO and the 3DISCO cleared samples

with pronounced dark color had improper perfusions. Therefore, this may have been the reason for the low clearing results. As Ertürk et al. (2012a) describe in their troubleshooting section, improper fixation may cause blood to remain in the tissues. In turn, the transparency of the samples diminishes (Ertürk et al., 2012a)

Besides clearing, we also notice the impact that poor perfusion has on staining vessels. From the experiment where we used mice of different ages, 3 out of 5 samples did not have homogeneous labeling: there were areas in the coronal slab with no labeling. From them, 2 had unsuccessful perfusion. We take into consideration parameters that will enable successful perfusions. For instance, we use 16% liquid PFA diluted to 4% and low perfusion flow rates to prevent perfusion artifacts (Cahill et al., 2011). Moreover, we warm our PBS and PFA solutions to 37°C in a warm water bath prior to perfusion. This reduces vasoconstriction. If vasoconstriction occurs in arterioles, then the surrounding vasculature may not be properly perfused (Fix and Garman, 2000). As Fix and Garman (2000) explain, this may occur when the perfusion flow rate is too low, or the fixative is too cold. Finally, we also add heparin into our PBS which is an anticoagulant. In summary, we take care to prepare for successful perfusions. Other challenges may occur during perfusion itself. For one, the cut at the atrium can be too small such that the flow of the perfusate entering the heart will be too high relative to the flow leaving. This builds up pressure that can burst the vessels. Failed perfusions also occur when the needle pierces the right ventricle (Wu et al., 2021). Both these cases may lead to fluids flowing out of the nose. As such, the perfusion impacts the tissue clearing and vessel staining qualities. From these 5 mice, we did notice a case where even though the perfusion seemed to have gone well, we still had incomplete staining that we could not account for.

Clearing coronal slabs with iDISCO+ and 3DISCO

The use of coronal slabs increases the number of samples available for comparisons. When evaluating the transparency of the slabs, both iDISCO+ and 3DISCO resulted in optically cleared coronal sections (see also: Renier et al., 2016, Ertürk et al., 2012a). In other words, the millimetric grid placed underneath the tissue was visible. As such, our results concord with these organic solvent clearing protocols. Incidentally, we notice that refreshing the RI matching solvent improves transparency. In fact, Ertürk et al. (2012a) also recommend this tip. On another note, the mice's age variation did not impact the clearing. However, in terms of different slab thicknesses,

we notice that 2 mm slabs become slightly more transparent. Nonetheless, we get good clearing for both 2 mm and 3 mm slabs. Additionally, by following the incubation steps described for clearing rat hemispheres (Branch et al., 2021), we also noticed cleared tissue slabs from the rat brains.

Tissue shrinkage with the 3DISCO clearing averages to 20-30%. This behavior is expected because dehydration with THF shrinks tissue samples (Tainaka et al., 2016; Becker et al., 2012). We base our 3DISCO protocol on Todorov et al.'s instructions who also report tissue shrinkage (Todorov et al., 2020). A gradual increase of the dehydrating agent's concentration minimizes the shrinkage and distortions (Ertürk et al., 2012a). For iDISCO+ clearing, similar to the published iDISCO+ protocol (Renier et al., 2016), we do not observe shrinkage. This change in behavior may be due to the usage of methanol instead of THF. Renier et al., (2016) indicate that the elimination of shrinkage facilitates automated registration of microscopy data to the brain atlas. On the other hand, Pan et al., (2016) put in perspective the advantages of tissue shrinkage. It facilitates organ imaging if the only available microscope can only support small imaging chambers, or it only has objectives with a short working distance and high numerical aperture (Pan et al., 2016). Additionally, methods such as vDISCO use the feature of tissue shrinkage to perform whole-body mouse imaging (Cai et al., 2019). However, a reduction in sample size could also lead to a reduction in resolution (Pan et al., 2016). Although it has been suggested that these clearing methods result in isotropic shrinkage and cause no distortions (Renier et al., 2016, Ertürk et al., 2012a), we sometimes observed some bending at the edges of our $\frac{1}{2}$ coronal slabs. We also saw noticeable distortions after clearing whenever minor cuts occurred during brain extraction or cutting.

Clearing coronal slabs with CUBIC

All coronal samples cleared with CUBIC became transparent. However, as tissue size increases, the clearing time increases. The use of a 3 mm mouse coronal slab also slows down the process relative to the mouse 2 mm slab. Thus, the process may take longer for larger samples as it may take more time for the delipidating solvents to penetrate all the way to the center of the sample and take effect on the tissue.

For complete clearing, we need to make sure there is sufficient delipidation before immersing our samples in the RI solution. In fact, we observed an incomplete clearing during our

whole brain processing as some areas remained white and cloudy. We followed the recommendation from the paper that brought forth CUBIC-L/R clearing (Tainaka et al., 2018). They recommend, for mouse organs and body clearing, 3-7 days of incubation at 37°C. However, Tainaka et al. also use an optional step during perfusion with a solvent called CUBIC-P. This may play a role in the increased rate of delipidation. Nonetheless, with coronal slabs, we extended the delipidation time and noticed good optical clearing. Other papers have also found the need to increase delipidation time. Rocha et al. (2019) clear an adult songbird brain with the original CUBIC protocol. They increased the delipidation time to 10 days instead of the recommended 7 days and saw that the tissue transparency obtained at the end of the process improved (Rocha, 2019). In fact, the effectiveness of delipidation impacts the final tissue transparency (Tainaka et al., 2018).

Some of our coronal slabs were delipidated at room temperature while others were at 37°C. Incubating at 37°C speeds the clearing process. However, we found that as the number of incubation days increased, the tissue started to lose its integrity. This was especially true with incubations at 37°C. By inspecting our CUBIC imaging data, we can see the slabs lose their structure at the regions of the surface of the brain: the edges of the samples look broken.

In summary, a long incubation time makes the tissues fragile, whereas a short incubation time results in incomplete lipid removal. This leads to reduced clearing efficiency (Tainaka et al., 2016). Finally, we notice an increase in tissue size. This is depicted by Nehrhoff et al. (2017) as well. Our solutions are slightly basic which can cause swelling (Tainaka et al., 2016).

Imaging vasculature with vessel labeling and DISCO clearing

For labeling the vascular system, we mainly use WGA Alexa Fluor in combination with organic solvent clearing. Renier *et al.* also use Alexa Fluor in their iDISCO and iDISCO+ immunolabelling protocols since these probes resist well in organic solvents and are stable long-term even at room temperature (Renier et al., 2014, Renier et al., 2016). In fact, we still had strong fluorescent signals while imaging our coronal slabs 1.5 months following the initial microscopy imaging. We note that we store our tissue at 4°C.

We initially used Alexa Fluor 594, following Todorov et al.'s protocol. However, the excitation laser available to us is a 561 nm solid-state laser. At this value, only about 50% of the

fluorophores in Alexa Fluor 594 are excited, based on the excitation spectrum (Thermo Fisher Scientific). Therefore, we switched to using Alexa Fluor 647. The excitation laser available for Alexa Fluor 647 is a 640 nm solid-state laser. For our mouse coronal slabs that were stained with Alexa Fluor 594 and cleared with iDISCO+, we can see background fluorescence around in the cortex area. This is not observed in the mouse slabs stained with Alexa Fluor 647 and cleared with iDISCO+. Some use Alexa Fluor 647 purposefully to overcome autofluorescence (Luong et al., 2021). In fact, it is best to use fluorophores in the red or far-red spectrum (e.g.: Alexa Fluor 594 and 647) since tissues generate autofluorescence in the blue/green spectrum (Renier et al., 2014).

When we compared iDISCO+ images to 3DISCO qualitatively and quantitatively, we observed a smaller 3DISCO signal-to-background ratio. Although the reason is not entirely clear, one possible explanation is that autofluorescence may arise due to the changes in a tissue's biochemical properties during clearing (Seo et al., 2016) or due to tissue shrinkage (Pan et al., 2016).

In terms of vasculature labeling with different volumes of dye, $\frac{3}{4}$ of our mice had good perfusion-staining. The larger vessels are easily identifiable in this dataset. However, at the capillary level, we noticed that the micro-vessels are harder to visualize in the mouse that received a volume of 100 μ l of Alexa Fluor (1.67 mg/ml). The 200 μ l and 250 μ l injection volumes yielded the best results. The 150 μ l dye volume did not give a good result due to poor perfusion. Even though this experiment was performed only once, we can still see a trend where the signal-to-background ratio is greater with 200 μ l and 250 μ l dye volumes relative to 100 μ l (Figures 25 and 26). Others have also evaluated the ideal quantity of dye necessary to stain vessels. Although they find a minimum, an upper threshold is not reported. For one, Robertson et al. (2015) vary the amount of LEL DyLight 649 to stain mouse vasculature (25 μ g, 50 μ g, and 100 μ g). They find low labeling intensity with 25 μ g (1 mg/ml) of the dye and the most distinguishable results at 100 μ g (1 mg/ml). Battistella et al. (2021) investigate a similar question. They intracardially stain with 5 ml WGA-FITC during perfusion using different concentrations: 5 μ g/ml, 50 μ g/ml, 125 μ g/ml. 125 μ g/ml gives the best signal-to-noise ratio. We saw a similar pattern in our mouse experiment where a higher volume gave a better signal-to-background ratio. We also looked at different volumes in rats: 1.2 ml vs 0.6 ml of Alexa Fluor 647 (1.67 mg/ml). We found that a volume of 1.2 ml gave a greater signal-to-background ratio compared to 0.6 ml.

Based on this result, we would need to increase the volume of the dye a lot to get high signal-to-background ratio. This will increase the cost significantly. But, when should one stop increasing the volume? We recommend evaluating the required volume against the required results. To test whether the increase in volume is indeed necessary, an automatic analysis – such as segmentation with convolutional neural networks – can be performed, to identify the specific features of interest: in our case, this would be the capillaries. To analyze the cost-effective optimal concentration, one can apply such an automatic analysis and verify the results by inspection. This would include inspecting the images and identifying true positive detection, false positive and false negative (true negative is the default outcome in such an experiment). The volume should be increased to achieve the required percentage of the true positive, false positive and false negative detection. We recommend doing a similar evaluation in similar future studies, to analyze the cost-effectiveness of increasing stain or antibody concentration and the corresponding cost, based on the specific aims of the study.

In terms of the dye injection site, when we performed Alexa Fluor 647 tail vein injections in rats, we can see homogenous labeling. In contrast, we noticed that the brightness obtained with intracardiac injections in mice varied between different regions of the slabs. This was mainly noticeable with Alexa Fluor 594. For instance, the larger vessels are significantly brighter than the capillaries. This makes it harder to visualize the capillaries with simple image processing techniques because visualization of the larger vessels without cropping their brightness requires a wide dynamic range. A similar result is discussed by Robertson *et al.* (2015). They compared different parameters of injection in mice. Although both intracardiac and intravenous labeling showed homogenous labeling, the intensities observed with intracardiac labeling varied between different regions (Robertson *et al.*, 2015). However, it is important to note that our results may be attributed to the different species we used (homogeneous and non-homogeneous labeling in rats and mice, respectively) and not the pathway of fluorophore injection (intravenous or intra-cardiac). Although we initially attempted tail vein injection in mice as well, we decided to abandon the idea, because it was difficult to localize the lateral vein. In fact, Berry-Pusey *et al.* (2013) demonstrate the difficulty of tail vein injection. They use 3 trained injectors to perform 7 tail vein injections of radiolabeled probes. They find that $13.9\% \pm 12.3\%$ of the injection dose remains in the tail vein.

Imaging vasculature with vessel labeling and CUBIC clearing

We injected a total of 5 mice intracardially to label with dextran-FITC and cleared their brains with CUBIC. We used mice of different ages and cut the slabs into different thicknesses. Only one out of the 5 mice had labeled vasculature. From the mouse in which dextran-FITC staining worked, we noticed that many of the capillaries were difficult to see as they blended with the background (low signal-to-background ratio). In fact, this makes sense as FITC's excitation is in the green spectrum. At this spectrum, the autofluorescence in mouse brain is high, to the extent that some studies use it to annotate brain regions (Ariel 2017). We also notice from this data that other cellular structures were labeled as well. We used dextran-FITC with a molecular weight of 2000kDa to follow Susaki et al.'s (2015) staining protocol. Therefore, with this molecular weight, dextran is not expected to cross the blood-brain barrier (Choi et al., 2010). Some discourage the use of dextran-FITC because, although dextran-FITC fills the blood vessels, it does not bind to it (Li et al., 2008). Therefore, as the tissue gets compressed during processing (e.g.: cutting brain slabs) the dye may escape from some of the vessels and we may observe fragmented vascular patterns (Li et al., 2008). CUBIC clearing leads to swelling at the cellular level (Nehrhoff et al, 2017). The removal of lipids interrupts the cell membrane's integrity which leads to the solvents passing through the cells (Nehrhoff et al, 2017). Perhaps, the breakup of the cellular integrity and the swelling of the structures may also cause dextran-FITC to escape the vessels. Therefore, the reason for the signal of the structures in the background may be due to the tissue's autofluorescence itself or due to dextran-FITC escaping the vessels. To help understand if the observed cellular structures are visible because of the tissue's autofluorescence, a good approach would be to perform imaging of a control sample with no dye.

We also performed CUBIC clearing following intracardiac injection of Alexa Fluor 647. In our mouse results, we do notice staining of vessels after the completion of the clearing. As for the rats, we obtain vessel signals from only 1 out of the 3 rats. The clearing of the rat coronal slabs takes longer. In other words, the samples were incubated at 37°C for a longer period which may have affected the signal's strength. For the data in which we observed vessels (with Alexa Fluor 647), we noticed a relatively high level of background signal similar to what we observed with the background signal in mice injected with dextran-FITC. This is interesting since Alexa Fluor 647 is in the far red and we would expect a reduction in autofluorescence. However, conversely, to dextran-FITC, we no longer observe the staining of other cellular compounds with the WGA Alexa

Fluor. Nehrhoff *et al.* (2017) stained the heart vasculature by injecting LEL-FITC and LEL DyLight-649 into the vascular system. They found that using LEL DyLight-649 generally gives more microvessel labelling and less background relative to FITC fluorophore. Another group that used FITC conjugated to a lectin is Di Giovanna, et al (2018). They compared it to the use of albumin-conjugated FITC dissolved in porcine skin gelatin, and they performed CLARITY clearing. They concluded that staining with FITC-gel gives a higher signal-to-noise ratio.

Imaging vasculature with Immersion staining and CUBIC clearing

In general, immersion staining with WGA Alexa Fluor did not work. However, it worked with brain slabs labeled with LEL DyLight after delipidation. For the slabs that were stained before delipidation, we saw much fewer vessels. Mainly larger vessels were labeled. By removing the lipids, we permeabilize the tissues. Therefore, the fluorescent probes travel into the sample more easily (Molbay, M., et al. 2021). Additionally, the dye penetration into the samples increases with higher incubation temperature (Xiao X. et al., 2018). As we saw, the slabs at room temperature incubation resulted in minimal vascular staining.

WGA and LEL both bind to glycoproteins on the cell membranes. More specifically, LEL binds to poly-N-acetyllactosamine residues (Robertson et al., 2015). WGA binds to N-Acetylglucosamine and sialic acid (Robertson B., 1990, Bensley et al 2016). These glycoconjugates are also found on neuronal and microglia membranes (Robertson 1990, Brawek et al., 2019, Battistella et al., 2021). They are also highly abundant on endothelial membranes like the apical surface of capillaries (Bensley et al., 2016, Robertson et al., 2015). Therefore, since these glycoproteins are common constituents of many cells, it is reasonable to see elements - other than the vasculature - labeled too. Battistella *et al.*, (2021) performed immunohistology on 100 μm brain slices with WGA and LEL at different concentrations (5 $\mu\text{g/ml}$, 10 $\mu\text{g/ml}$, and 20 $\mu\text{g/ml}$). They conclude that the lowest concentration gives the smallest background. Additionally, similar to us, they find that LEL gives superior immunostaining of vasculature compared to WGA.

Limitations & Future steps

The end goal of our experiment was to set up a staining and clearing protocol that would allow us to image blood vessels down to the capillary level. For this, we evaluate the results obtained from varying a number of parameters involving the dyes used, the dye volumes, the

labeling methods, the clearing methods, and the rodent's age. We achieve the best results with rats intravenously labeled with 1.2 ml of WGA Alexa Fluor 647 and cleared with iDISCO+.

A limitation is an unpredictability of staining quality in mouse perfusion. Although we are making sure all controllable aspects are done properly (filtering the PBS before use, the use of heparin, warming the perfusates, etc.), we still had cases in mice where their perfusion seemed to have gone well but the staining of the vasculature was inconsistent.

We concluded that tail vein dye injection in rats gave one of the best results. However, it may be because of an interspecies aspect: we currently have data from rats injected in the tail vein and mice that received intra-cardiac injections. Regardless, we observed that tail vein injection of WGA Alexa Fluor 647 in rats with organic solvent (iDISCO+) clearing seems to give the best result.

The next steps to accomplish include finalizing the optimal volume of WGA Alexa Fluor needed to label rat vasculature. Once the optimization is complete, the next step is to image larger brain sections and perform quantitative analysis. More future work involves incorporating the information in models of fMRI, for better modeling of the mechanisms underlying fMRI.

CHAPTER VI – REFERENCES

- Ariel, P., (2017) A beginner's guide to tissue clearing. *The International Journal of Biochemistry & Cell Biology*. 84: 35-39. Doi: 10.1016/j.biocel.2016.12.009
- Battistella, R., Kritsilis, M., Matuskova, H., Haswell, D., Cheng, A.X., Meissner, A., Nedergaard, M., and Lundgaard, I. (2021) Not All Lectins Are Equally Suitable for Labeling Rodent Vasculature. *International Journal of Molecular Sciences*. 22(21): 11554. Doi: 10.3390/ijms222111554
- Becker, K., Hahn, C.M., Saghafi, S., Jährling, N., Wanis, M., and Dodt, H.-U. (2014). Reduction of Photo Bleaching and Long Term Archiving of Chemically Cleared GFP-Expressing Mouse Brains. *PLoS One*. 9(12): e114149. Doi: 10.1371/journal.pone.0114149
- Becker, K., Jährling, N., Saghafi, S., Weiler, R., and Dodt, H.U. (2012) Chemical Clearing and Dehydration of GFP Expressing Mouse Brains. *PLoS One*. 7(3): e33916. Doi: 10.1371/journal.pone.0033916
- Bensley, J.G., De Matteo, R., Harding, R., and Black, M.J. (2016) Three-dimensional direct measurement of cardiomyocyte volume, nuclearity, and ploidy in thick histological sections. *Scientific Reports*. 6: 23756. Doi: 10.1038/srep23756
- Berry-Pusey, B.N., Chang, Y.C., Prince, S.W., Chu, K., David, J., Taschereau, R., Silverman, R.W., Williams, D., Ladno, W., Stout, D., Tsao, T.C., and Chatziioannou, A. (2012) A semi-automated vascular access system for preclinical models. *Physics in Medicine and Biology*. 58(16): 5351-5362. Doi: 10.1088/0031-9155/58/16/5351.
- Branch, A., Tward, D., Kolstad, A.C., Pulyadi, V., Vogelstein, J.T., Wu, Z., and Gallagher, M. (2021) An optimized tissue clearing protocol for rat brain labeling, imaging, and high throughput analysis. *bioRxiv* 639674; Doi: 10.1101/639674
- Brawek B., del Moral M. O., and Garaschuk O. (2019) In Vivo Visualization of Microglia Using Tomato Lectin. In: Garaschuk O., Verkhratsky A. (eds) *Microglia. Methods in Molecular Biology*. 2034:165-175. Humana, New York, NY. Doi: 10.1007/978-1-4939-9658-2_12
- Bryson, J.L., Coles, M.C., and Manley, N.R. (2011) A Method for Labeling Vasculature in Embryonic Mice. *Journal of Visualized Experiments*. (56): e3267. Doi: 10.3791/3267.
- Cahill, L.S., Laliberte, C.L., Ellegood, J., Spring, S., Gleave, J.A., van Eede, M.C., Lerch, J.P., and Henkelman, R.M. (2012) Preparation of fixed mouse brains for MRI. *NeuroImage*. 60(2): 933–939. Doi: 10.1016/j.neuroimage.2012.01.100
- Cai, R., Pan, C., Ghasemigharagoz, A., Todorov, M.I., Förstera, B., Zhao, S., Bhatia, H.S., Parra-Damas, A., Mrowka, L., Theodorou, D., Rempfler, M., Xavier, A.L.R., Kress, B.T., Benakis, C., Steinke, H., Liebscher, S., Bechmann, I., Liesz, A., Menze, B., Kerschensteiner, M., Nedergaard, M., and Ertürk, A. (2019). Panoptic imaging of transparent mice reveals whole-body neuronal projections and skull–meninges connections. *Nature Neuroscience*. 22(2): 317–327. Doi: 10.1038/s41593-018-0301-3

Carrillo, M., Chuecos, M., Gandhi, K., Bednov, A., Moore, D.L., Maher, J., Ventolini, G., Ji, G.C., and Schlabritz-Loutsevitch, N. (2018). Optical tissue clearing in combination with perfusion and immunofluorescence for placental vascular imaging. *Medicine*. 97(39): e12392. Doi: 10.1097/MD.00000000000012392

Choi, J. J., Wang, S., Tung, Y. S., Morrison, B., 3rd, and Konofagou, E. E. (2010). Molecules of various pharmacologically-relevant sizes can cross the ultrasound-induced blood-brain barrier opening in vivo. *Ultrasound in medicine & biology*, 36(1): 58–67. Doi: 10.1016/j.ultrasmedbio.2009.08.006

Chung, K., Wallace, J., Kim, S.Y., Kalyanasundaram, S., Andalman, A.S., Davidson, T.J., Mirzabekov, J.J., Zalocusky, K.A., Mattis, J., Denisin, A.K., Pak, S., Bernstein, H., Ramakrishnan, C., Grosenick, L., Gradinaru, V., and Deisseroth, K. (2013) Structural and molecular interrogation of intact biological systems. *Nature*. 497(7449): 332-337. Doi: 10.1038/nature12107

d'Esposito, A., Nikitichev, D., Desjardins, A., Walker-Samuel, S., and Lythgoe, M.F. (2015). Quantification of light attenuation in optically cleared mouse brains. *Journal of Biomedical Optics*. 20(8): 080503. Doi: 10.1117/1.JBO.20.8.080503

Di Giovanna, A.P., Tibo, A., Silvestri, L., Müllenbroich, M.C., Costantini, I., Mascaro, A.L.A., Sacconi, L., Frascioni, P., and Pavone, F.S. (2018). Whole-Brain Vasculature Reconstruction at the Single Capillary Level. *Scientific reports*. 8: 12573. Doi: 10.1038/s41598-018-30533-3

Dotd, H-U., Leischner, U., Schierloh, A., Jährling, N., Mauch, C.P., Deininger, K., Deussing, J.M., Eder, M., Zieglgänsberger, W., and Becker, K. (2007). Ultramicroscopy: three-dimensional visualization of neuronal networks in the whole mouse brain. *Nature Methods*. 4(4): 331–336. Doi: 10.1038/nmeth1036

Du, H., Hou, P., Zhang, W., & Li, Q. (2018). Advances in CLARITY-based tissue clearing and imaging (Review). *Experimental and therapeutic medicine*. 16(3): 1567–1576. Doi: 10.3892/etm.2018.6374

Ertürk, A., Becker, K., Jährling, N., Mauch, C.P., Hojer, C.D., Egen, J.G., Hellal, F., Bradke, F., Sheng, M., and Dotd, H.U. (2012) (a) Three-dimensional imaging of solvent-cleared organs using 3DISCO. *Nature Protocols* 7(11): 1983-1995. Doi: 10.1038/nprot.2012.119

Ertürk, A., Mauch, C.P., Hellal, F., Forstner, F., Keck, T., Becker, K., Jährling, N., Steffens, H., Richter, M., Hubener, M., Kramer, E., Kirchhoff, F., Dotd, H.U., and Bradke, F. (2012) (b) Three-dimensional imaging of the unsectioned adult spinal cord to assess axon regeneration and glial responses after injury. *Nature Medicine*. 18(1): 166–171. Doi: 10.1038/nm.2600

Fix, A.S., and Garman, R.H. (2000). Practical Aspects of Neuropathology: A Technical Guide for Working with the Nervous System. *Toxicologic Pathology*. 28(1): 122-131. Doi: 10.1177/019262330002800115

Fumoto, S., Kinoshita, E., Ohta, K., Nakamura, K. I., Hirayama, T., Nagasawa, H., Hu, D., Okami, K., Kato, R., Shimokawa, S., Ohira, N., Nishimura, K., Miyamoto, H., Tanaka, T., Kawakami, S., and Nishida, K. (2020). A pH-Adjustable Tissue Clearing Solution That Preserves Lipid Ultrastructures: Suitable Tissue Clearing Method for DDS Evaluation. *Pharmaceutics*. 12(11): 1070. Doi: 10.3390/pharmaceutics12111070.

Hahn, C., Becker, K., Saghafi, S., Pende, M., Avdibašić, A., Foroughipour, M., Heinz, D.E., Wotjak, C.T., and Dodt, H-U. (2019) High-resolution imaging of fluorescent whole mouse brains using stabilised organic media (sDISCO). *Journal of Biophotonics*. 12(8): e201800368. Doi: 10.1002/jbio.201800368

Haseloff, R.F., Blasig, I.E., Meffert, H., and Ebert B. (1990). Hydroxyl radical scavenging and antipsoriatic activity of benzoic acid derivatives. *Free Radical Biology and Medicine*. 9(2): 111-115. Doi: 10.1016/0891-5849(90)90113-W

Hildebrand, S., Schueth, A., von Wangenheim, K., Mattheyer, C., Pampaloni, F., Bratzke, H., Roebroek, A.F., and Galuske, R.A.W. (2020) hFRUIT: An optimized agent for optical clearing of DiI-stained adult human brain tissue. *Scientific Reports* 10(1): 9950. Doi: 10.1038/s41598-020-66999-3

Huber, L.R., Poser, B.A., Kaas, A.L., Fear, E.J., Dresbach, S, Berwick, J, Goebel, R, Turner, R, and Kennerley, A.J. (2021) Validating layer-specific VASO across species. *NeuroImage*, 237: 118195. Doi: 10.1016/j.neuroimage.2021.118195.

Hughes S., Dashkin O., and DeFazio R.A. (2014) Vessel Painting Technique for Visualizing the Cerebral Vascular Architecture of the Mouse. In: Milner R. (eds) *Cerebral Angiogenesis: Methods in Molecular Biology*, Humana Press, New York, NY. 1135: 127-138 Doi: 10.1007/978-1-4939-0320-7_12

Hou, B., Zhang, D., Zhao, S., Wei, M., Yang, Z., Wang, S., Wang, J., Zhang, X., Liu, B., Fan, L., Li, Y., Qiu, Z., Zhang, C., and Jiang, T. (2015). Scalable and DiI-compatible optical clearance of the mammalian brain. *Frontiers in Neuroanatomy*. 9: 19. Doi: 10.3389/fnana.2015.00019

Jackson, H.L., McCormack, W.B., Rondestvedt, C.S., Smeltz, K.C., and Viele, I.E. (1970). Control of peroxidizable compounds. *Journal of Chemical Education*. 47(3): A175-A188. Doi: 10.1021/ed047pA175.

Jing, D., Zhang, S., Luo, W., Gao, X., Men, Y., Ma, C., Liu, X., Yi, Y., Bugde, A., Zhou, B.O., Zhao, Z., Yuan, Q., Feng, J.Q., Gao, L., Ge W-P., and Zhao, H. (2018). Tissue clearing of both hard and soft tissue organs with the PEGASOS method. *Cell Research*. 28(8): 803–818. Doi:10.1038/s41422-018-0049-z

Kataoka, H., Ushiyama, A., Kawakami, H., Akimoto, Y., Matsubara, S., and Iijima, T. (2016). Fluorescent imaging of endothelial glycocalyx layer with wheat germ agglutinin using intravital microscopy. *Microscopy Research and Technique*. 79(1): 31–37. Doi: 10.1002/jemt.22602

Kuwajima, T., Sitko, A.A., Bhansali, P., Jurgens, C., Guido, W., and Mason, C. (2013). ClearT: a detergent- and solvent-free clearing method for neuronal and non-neuronal tissue. *Development*. 140 (6): 1364–1368. Doi: 10.1242/dev.091844

Lee, S.H., Choe, Y.H., Kang, R.H., Kim, Y.R., Kim, N.H., Kang, S., Kim, Y., Park, S., Hyun, Y.M., and Kim, D. (2019) A bright blue fluorescent dextran for two-photon in vivo imaging of blood vessels. *Bioorganic Chemistry*. 89:103019. Doi: 10.1016/j.bioorg.2019.103019

Li, C., Zhang, Y., Wang, M., Zhang, Y., Chen, G., Li, L., Wu, D., and Wang, Q. (2014) In vivo real-time visualization of tissue blood flow and angiogenesis using Ag2S quantum dots in the NIR-II window. *Biomaterials*. 35(1): 393-400. Doi: 10.1016/j.biomaterials.2013.10.010.

Li, Y.S., Xu, J.Y., Wan, P., Yu, T.T., and Zhu, D. (2018) Optimization of GFP Fluorescence Preservation by a Modified uDISCO Clearing Protocol. *Frontiers in Neuroanatomy* 12:67. Doi: 10.3389/fnana.2018.00067

Li, Y.W., Song, Y., Zhao, L., Gaidosh, G., Laties, A.M., and Wen, R. (2008) Direct labeling and visualization of blood vessels with lipophilic carbocyanine dye DiI. *Nature Protocols*. 3(11): 1703-1708 Doi: 10.1038/nprot.2008.172

Liu, P.F., Mu, X.Y., Zhang, X.-D., and Ming, D. (2020) The Near-Infrared-II Fluorophores and Advanced Microscopy Technologies Development and Application in Bioimaging. *Bioconjugate Chemistry*. 31(2):260–275. Doi: 10.1021/acs.bioconjchem.9b00610

Luong, Q.V., Israel, A., Sharma, R., Ussar, S., and Lee, K.Y. (2021) Development of an Optimized Clearing Protocol to Examine Adipocyte Subpopulations in White Adipose Tissue. *Methods and Protocols*. 4(2): 39. Doi: 10.3390/mps4020039

Mahmoudian, J., Hadavi, R., Jeddi-Tehrani, M., Mahmoudi, A. R., Bayat, A. A., Shaban, E., Vafakhah, M., Darzi, M., Tarahomi, M., and Ghods, R. (2011). Comparison of the Photobleaching and Photostability Traits of Alexa Fluor 568- and Fluorescein Isothiocyanate-conjugated Antibody. *Cell journal*. 13(3): 169–172. Doi: <https://www.ncbi.nlm.nih.gov.proxy3.library.mcgill.ca/pmc/articles/PMC3584473/>

Matsumoto, K., Mitani, T.T., Horiguchi, S.A., Kaneshiro, J., Murakami, T.C., Mano, T., Fujishima, H., Konno, A., Watanabe, T.M., Hirai H., and Ueda, H.R. (2019). Advanced CUBIC tissue clearing for whole-organ cell profiling. *Nature Protocols*. 14(12): 3506–3537. Doi: 10.1038/s41596-019-0240-9.

Molbay, M., Kolabas, Z.I., Todorov, M.I., Ohn, T-L., and Ertürk, A. (2021). A guidebook for DISCO tissue clearing. *Molecular System Biology*. 17(3): e9807 Doi: 10.15252/msb.20209807

Murray, E., Cho, J.H., Goodwin, D., Ku, T., Swaney, J., Kim, S.Y., Choi, H., Park, Y.G., Park, J.Y., Hubbert, A., Mccue, M., Vassallo, S., Bakh, N., Frosch, M.P., Wedeen, V.J., Seung, H.S., and Chung, K. (2015) Simple, scalable proteomic imaging for high-dimensional profiling of intact systems. *Cell*. 163(6): 1500-1514. Doi: 10.1016/j.cell.2015.11.025

Nachbar, M.S., Oppenheim, J.D., and Thomas, J.O. (1980) Lectins in the U.S. Diet. Isolation and characterization of a lectin from the tomato (*Lycopersicon esculentum*). *Journal of Biological Chemistry*. 255(5): 2056-2061. Doi: 10.1016/S0021-9258(19)85992-6

Nehrhoff, I., Ripoll, J., Samaniego, R., Desco, M., and Gómez-Gavero, M.V. (2017). Looking inside the heart: a see-through view of the vascular tree. *Biomedical optics express*. 8(6): 3110–3118. Doi: 10.1364/BOE.8.003110

Pan C., Cail, R., Quacquarelli, F.P., Ghasemigharagoz, A., Lourbopoulos, A., Matryba, P., Plesnila, N., Dichgans, M., Hellal, F., and Ertürk, A. (2016) Shrinkage-mediated imaging of entire organs and organisms using uDISCO. *Nature Methods*. 13(10): 859-867. Doi: 10.1038/nmeth.3964

Panchuk-Voloshina, N., Haugland, R.P., Bishop-Stewart, J., Bhalgat, M.K., Millard, P.J., Mao, F., Leung, W.Y., and Haugland, R.P. (1999) Alexa Dyes, a Series of New Fluorescent Dyes that Yield Exceptionally Bright, Photostable Conjugates. *The Journal of Histochemistry & Cytochemistry*. 47(9): 1179–1188. Doi: 10.1177/002215549904700910

Paxinos, G., and Franklin, K.B.J. (2001) *The mouse brain in stereotaxic coordinates*, Second Edition. Elsevier Academic Press.

Paxinos, G., and Watson, C. (2005). *The Rat Brain in Stereotaxic Coordinates*, Fifth Edition. Boston, MA: Elsevier Academic Press.

Peeters, G., Debbaut, C., Laleman, W., Monbaliu, D., Vander Elst, I., Detrez, J.R., Vandecasteele, T., De Schryver, T., Van Hoorebeke, L., Favere, K., Verbeke, J., Segers, P., Cornillie, P., and De Vos, W.H., (2017) A multilevel framework to reconstruct anatomical 3D models of the hepatic vasculature in rat livers. *Journal of Anatomy*. 230(3): 471-483. Doi: 10.1111/joa.12567

Pichat, J., Iglesias, J. E., Yousry, T., Ourselin, S., and Modat, M. (2018) A Survey of Methods for 3D Histology Reconstruction. *Medical Image Analysis*. 46: 73-105. Doi: 10.1016/j.media.2018.02.004

Qi, Y., Yu, T., Xu, J., Wan, P., Ma, Y., Zhu J., Li, Y., Gong, H., Luo, Q. and Zhu D. (2019) FDISCO: Advanced solvent-based clearing method for imaging whole organs. *Science Advances* 5(1): eaau8355. Doi: 10.1126/sciadv.aau8355

Renier, N., Adams, E.L., Kirst, C., Wu, Z., Azevedo, R., Kohl, J., Autry, A.E., Kadiri, L., Venkataraju, K.U., Zhou, Y., Wang, V.X., Tang, C.Y., Olsen, O., Dulac, C., Osten, P., and Tessier-Lavigne, M. (2016) Mapping of Brain Activity by Automated Volume Analysis of Immediate Early Genes. *Cell*. 165(7): 1789– 1802. Doi: 10.1016/j.cell.2016.05.007

Renier, N., Wu, Z., Simon, D.J., Yang, J., Ariel, P., and Tessier-Lavigne, M. (2014). iDISCO: A Simple, Rapid Method to Immunolabel Large Tissue Samples for Volume Imaging. *Cell*. 159(4): .896-910 Doi: 10.1016/j.cell.2014.10.010

Richardson, D.S., and Lichtman, J.W. (2015). Clarifying Tissue Clearing. *Cell* 162(2): 246-257. Doi: 10.1016/j.cell.2015.06.067

Robertson, B. (1990) Wheat germ agglutinin binding in rat primary sensory neurons: a histochemical study. *Histochemistry* 94(1): 81–85. Doi: 10.1007/BF00266793

Robertson, R.T., Levine, S.T., Haynes, S.M., Gutierrez, P., Baratta, J.L., Tan, Z.Q., and Longmuir, K.J. (2015) Use of labeled tomato lectin for imaging vasculature structures. *Histochemistry and Cell Biology*. 143(2): 225–234. Doi: 10.1007/s00418-014-1301-3.

Rocha, D.R., Düring, D.N., Bethge, P., Voigt, F.F., Hildebrand, S., Helmchen, F., Pfeifer, A., Hahnloser, R.H.R., and Gahr, M. (2019). Tissue Clearing and Light Sheet Microscopy: Imaging the Unsectioned Adult Zebra Finch Brain at Cellular Resolution. *Frontier in Neuroanatomy*. 13:13 Doi: 10.3389/fnana.2019.00013.

Salehi, A., Jullienne, A., Wendel, K.M., Hamer, M., Tang, J.P., Zhang, J.H., Pearce, W.J., DeFazio, R.A., Vexler, Z.S., and Obenaus, A. (2019). A Novel Technique for Visualizing and Analyzing the Cerebral Vasculature in Rodents. *Translational Stroke Research*. 10(2): 216–230. Doi: 10.1007/s12975-018-0632-0.

Saltman, A.J., Barakat, M., Bryant, D.M., Brodovskaya, A., and Whited, J.L. (2017) DiI Perfusion as a Method for Vascular Visualization in *Ambystoma mexicanum*. *JoVE-Journal of Visualized Experiments*. (124): 55740. Doi: 10.3791/55740.

Sarkar, P., Sridharan, S., Luchowski, R., Desai, S., Dworecki, B., Nlend, M., Gryczynski Z., and Gryczynski, I. (2010) Photophysical properties of a new DyLight 594 dye. *Journal of Photochemistry and Photobiology B-Biology*. 98(1): 35-39. Doi: 10.1016/j.jphotobiol.2009.10.005

Schwarz, M.K., Scherbarth, A., Sprengel, R., Engelhardt, J., Theer, P., and Giese, G. (2015) Fluorescent-protein stabilization and high-resolution imaging of cleared, intact mouse brains. *PLoS One*. 10(5): e0124650. Doi: 10.1371/journal.pone.0124650

Seo, J., Choe, M., and Kim, S-Y. (2016) Clearing and Labeling Techniques for Large-Scale Biological Tissues. *Molecules and Cells*. 39(6): 439–446. Doi: 10.14348/molcells.2016.0088

Siedentopf, H. & Zsigmondy, R. Über Sichtbarmachung und Größenbestimmung ultramikroskopischer Teilchen, mit besonderer Anwendung auf Goldrubingläser. *Annalen der Physik* 10, 1–39 (1903).

Snyder, R. (1992). Ethel Browning's Toxicity and Metabolism of Industrial Solvents. Second Edition. Volume 3 Alcohols and Esters, Elsevier, New York, NY. 3:65.

Sotero, R.C., Bortel, A., Naaman, S., Mocanu, V.M., Kropf, P., Villeneuve, M.Y., and Shmuel, A. (2015) Laminar Distribution of Phase-Amplitude Coupling of Spontaneous Current Sources and Sinks. *Frontiers in Neuroscience*. 9:454 Doi: 10.3389/fnins.2015.00454

Spalteholz, W. Über das Durchsichtigmachen von menschlichen und tierischen Präparaten. (S. Hierzel, Leipzig, 1914)

Steinman, J., Koletar, M.M., Stefanovic, B., and Sled, J.G. (2017) 3D morphological analysis of the mouse cerebral vasculature: Comparison of in vivo and ex vivo methods. *PLoS One*. 12(10): e0186676. Doi: 10.1371/journal.pone.0186676

Susaki, E.A., Tainaka, K., Perrin, D., Yukinaga, H., Kuno, A., and Ueda, H.R. (2015). Advanced CUBIC protocols for whole-brain and whole-body clearing and imaging. *Nature Protocols*. 10 (11): 1709-1727. Doi: 10.1038/nprot.2015.085.

Tainaka, K., Kuno, A., Kubota, S.I., Murakami, T., and Ueda, H.R. (2016). Chemical Principles in Tissue Clearing and Staining Protocols for Whole-Body Cell Profiling. *Annual Review of Cell and Developmental Biology*. 32: 713-741 Doi: 10.1146/annurev-cellbio-111315-125001

Tainaka, K., Murakami, T.C., Susaki, E.A., Shimizu, C., Saito, R., Takahashi, K., Hayashi-Takagi, A., Sekiya, H., Arima, Y., Nojima, S., Ikemura, M., Ushiku, T., Shimizu, Y., Murakami, M., Tanaka, K.F., Iino, M., Kasai, H., Sasaoka, T., Kobayashi, K., Miyazono, K., Morii, E., Isa, T., Fukayama, M., Kakita, A., and Ueda, H.R. (2018) Chemical Landscape for Tissue Clearing Based on Hydrophilic Reagents, *Cell Reports*. 24(8): 2196-2210. Doi: 10.1016/j.celrep.2018.07.056.

Tanaka, N., Kaczynska, D., Kanatani, S., Sahlgren, C., Mitura, P., Stepulak, A., Miyakawa, A., Wiklund, P., and Uhlén, P. (2018). Mapping of the three-dimensional lymphatic microvasculature in bladder tumours using light-sheet microscopy. *British Journal of Cancer*. 118(7): 995-999. Doi: 10.1038/s41416-018-0016-y

Todorov, M.I., Paetzold, J.C., Schoppe, O., Tetteh, G., Shit, S., Efremov, V., Todorov-Völgyi, K., Düring, M., Dichgans, M., Piraud, M., Menze B., and Ertürk, A. (2020) Machine learning analysis of whole mouse brain vasculature. *Nature Methods* 17(4): 442–449. Doi: 10.1038/s41592-020-0792-1

Tong, X.Y., Liu, Y.J., Xu, X.Q., Shi, J.M., Hui, W., Ma, T., Cui, P., Lu, W.H., Pei, Z.L., Xu, M.Z., Zhang, F.F., Li, X., and Feng, Y. (2020) Ovarian Innervation Coupling With Vascularity: The Role of Electro-Acupuncture in Follicular Maturation in a Rat Model of Polycystic Ovary Syndrome. *Frontiers in Physiology*. 11: 474 Doi: 10.3389/fphys.2020.00474.

Ueda, H.R., Ertürk, A., Chung, K., Gradinaru, V., Chédotal, A., Tomancak, P., and Keller, P.J. (2020). Tissue clearing and its applications in neuroscience. *Nature Reviews Neuroscience*. 21(2): 61-79. Doi: 10.1038/s41583-019-0250-1

Uludağ, K. and Blinder, P. (2018). Linking brain vascular physiology to hemodynamic response in ultra-high field MRI. *NeuroImage* 168: 279-295. Doi: 10.1016/j.neuroimage.2017.02.063

Vigouroux, R.J., Belle, M., and Chédotal, A. (2017) Neuroscience in the third dimension: shedding new light on the brain with tissue clearing. *Molecular Brain*. 10(1): 33. Doi: 10.1186/s13041-017-0314-y

Wang, C-W., Ka, S-M., and Chen, A. (2014) Robust image registration of biological microscopic images. *Scientific Reports*. 4: 6050. Doi: 10.1038/srep06050

Wang, F.F., Wan, H., Ma, Z.R., Zhong, Y.T., Sun, Q.C, Tian, Y., Qu, L.Q., Du, H.T., Zhang, M.X., Li, L.L., Ma, H.L., Luo, J., Liang, Y.Y., Li, W.J., Hong, G.S., Liu, L.Q., and Dai, H.J. (2019). Light-sheet microscopy in the near-infrared II window. *Nature Methods*. 16(6): 545-552. Doi: 10.1038/s41592-019-0398-7

Walchli, T., Mateos, J.M., Weinman, O., Babic, D., Regli, L., Hoerstrup, S.P., Gerhardt, H., Schwab, M.E., and Vogel, J. (2015) Quantitative assessment of angiogenesis, perfused blood vessels and endothelial tip cells in the postnatal mouse brain. *Nature Protocols* 10(1): 53-74. Doi: 10.1038/nprot.2015.002.

Wu, J.Y., Cai, Y.Q., Wu, X.Y., Ying, Y., Tai, Y.L., and He, M. (2021) Transcardiac Perfusion of the Mouse for Brain Tissue Dissection and Fixation. *Bio-Protocol*. 11(5): e3988. Doi: 10.21769/BioProtoc.3988

Xiao, X., Feng, Y.P., Du, B., Sun, H.R. Ding, Y.Q., and Qi, J.G. (2018) Antibody incubation at 37°C improves fluorescent immunolabeling in free-floating thick tissue sections. *Biotechniques*. 62(3): 115-122. Doi: 10.2144/000114524

Xu, Y.Y., Li, P., Wang, M.Q., Zhang, J., and Wang, W. (2019) Imaging the brain in 3D using a combination of CUBIC and immunofluorescence staining. *Biomedical Optics Express*. 10(4): 2141–2149. Doi: 10.1364/BOE.10.002141

Yao, J.J., Maslov, K., Hu, S., and Wang, L.H.V. (2009) Evans blue dye-enhanced capillary-resolution photoacoustic microscopy in vivo. *Journal of Biomedical Optics*. 14(5): 054049. Doi: 10.1117/1.3251044

Yokoyama, T., Lee, J.K., Miwa, K., Opthof, T., Tomoyama, S., Nakanishi, H., Yoshida, A., Yasui, H., Iida, T., Miyagawa, S., Okabe, S., Sawa, Y., Sakata, Y., and Komuro, I. (2017) Quantification of sympathetic hyperinnervation and denervation after myocardial infarction by three-dimensional assessment of the cardiac sympathetic network in cleared transparent murine hearts. *PLoS ONE* 12(7): e0182072. Doi: 10.1371/journal.pone.0182072

Zhang, M., Yue, J., Cui, R., Ma, Z.R., Wan, H., Wang, F.F., Zhu, S.J., Zhou, Y., Kuang, Y., Zhong, Y.T., Pang, D.-W., and Dai, H.J. (2018). Bright quantum dots emitting at <1,600 nm in the NIR-IIb window for deep tissue fluorescence imaging. *Proceedings of the National Academy of Sciences of the USA* 115(26): 6590–6595. Doi: 10.1073/pnas.1806153115

Zhu, J.T., Yu, T.T., Li, Y.S., Xu, J.Y., Qi, Y.S., Yao, Y.T., Ma, Y.L., Wan, P., Chen, Z.L., Li, X.N., Gong, H., Luo, Q.M., and Zhu, D. (2020). MACS: Rapid Aqueous Clearing System for 3D Mapping of Intact Organs. *Advanced science*. 7(8): 1903185. Doi: 10.1002/advs.201903185

